Transmission electron microscopy:
fundamentals and application for battery materials

D. Batuk

Outline

1. The tool
    - lenses
    - holders
    - sample preparation
2. TEM modes:
    - Electron Diffraction
    - Imaging (conventional TEM, STEM)
    - Spectroscopy (elemental analysis)

Why electrons?

VLM

TEM

Ruska and Knoll 1930s

Resolution limit of an optical system (Rayleigh criterion): $\delta \approx 0.61\lambda/NA \approx \lambda/2$

Visible light: $\lambda \approx 500$ nm → δ [500nm] ≈ 250nm

Electrons:

$$\lambda = \frac{h}{\sqrt{2em_0U}} = \frac{12.26}{\sqrt{U}}$$

λ = 0.034Å (120kV); 0.020Å (300kV)

δ^{theor} [300kV] ≈ 0.02Å

δ^{real} [300kV] ≈ 0.5Å

Typical TEM tools (@EMAT, University of Antwerp)

FEI Tecnai G2

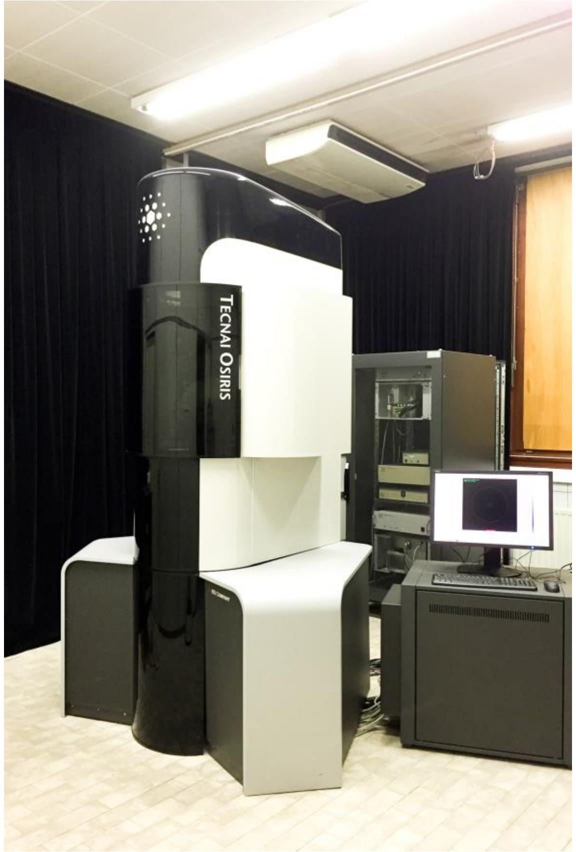

FEI Tecnai Osiris

FEI Titan

Microscope column

electron gun

condenser lenses

objective lens

projection lenses

observation unit

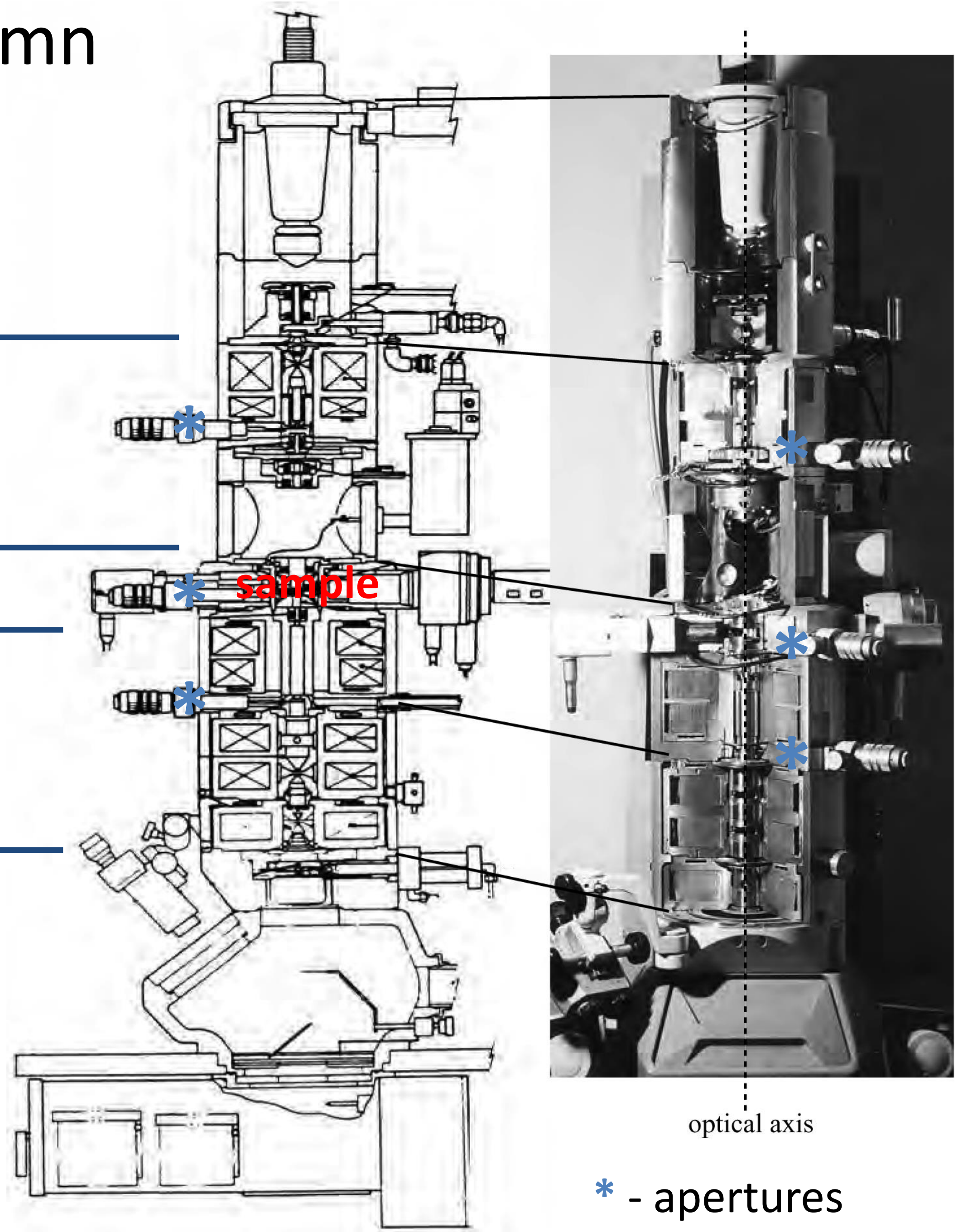

* - apertures

Electron source

Field Emission Guns (FEGs)

(1) Thermionic Gun

W tip
T = 2700 °C

LaB_6 tip
T = 1700 °C

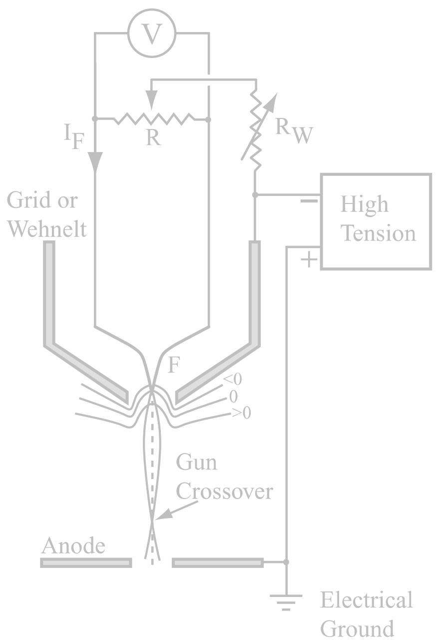

Typical HT: 60-300 kV

(2) Schottky FEG

W tip, T = 1800 °C

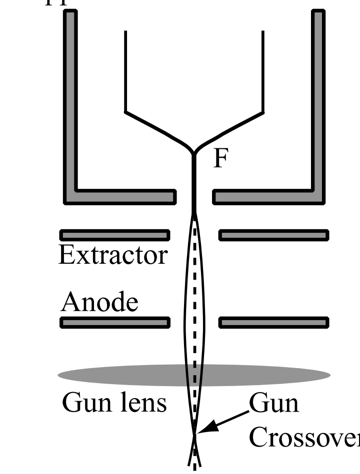

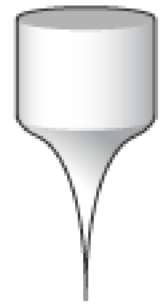

(3) cold FEG

W tip, RT

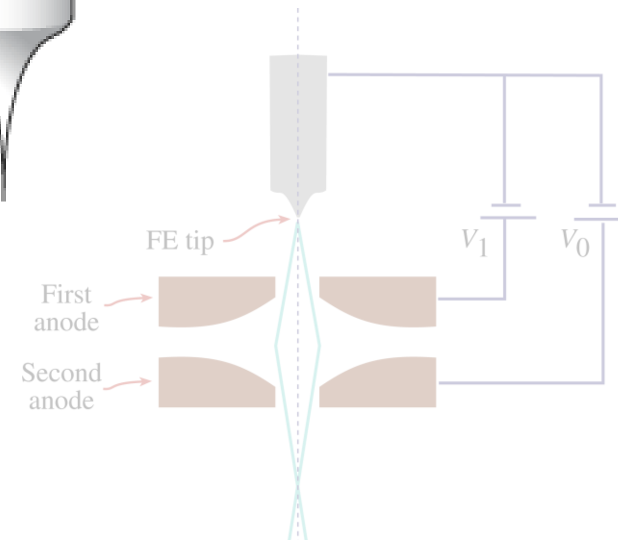

Advantages:

- ✓ high brightness
- ✓ high coherency
- ✓ small source size
- ✓ better stability

Electromagnetic lenses

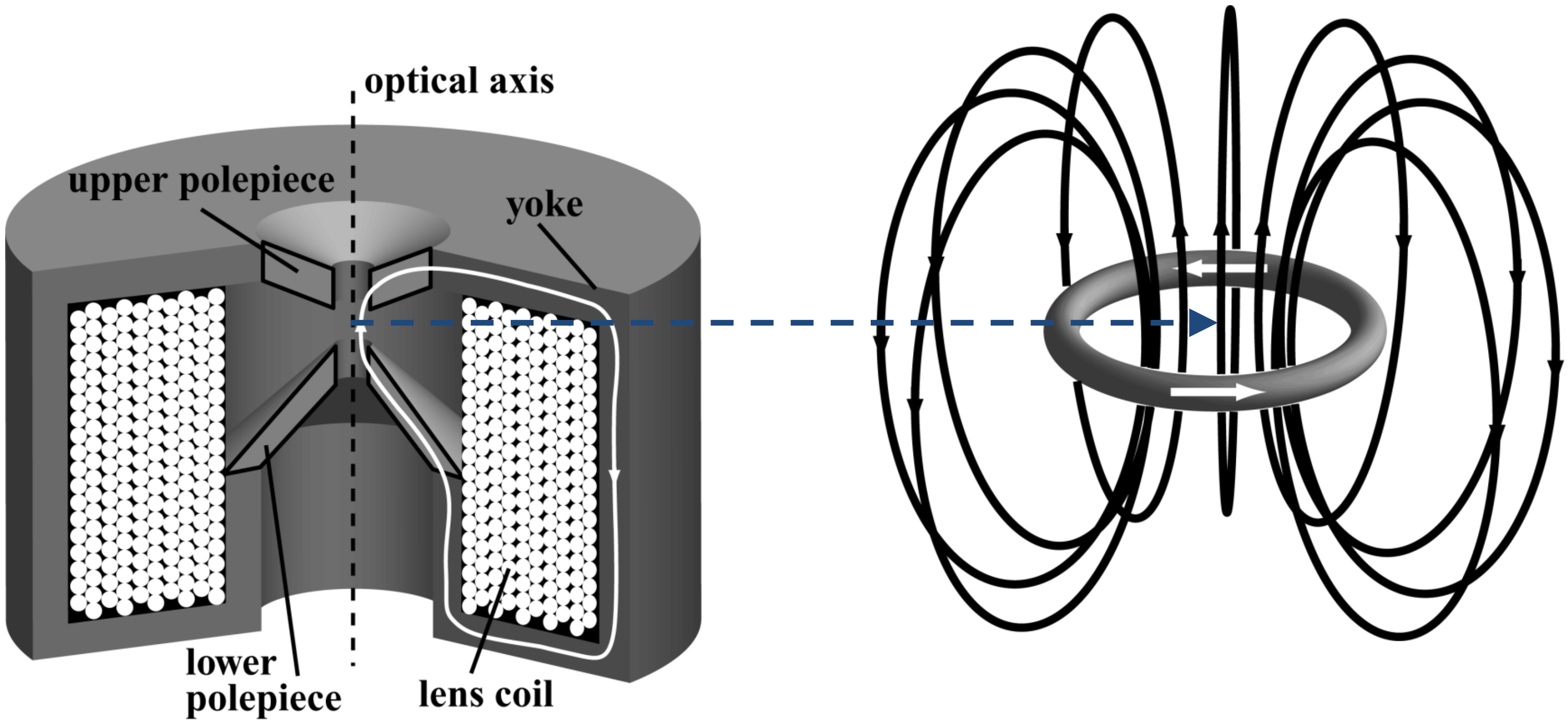

lens

magnetic field

Electromagnetic lenses

field

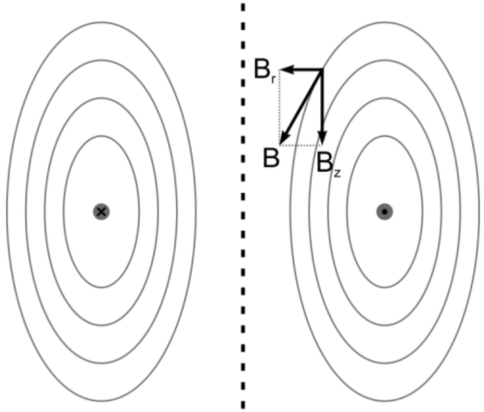

trajectory

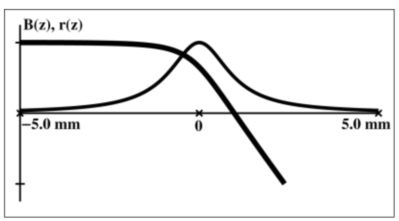

Radial plot

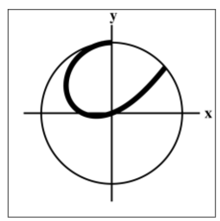

Azimuthal plot

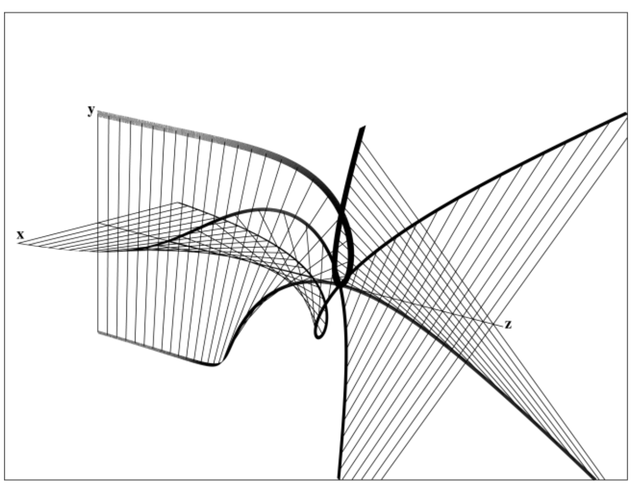

Perspective plot

Field: $\mathbf{B} = \mathbf{B}_z + \mathbf{B}_r$

Lorentz force: $\mathbf{F} = -e(\mathbf{v} \times \mathbf{B})$

$\mathbf{v}_z \parallel \mathbf{B}_z, \mathbf{v}_z \perp \mathbf{B}_r \Rightarrow \mathbf{F}_\theta = -e(\mathbf{v}_z \times \mathbf{B}_r)$

$\mathbf{v}_\theta \perp \mathbf{B}_z \Rightarrow \mathbf{F}_r = -e(\mathbf{v}_\theta \times \mathbf{B}_z)$

$\mathbf{F}_\theta$ – rotates about the optical axis

$\mathbf{F}_r$ – moves towards the optical axis

- spherical lens
- rotates the electron beam around the optical axis
- only focusing lenses
- variable focal length (strength) depending on the current

Functions of the lenses

condenser system:
- ✓ controls beam intensity
- ✓ controls convergence of the electron beam:
  - parallel-beam illumination
  - convergent-beam illumination

objective system:
- ✓ focusing of the electron beam on the sample

projection system:
- ✓ magnification
- ✓ switching between real space (imaging) and reciprocal space (diffraction)

Spherical aberrations

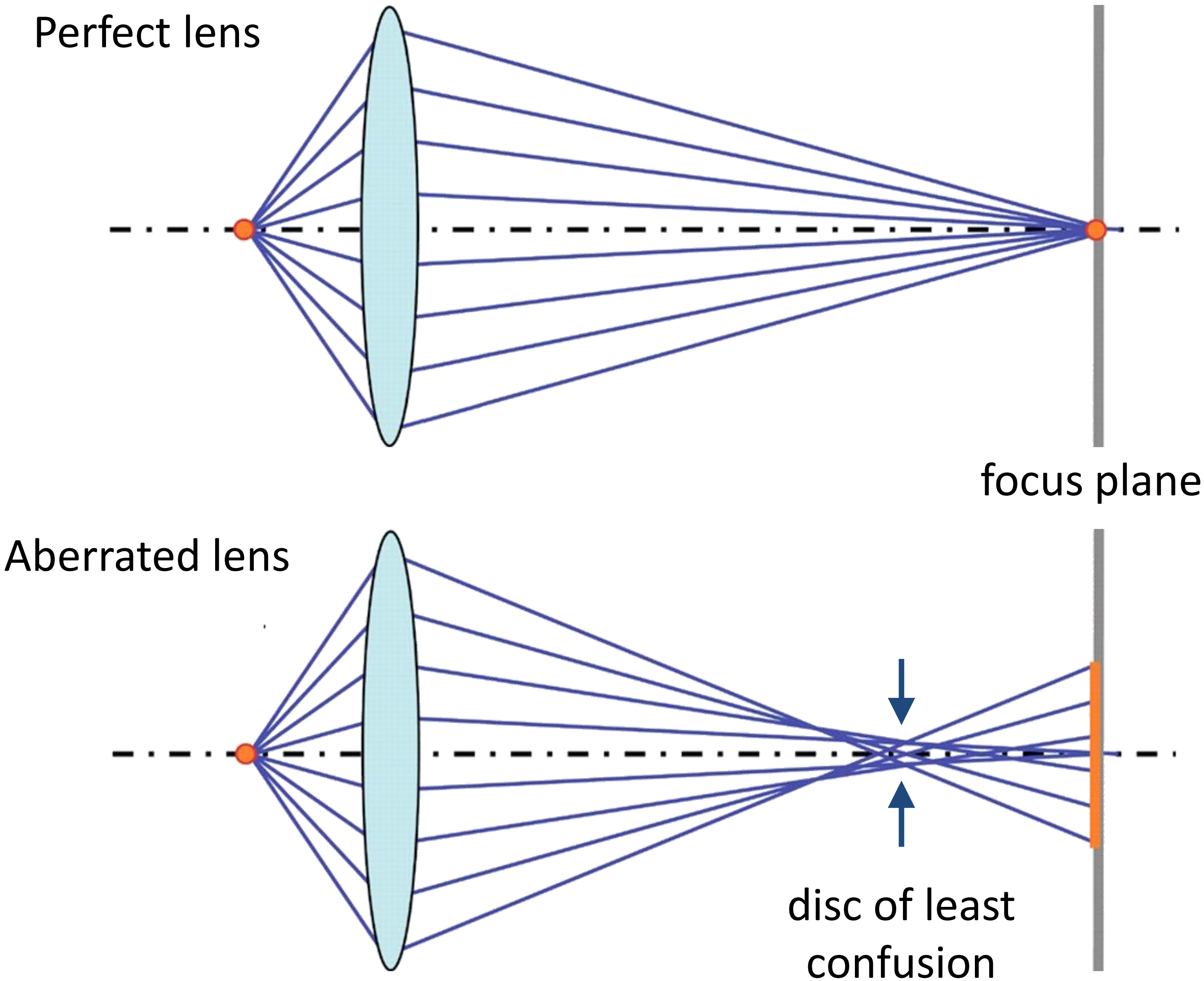

Spherical aberrations correction

Light optics: stacks of focusing and defocusing lenses

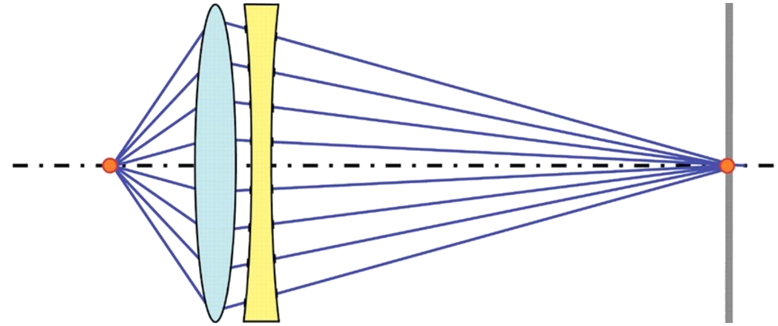

Electron optics: use of non-spherical elements

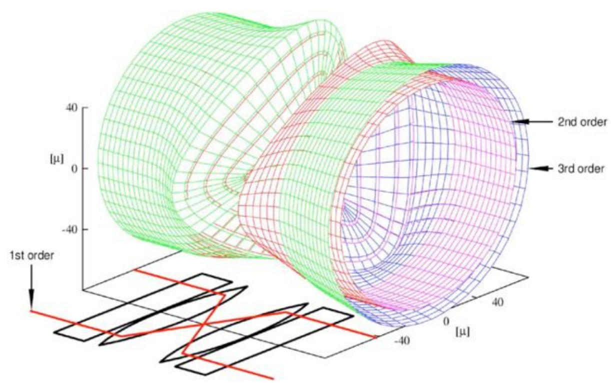

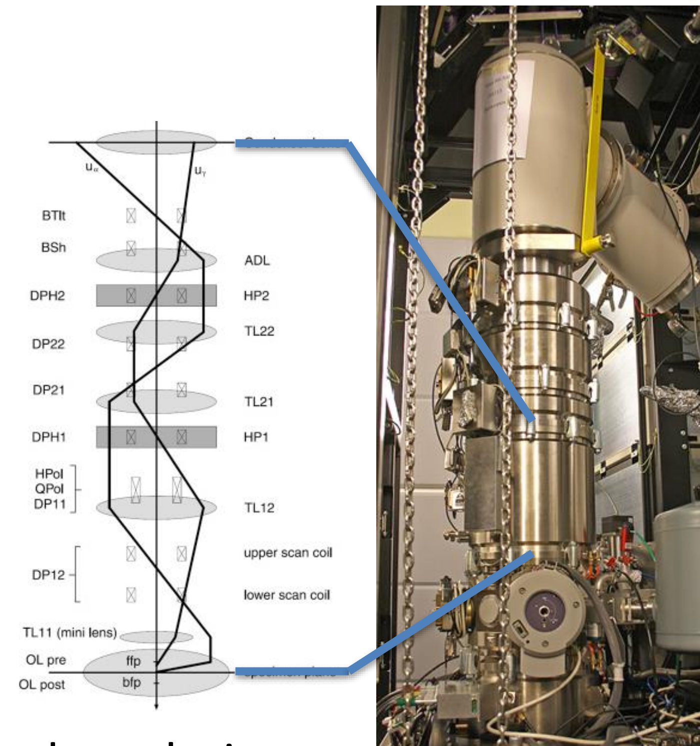

condensed system – probe corrector

objective system – image corrector

+ improved resolution

– high cost

– complex alignment

TEM sample holders

- single tilt
- tomography
- double tilt
- tilt-rotation
- cooling
- heating
- vacuum transfer
- *in situ* electrochemical testing
- mechanical testing
- …

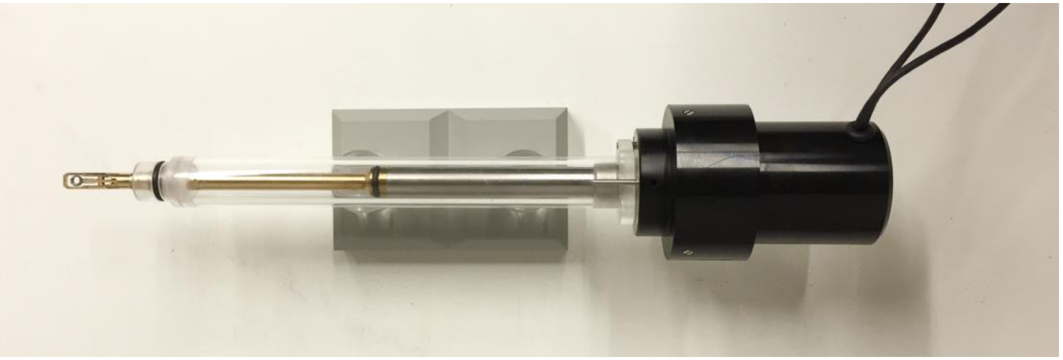

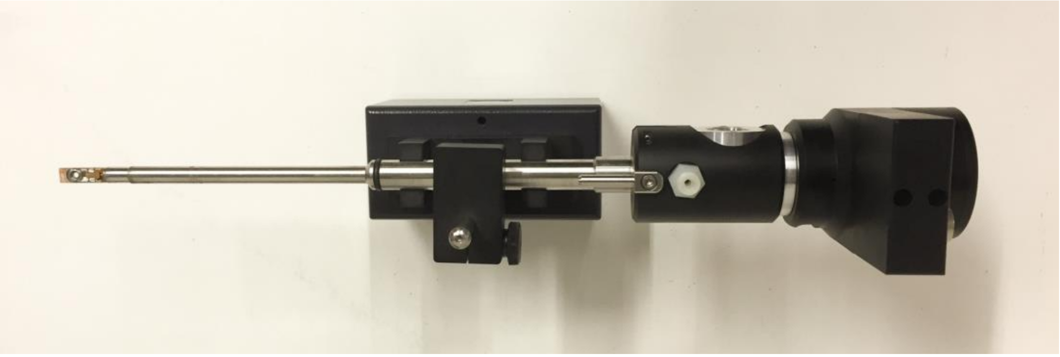

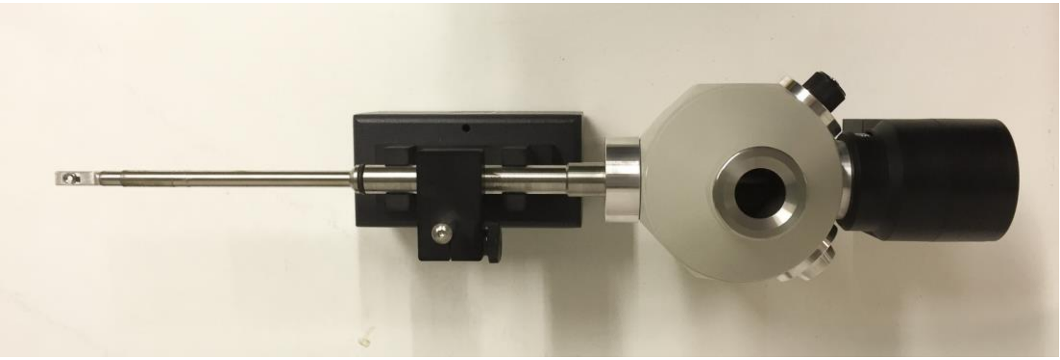

Tilts and TEM grids

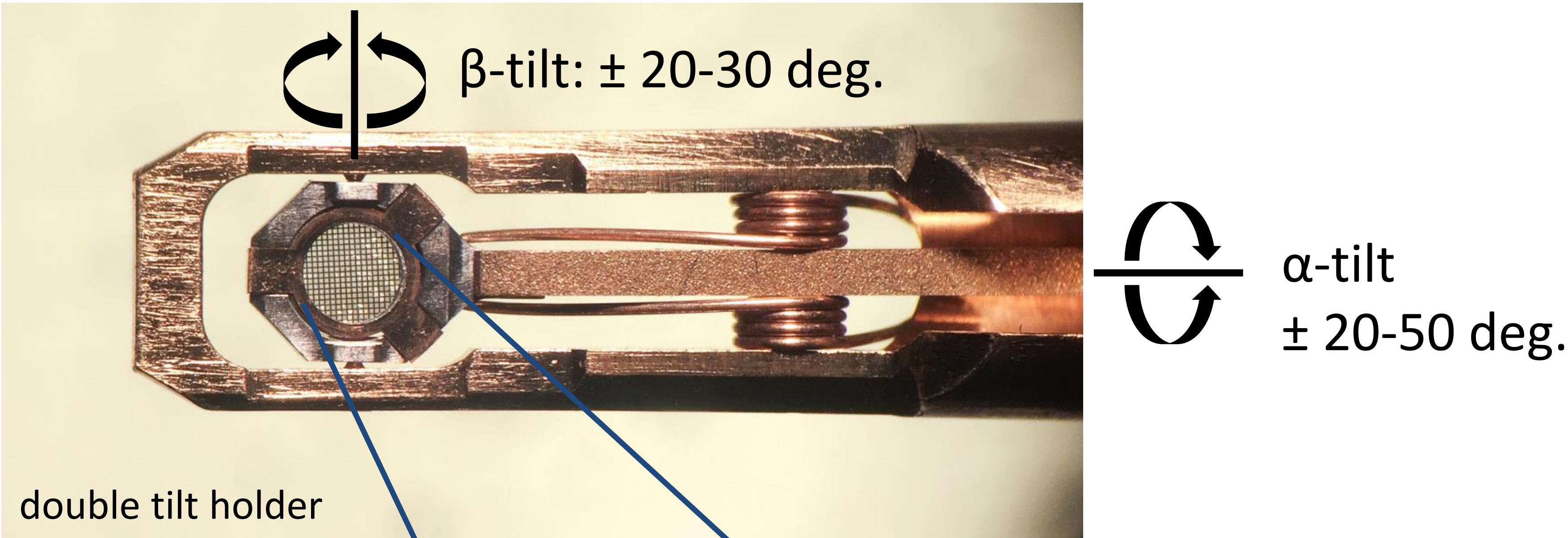

grids:

Cu (Ti, Ni, Mo) mesh

+

holey carbon foil

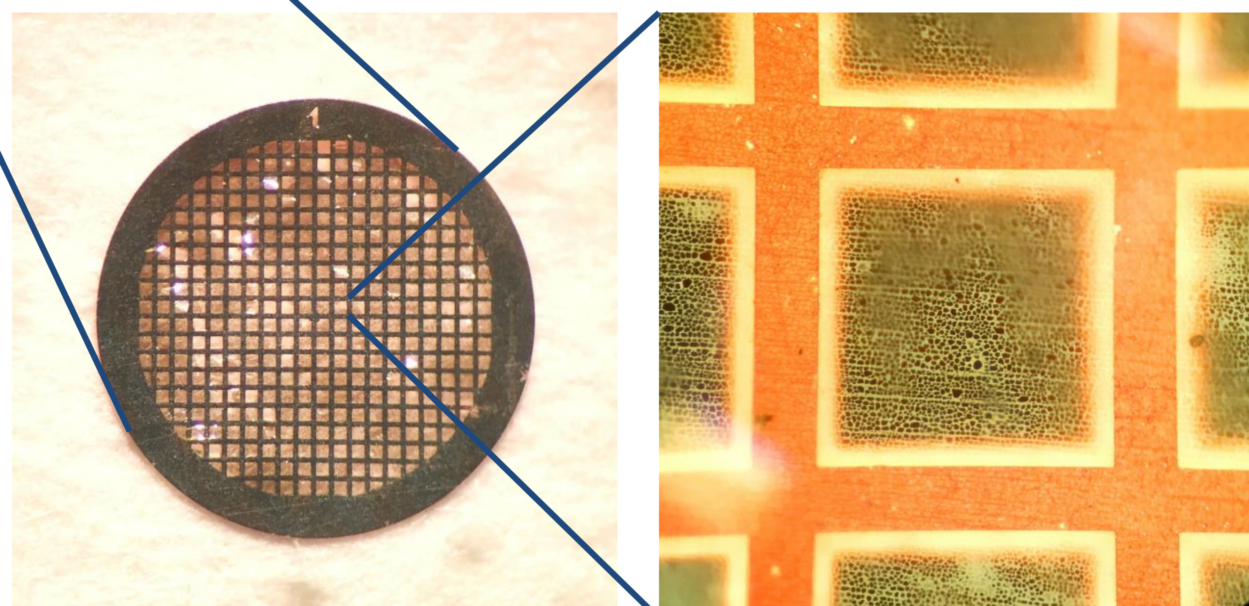

Sample preparation - powders

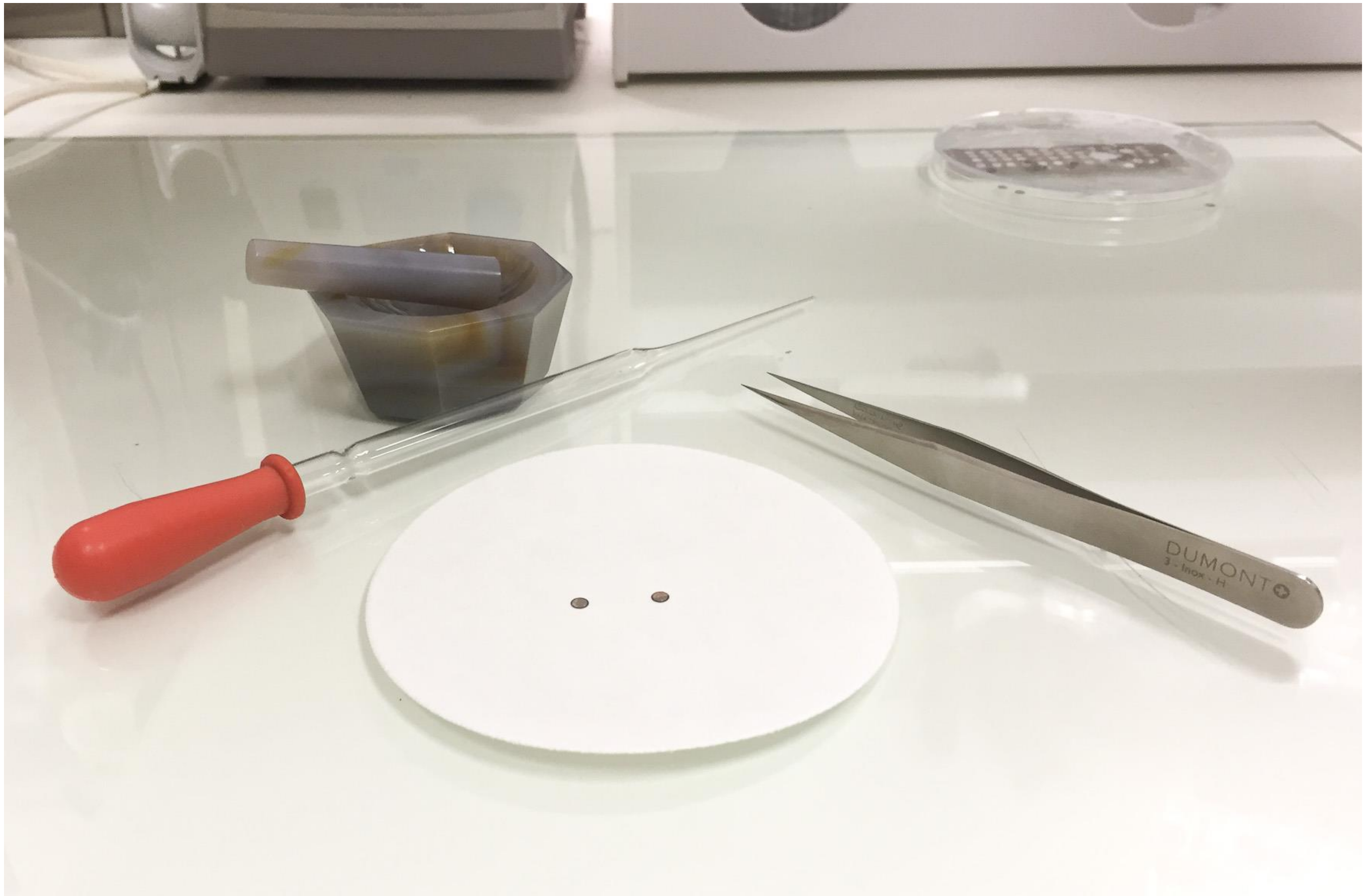

Method 1:

1. grinding under solvent (DMC, EtOH, hexane)
2. putting a few drops of dispersion on grids

Method 2:

1. no solvent
2. pressing TEM grid against dry powder

Air sensitive samples

Sample preparation in an Ar-filled glove box

Air-tight
double tilt holder

Transfer to the microscope under Ar

Focused Ion Beam (FIB)

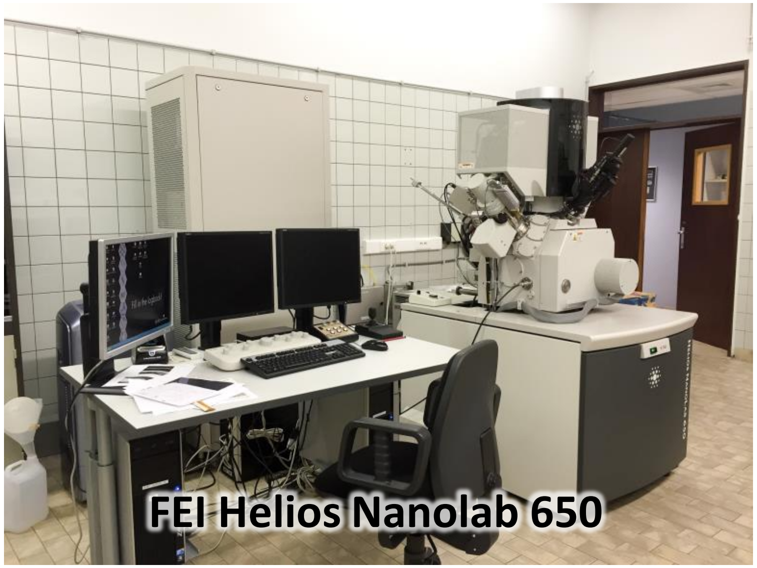

dual beam tool

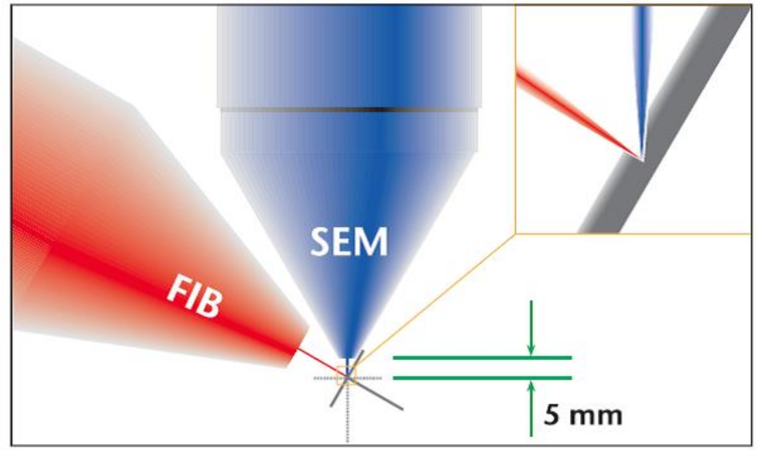

NaO_2 particles on carbon fibers

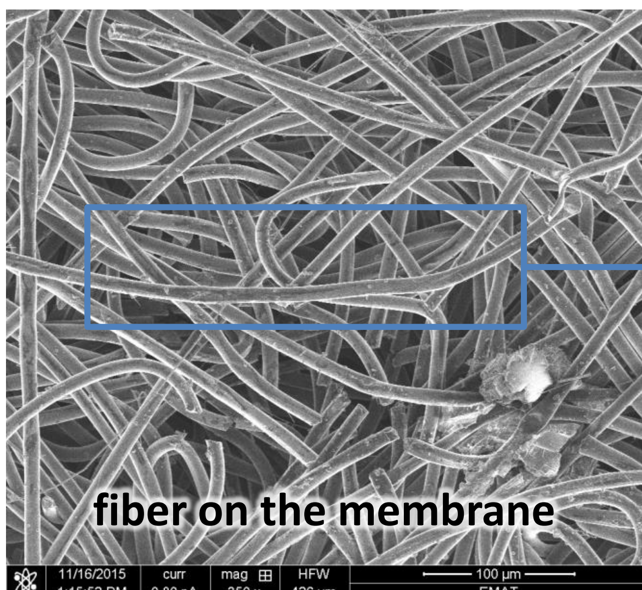

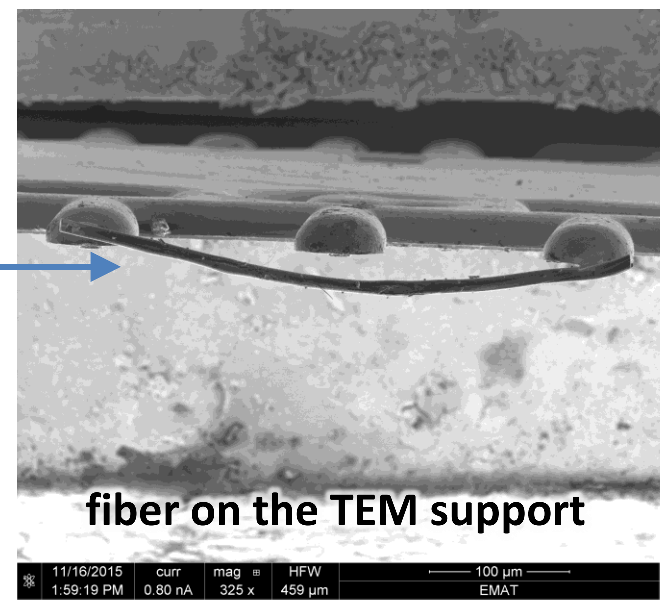

Electron interaction with the mater

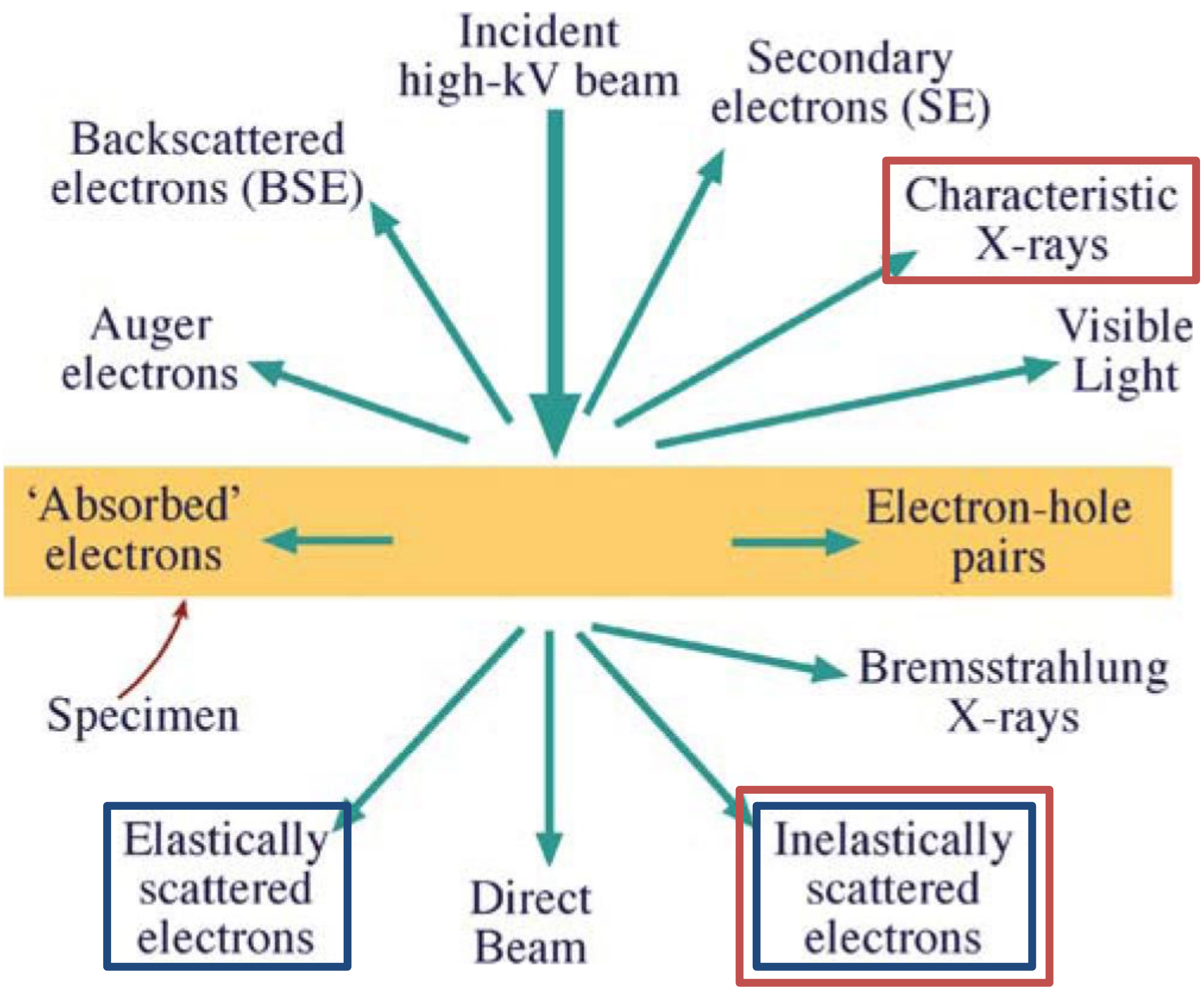

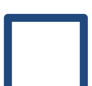
structural information

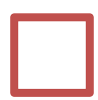
chemical information

Illumination modes

parallel-beam illumination

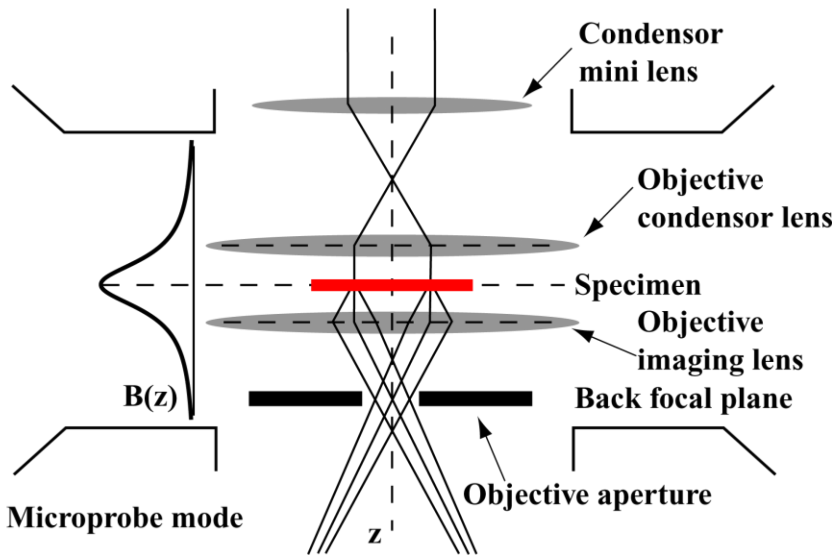

Electron Diffraction (ED)

low magnification TEM

High Resolution TEM (HRTEM)

focused-beam illumination

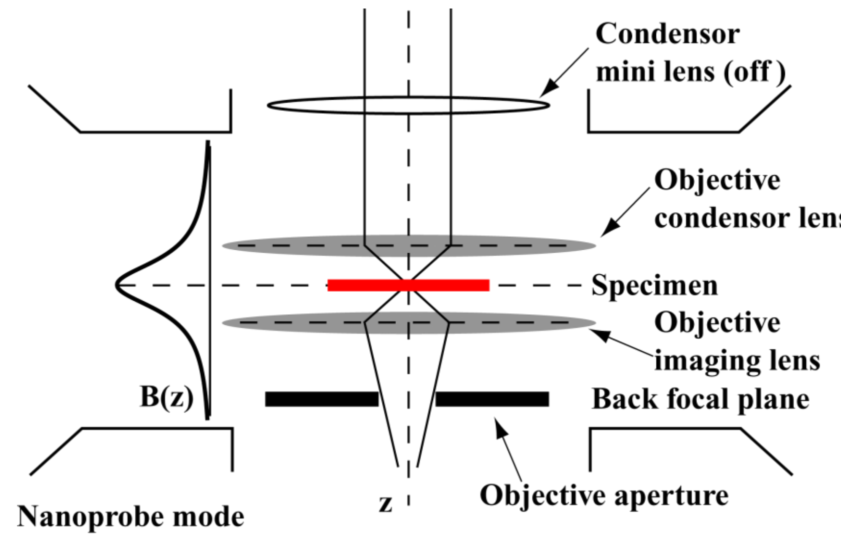

Scanning TEM (STEM)

HAADF-STEM and ABF-STEM

Parallel Illumination

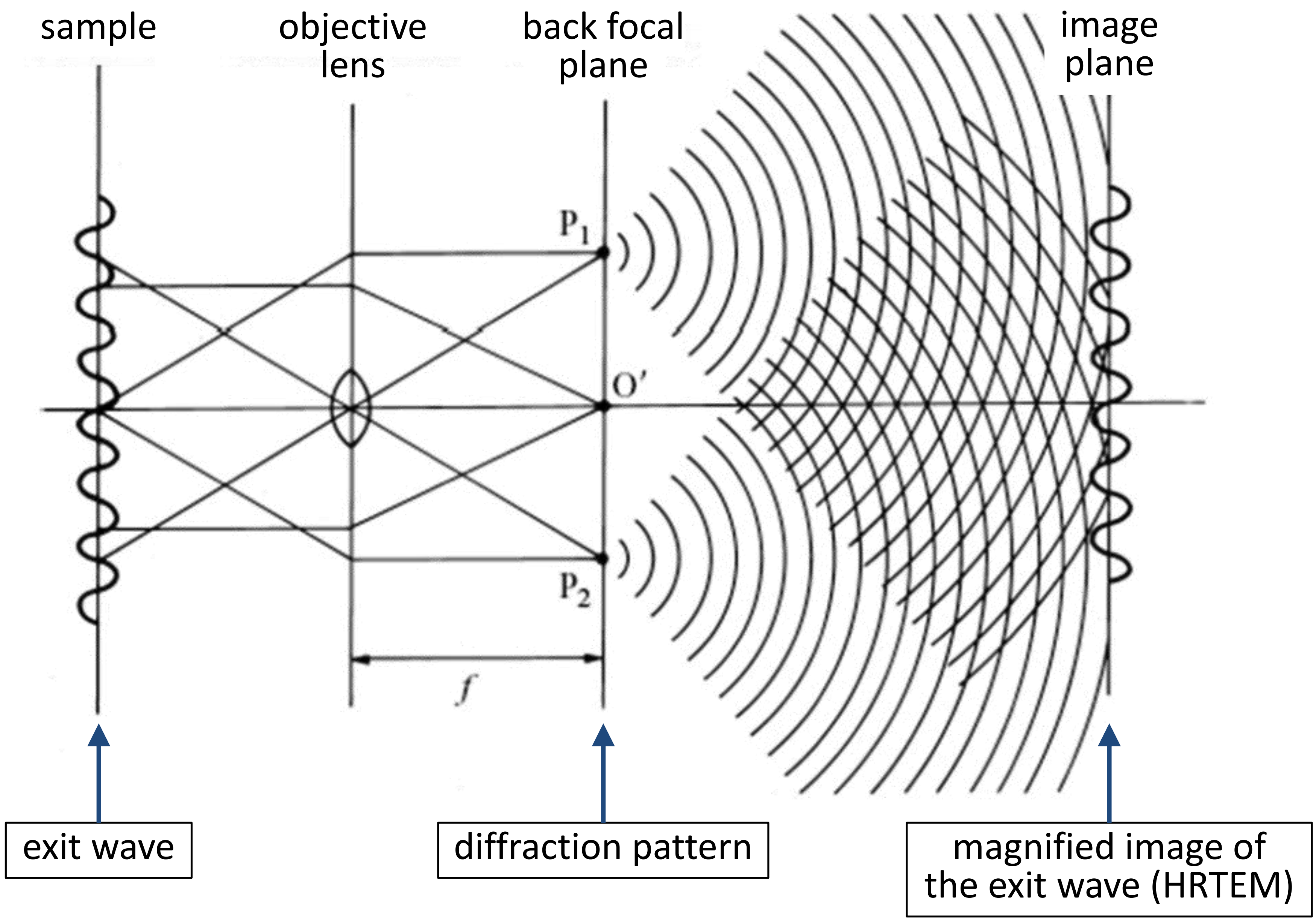

Real and reciprocal space in TEM

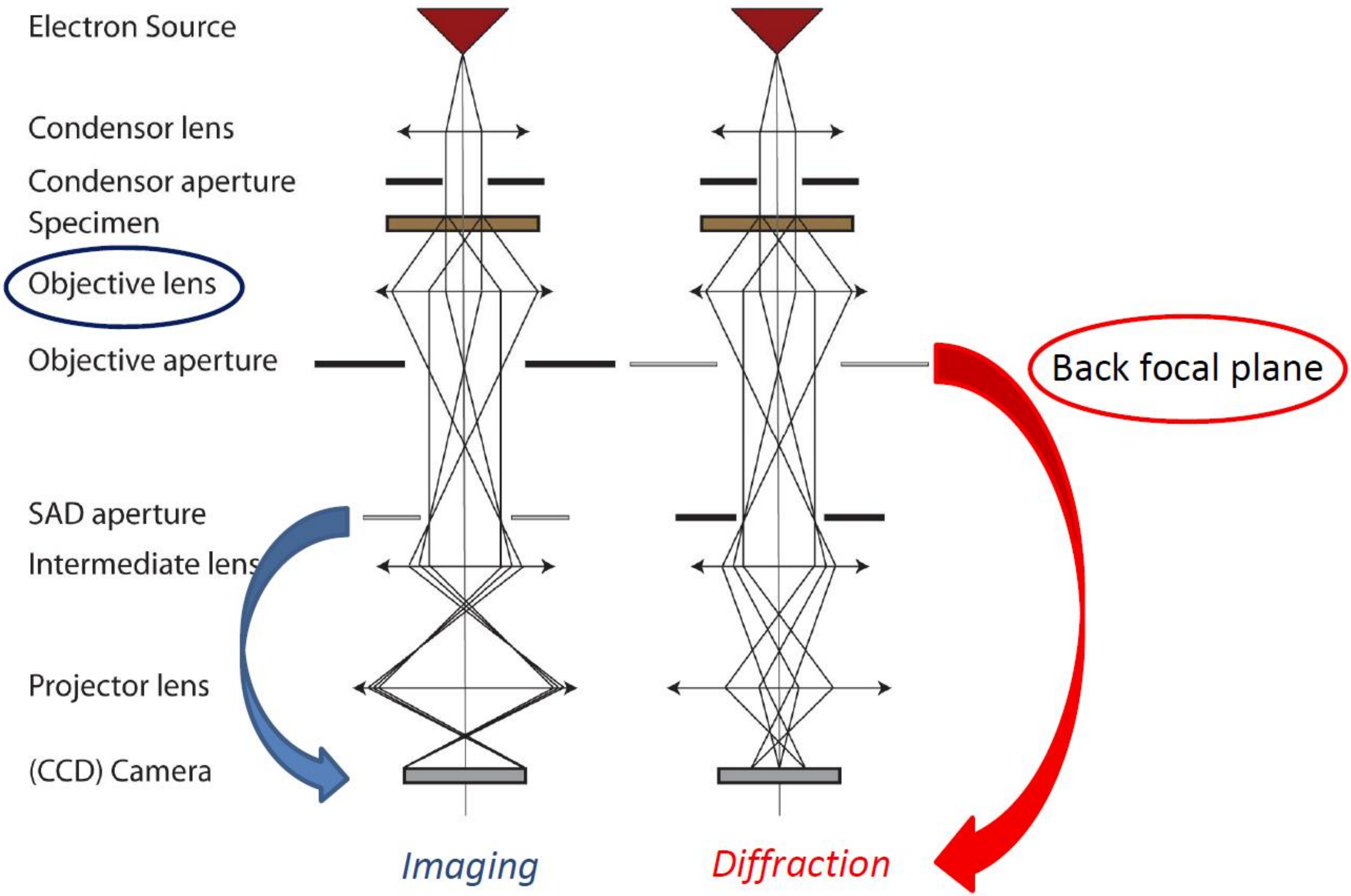

Selected Area Electron Diffraction (SAED)

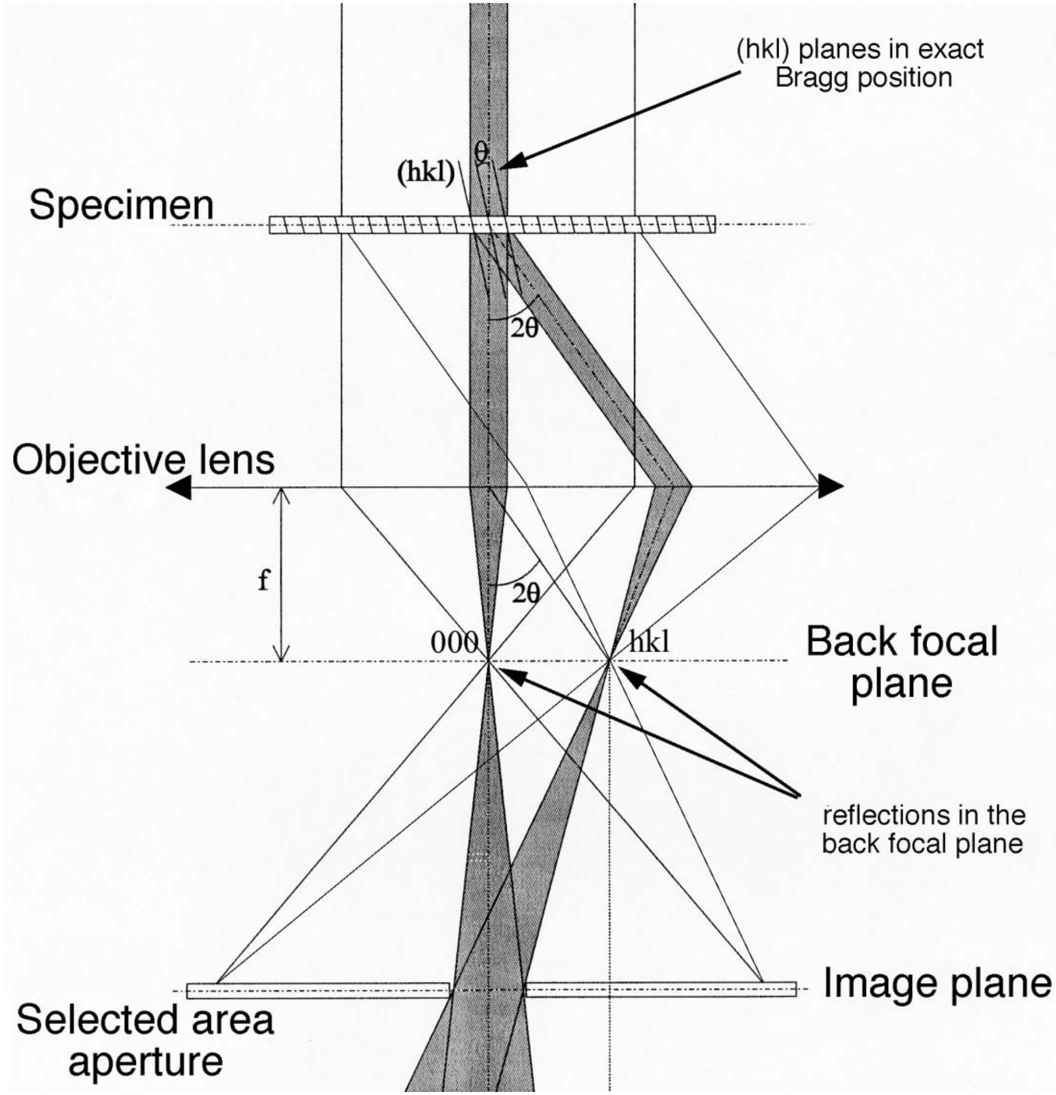

Tecnai G2: SAED aperture 10μm → ~100nm circle on the sample

Diffraction conditions – Ewald sphere

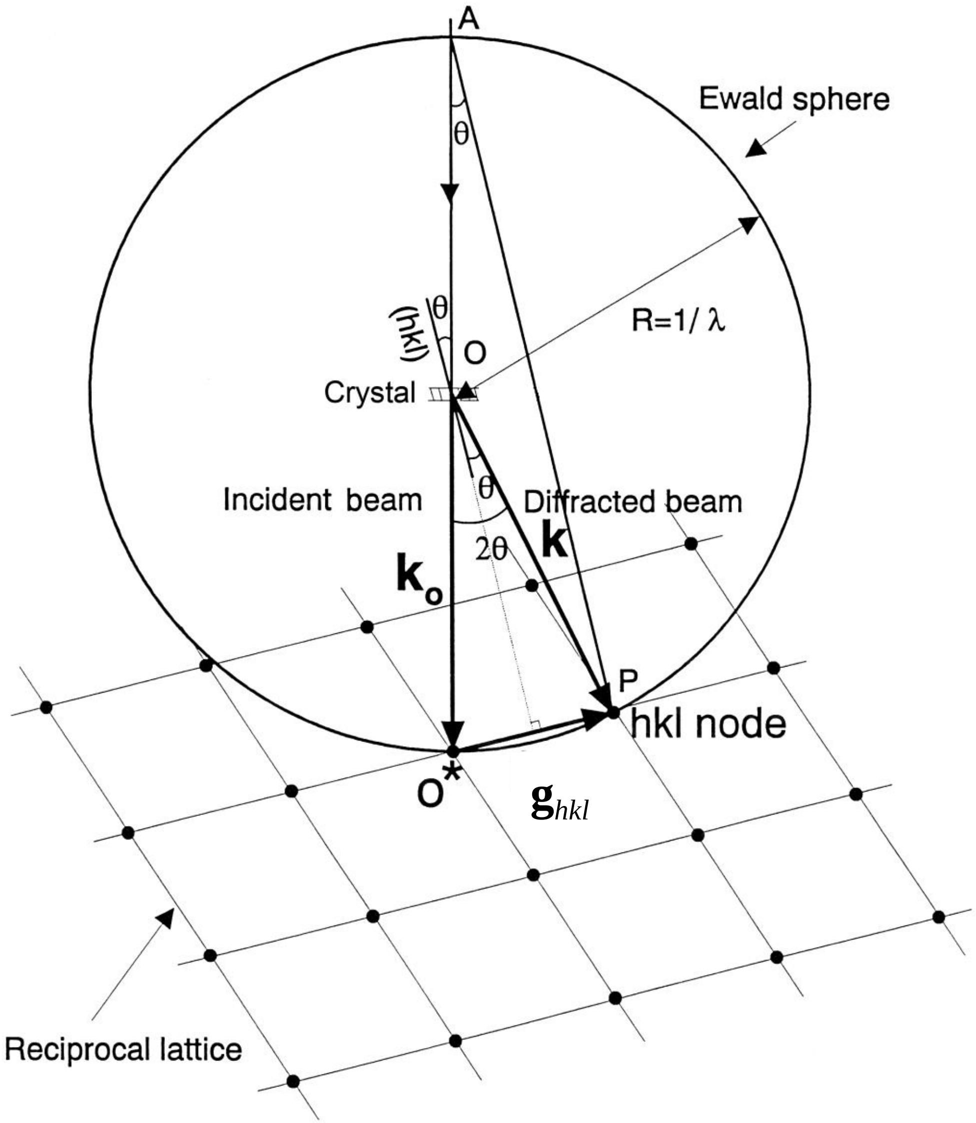

1. Radius: $1/\lambda$
2. Crystal (i.e. scattering center) at the center of the sphere
3. Incident beam - wave vector $\mathbf{k}_0$
4. Origin of the reciprocal lattice O* at the end of $\mathbf{k}_0$

1. Diffraction condition: when *hkl* node lies on the Ewald sphere (vectror **k**)

Diffraction conditions – Ewald sphere

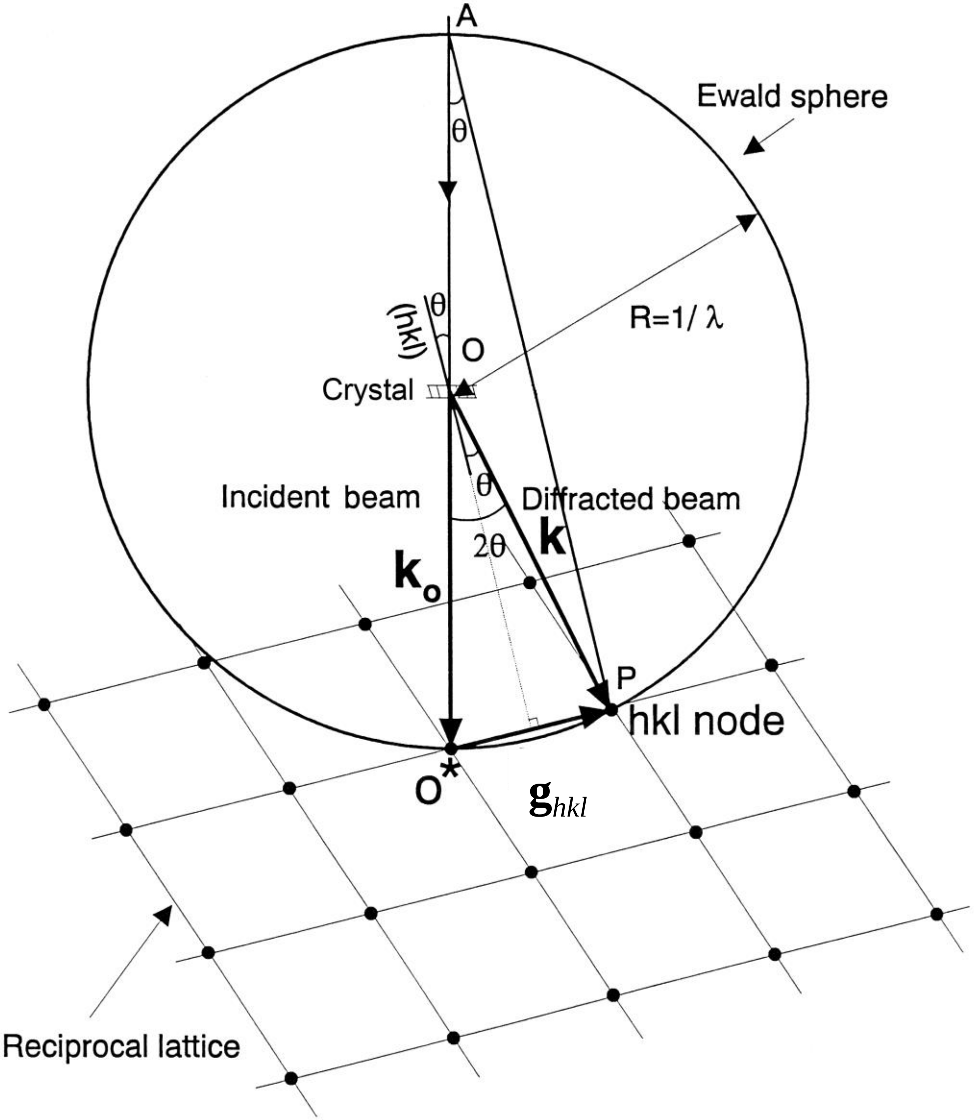

$\angle \mathbf{k},\mathbf{k}_0 = 2\theta$

$|\mathbf{k}| = |\mathbf{k}_0| = 1/\lambda$

$|\mathbf{g}_{hkl}| = 1/d_{hkl}$

$|\mathbf{g}_{hkl}| = 2|\mathbf{k}_0| sin\theta$

$1/d_{hkl} = 2/\lambda \sin\theta$

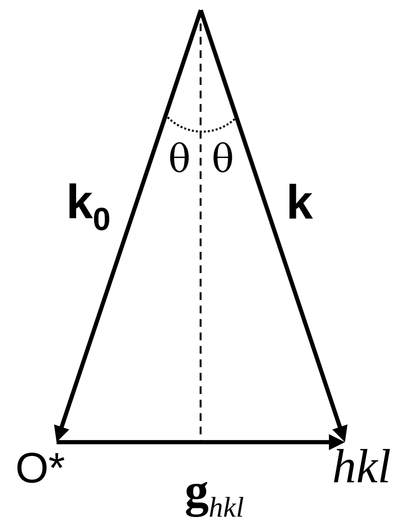

Electron Diffraction

X-rays:

$\lambda = 1.5406Å\ (CuK_{\alpha 1})$

Electrons:

$$\lambda = \frac{h}{\sqrt{2em_0U}} = \frac{12.26}{\sqrt{U}}$$

$\lambda = 0.034Å\ (120kV)$
$\lambda = 0.025Å\ (200kV)$
$\lambda = 0.020Å\ (300kV)$

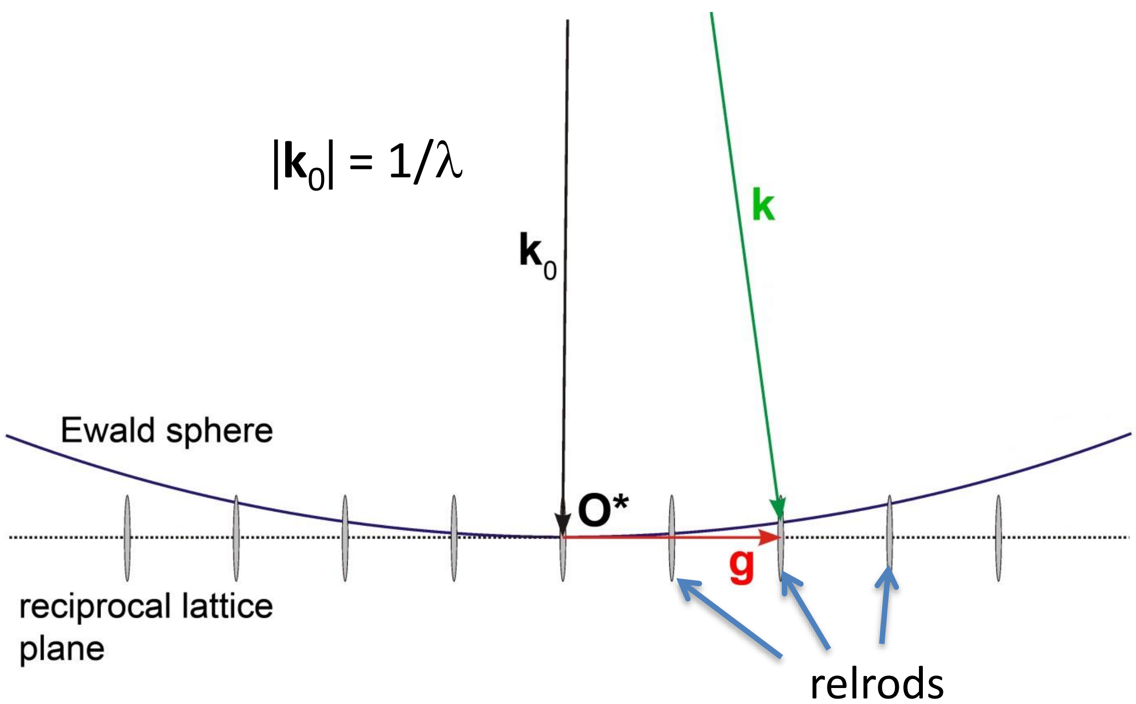

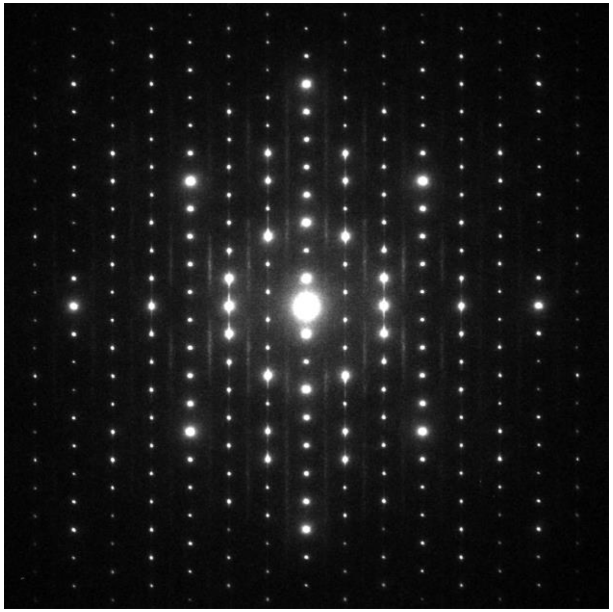

in-zone ED pattern

ED pattern is a section of the reciprocal lattice!

Orientation of the crystal

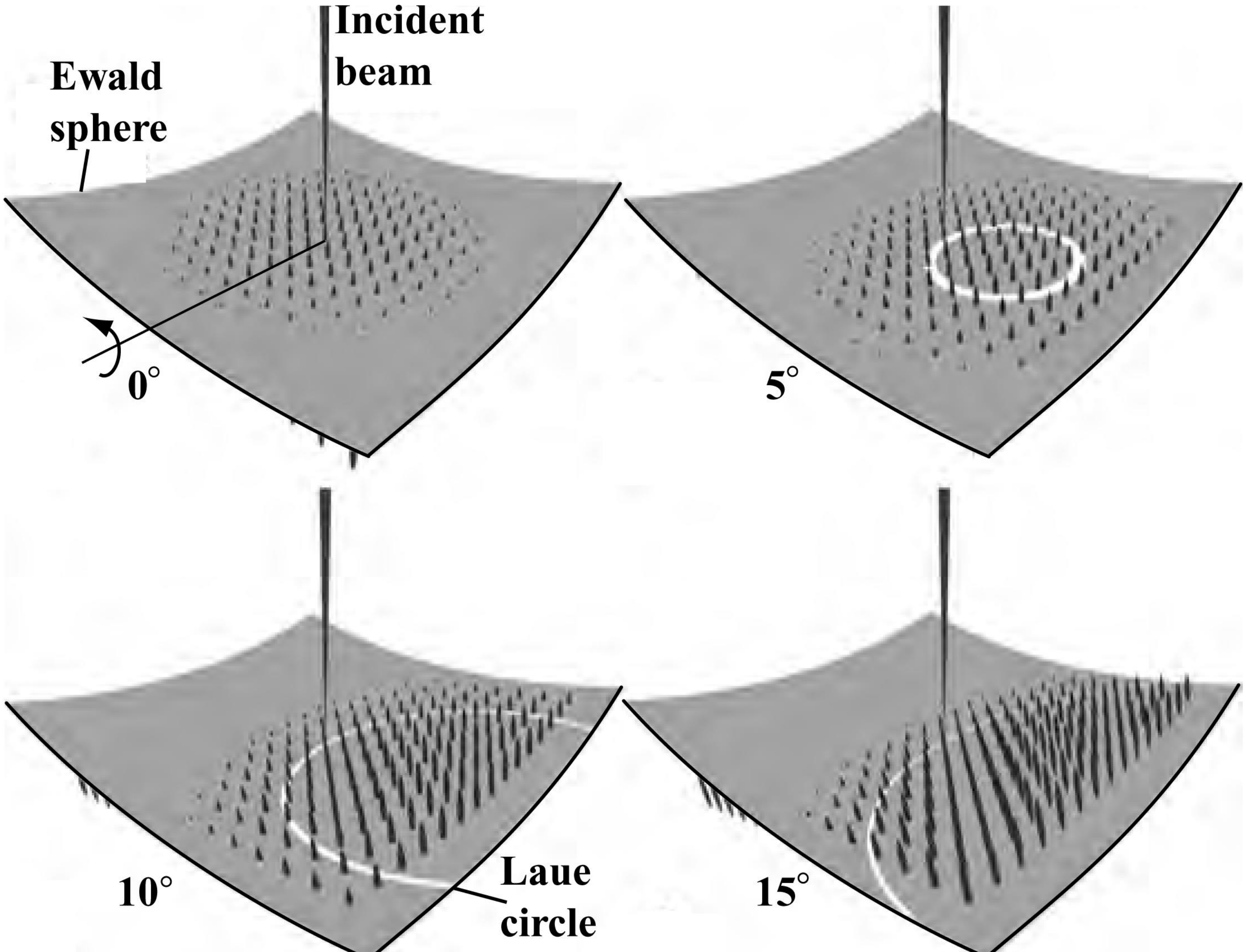

ED for Space Group determination $K_2Cu_2(SO_4)_3$

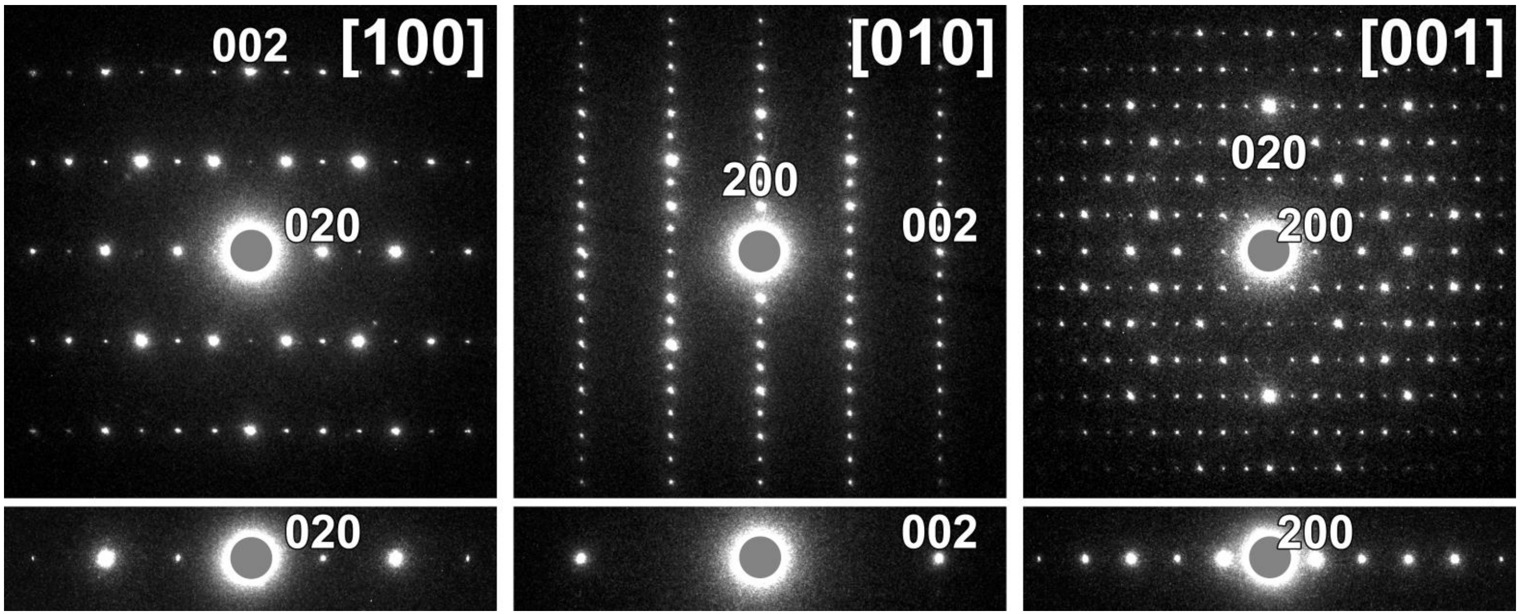

Reflection conditions

$h00$: $h = 2n$

$0k0$: $k = 2n$

$00l$: $l = 2n$

⇨ *S.G.* $P2_12_12_1$

Cell parameters (ED):

$a \approx 18.2$ Å, $b \approx 11.5$ Å, $c \approx 4.8$ Å

Lander L. *et al*, *Inorg. Chem.* **2017**, *56*, 2013–2021

Multiple scattering

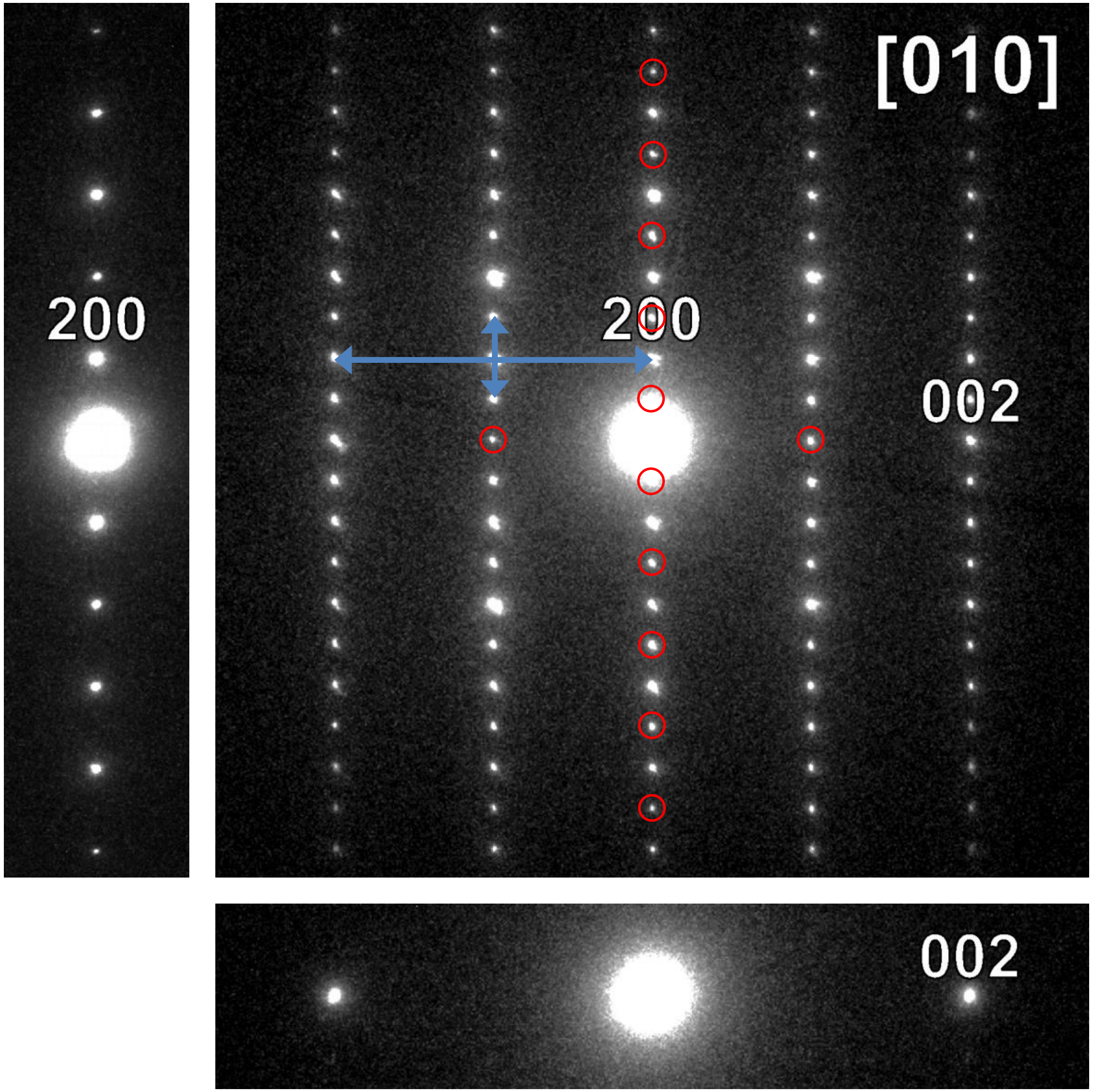

S.G. $P2_12_12_1$

$h00$: $h = 2n$

$0k0$: $k = 2n$

$00l$: $l = 2n$

Lander L. *et al*, *Inorg. Chem.* **2017**, *56*, 2013–2021

ED for Space Group determination $KVPO_4F$

Reflection conditions

$0kl$: $k + h = 2n$

$h0l$: $h = 2n$

$hk0$: –

⇨ *S.G. Pnam* or $Pna2_1$

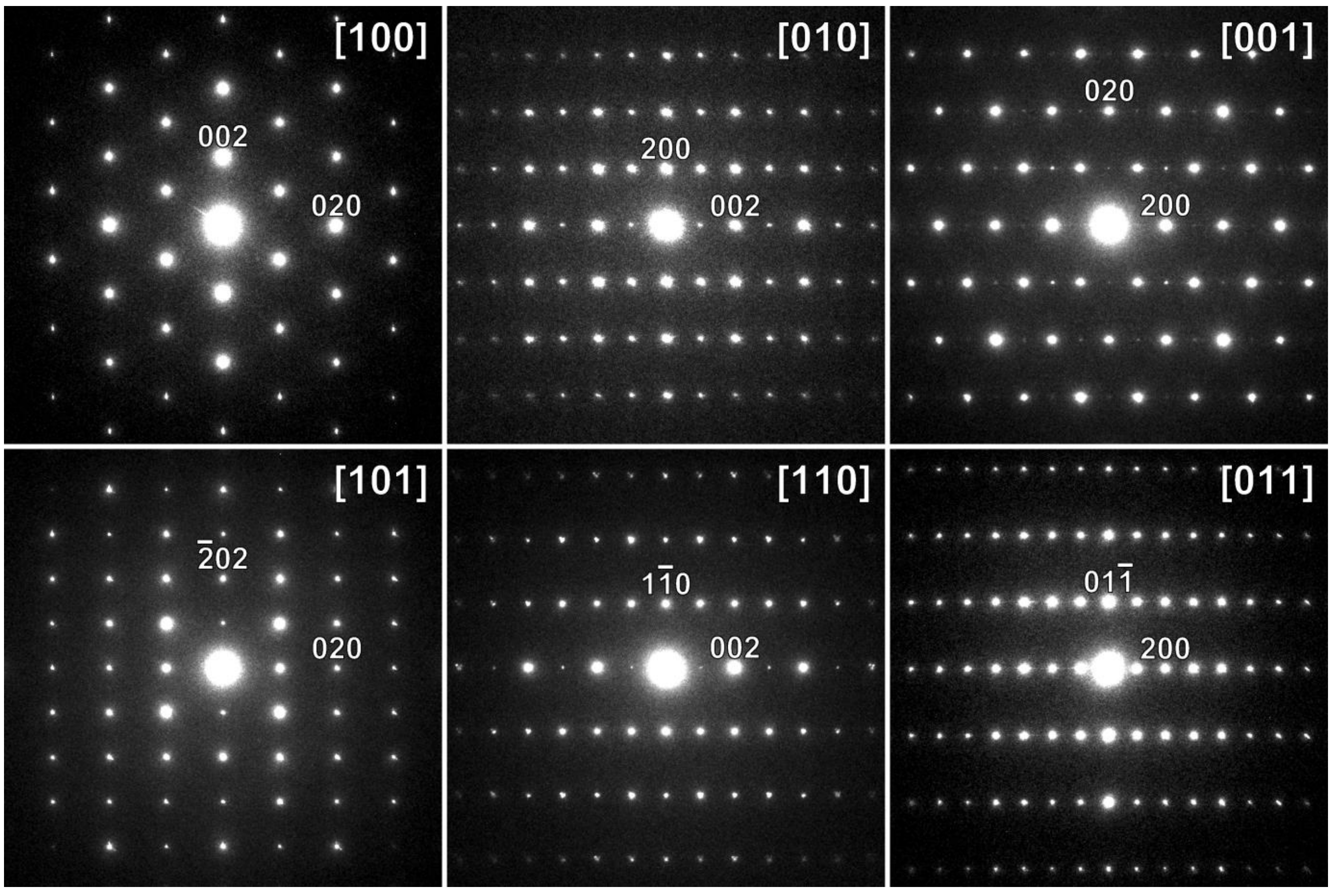

Fedotov S. S. *et al*, *Chem. Mater.* **2016**, *28*, 411–415

ED for Space Group determination $KVPO_4F$

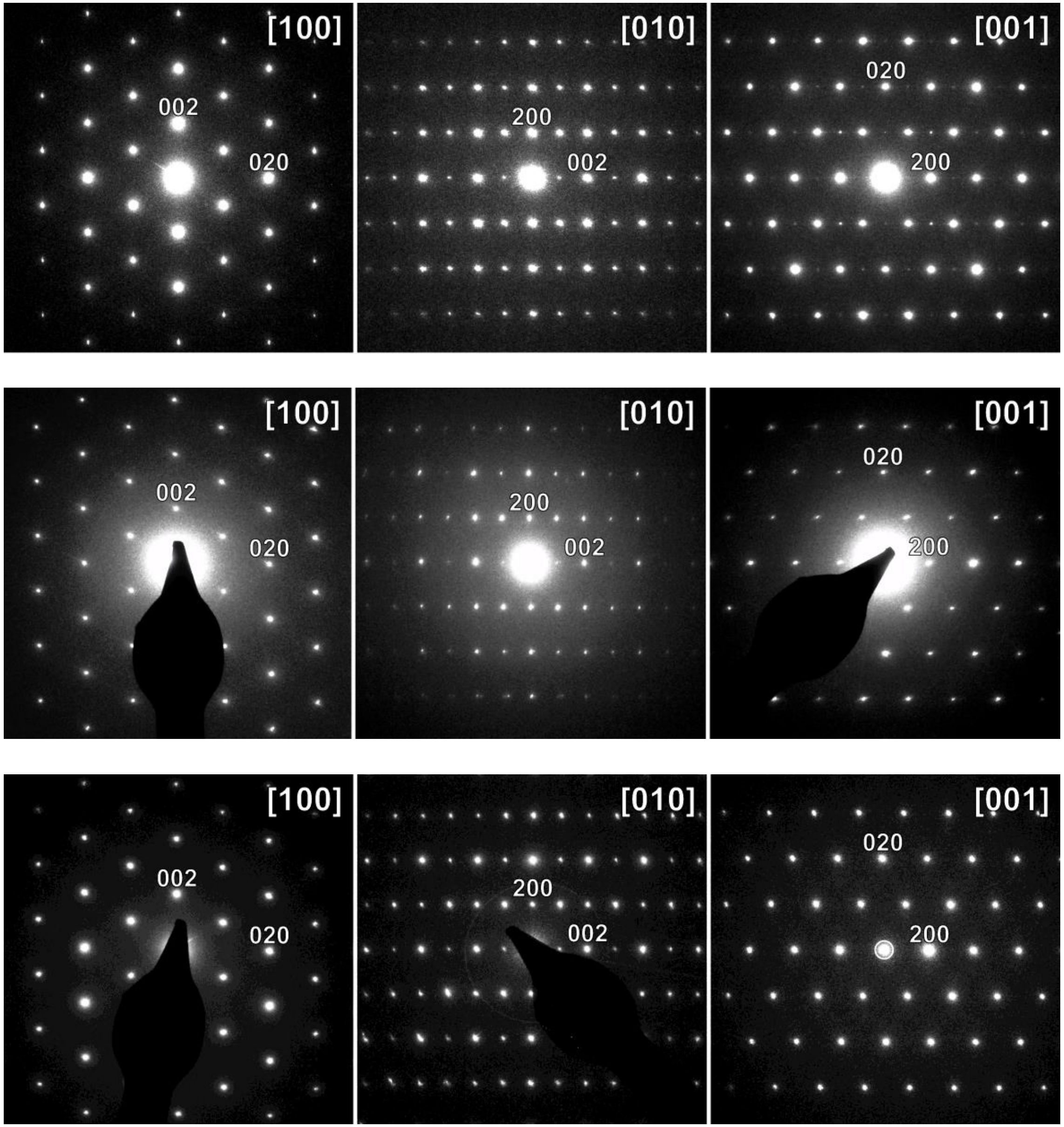

Pristine: KVO_4F

$0kl$: $k + h = 2n$
$h0l$: $h = 2n$
$hk0$: –

S.G. Pnam/Pna2_1

Charged: $K_{0.17}VO_4F$

$0kl$: $k + h = 2n$
$h0l$: $h = 2n$
$hk0$: $h + k = 2n$

S.G. Pnan

Discharged: $Li_{0.7}K_{0.12}VO_4F$

$0kl$: $k + h = 2n$
$h0l$: $h = 2n$
$hk0$: $h + k = 2n$

S.G. Pnan

Fedotov S. S. *et al*, *Chem. Mater.* **2016**, *28*, 411–415

ED tomography (EDT) for structure solution

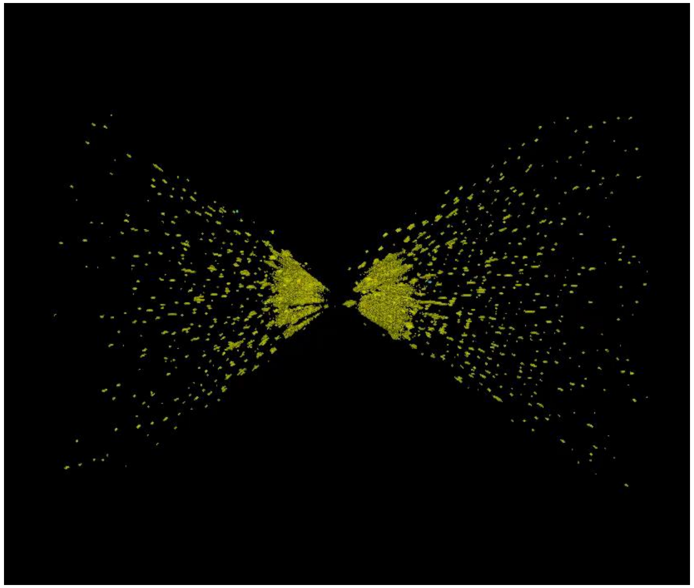

EDT workflow:

1. Data collection
    - ED pattern every 1°
    - avoiding main zone axes
2. 3D reciprocal space reconstruction
    –> quasi-kinematical intensities
3. Structure solution

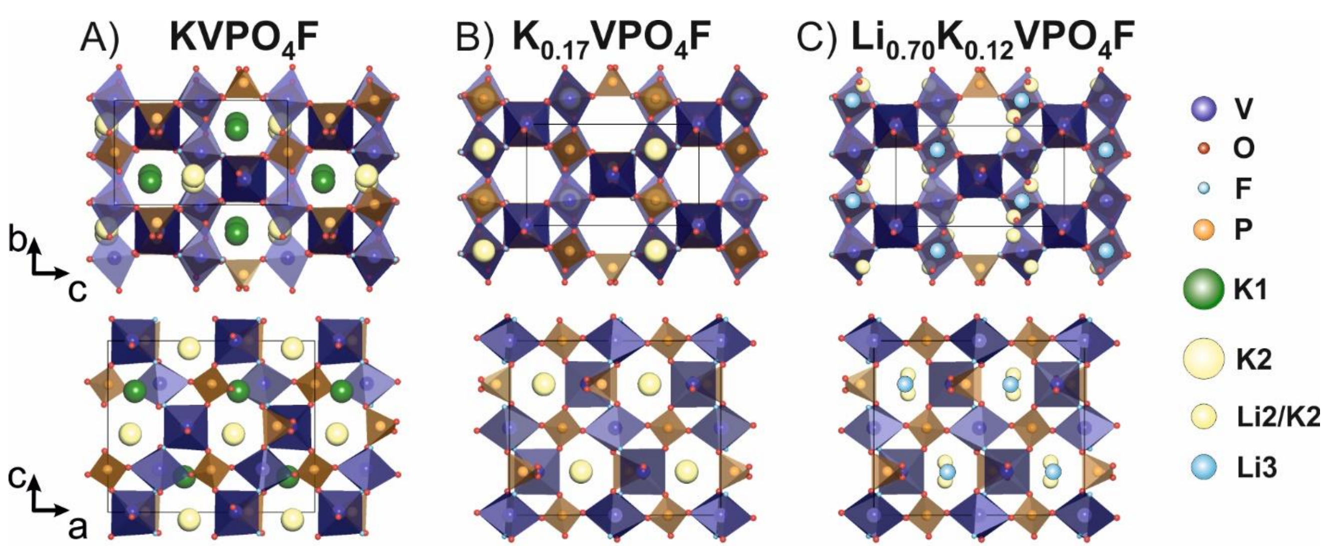

Fedotov S. S. *et al*, *Chem. Mater.* **2016**, *28*, 411–415

courtesy O. Karakulina, EMAT

High Resolution TEM (HRTEM)

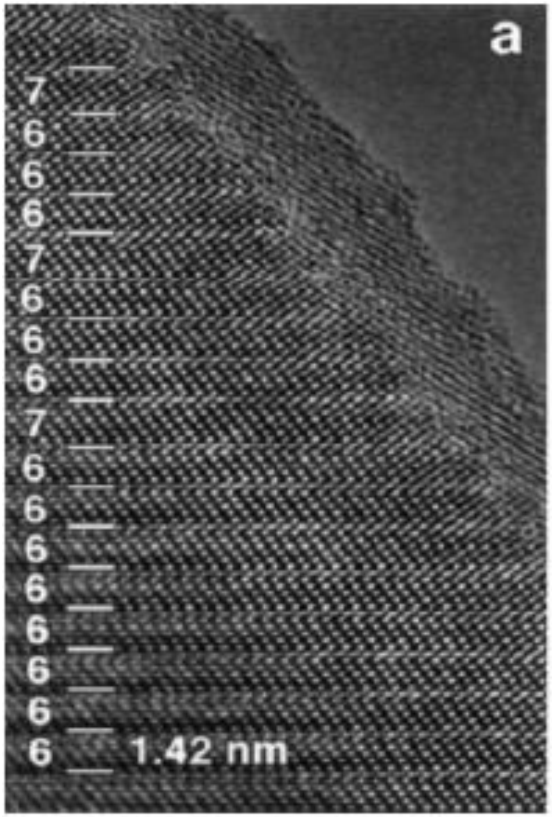

experimental image

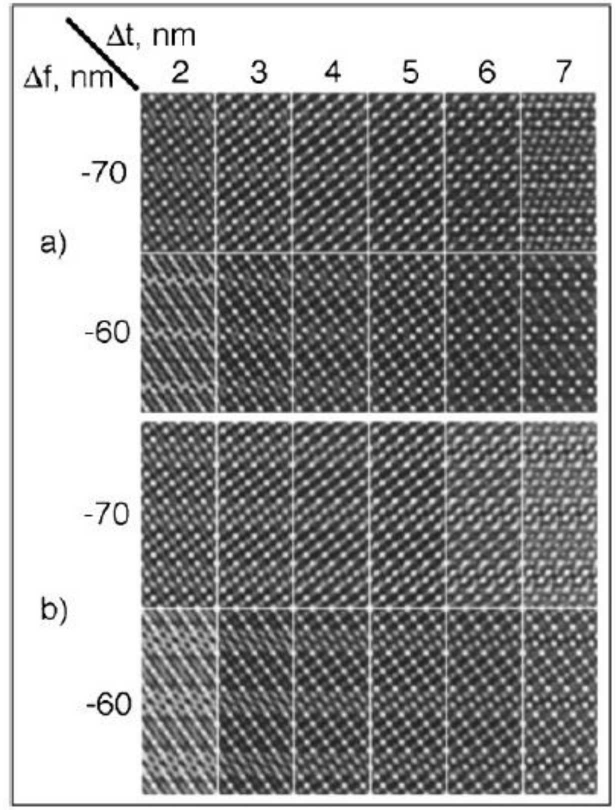

simulation

- high dose rate -> bad for beam sensitive materials
- extremely sensitive to misorientaions
- contrast depends on the thickness and defocus

High Resolution TEM (HRTEM)

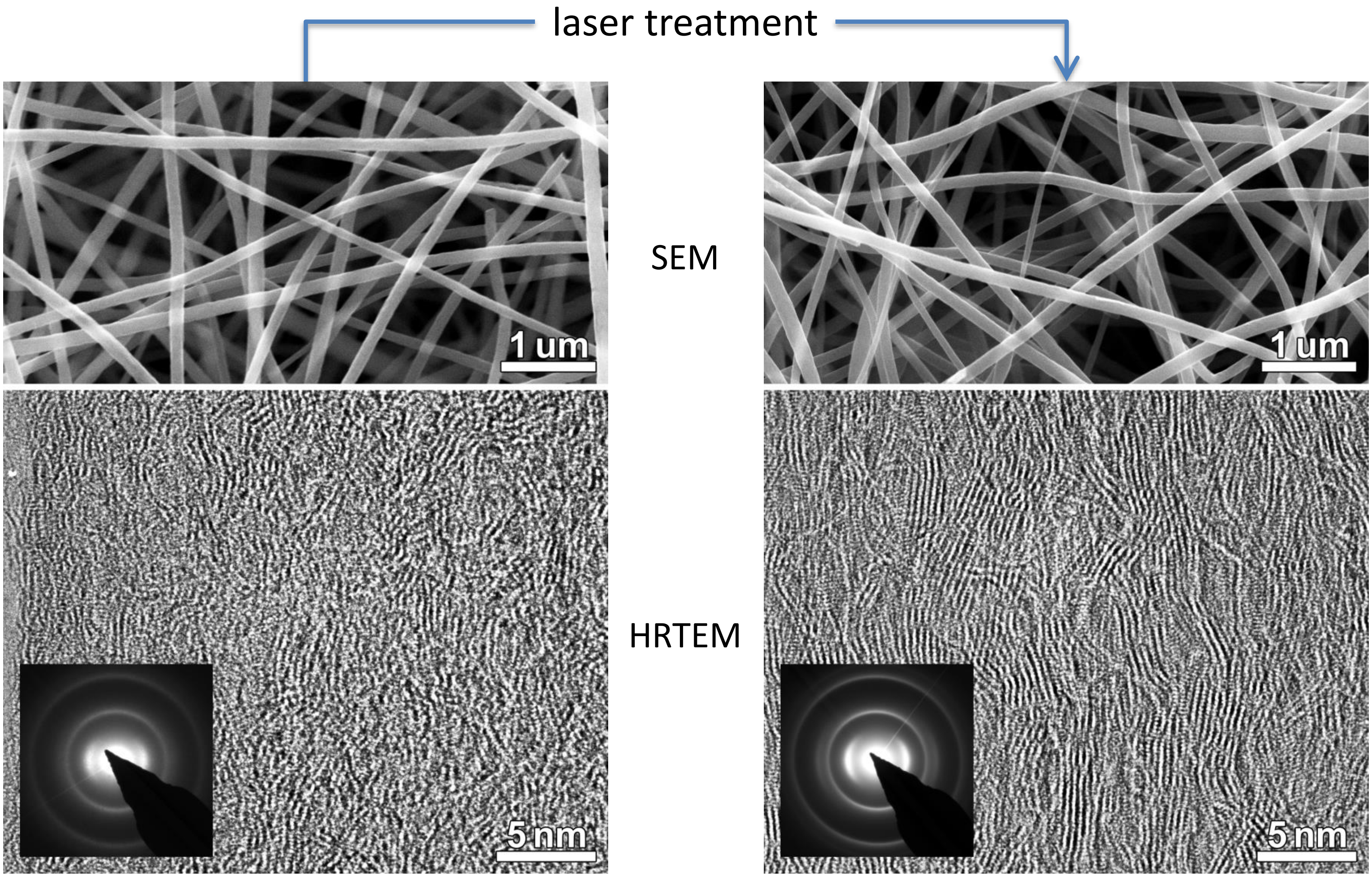

Zhang B. *et al*, *Adv. Mater. Technol.* **2016**, 1600227

Focused beam illumination, HAADF-STEM

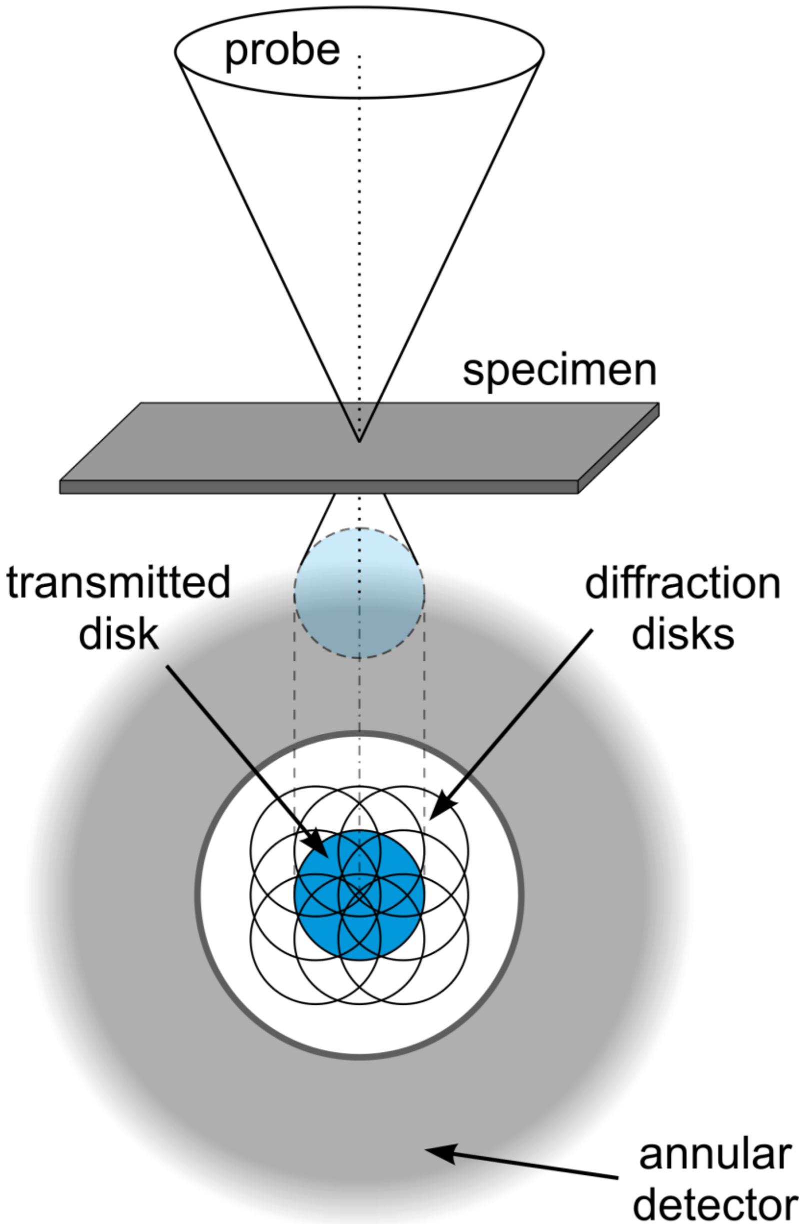

- Focused probe ~1Å
- Detector in the diffraction plane
- Image: Intensity vs. position of the probe
- Annular-shape detector

High Angle Annular Dark Field Scanning Transmission Electron Microscopy (HAADF-STEM)

$I \sim Z^{1.6-1.9}$ (Z - average at. number)

Li_xRhO_2

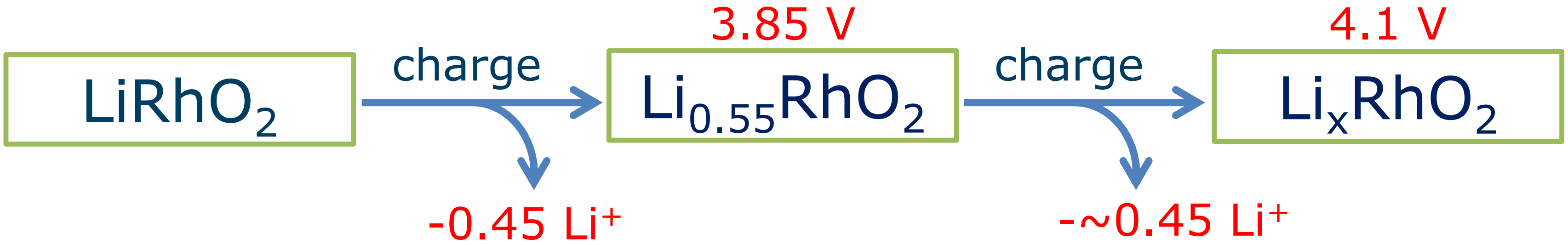

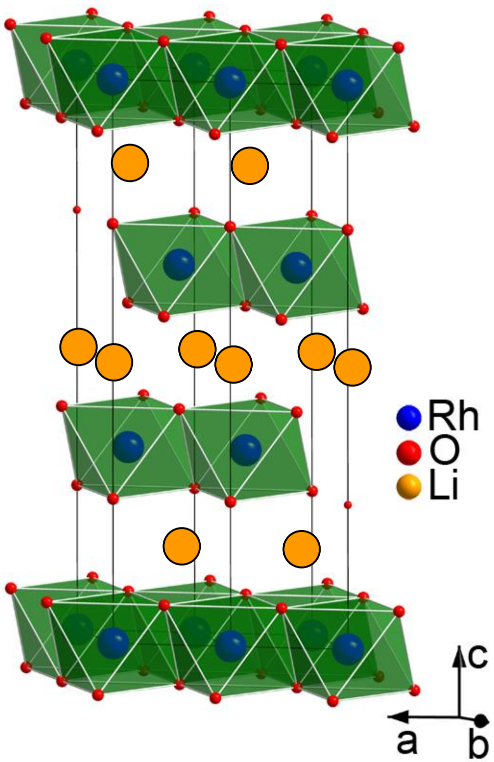

In-situ synchrotron powder diffraction in electrochemical test cells

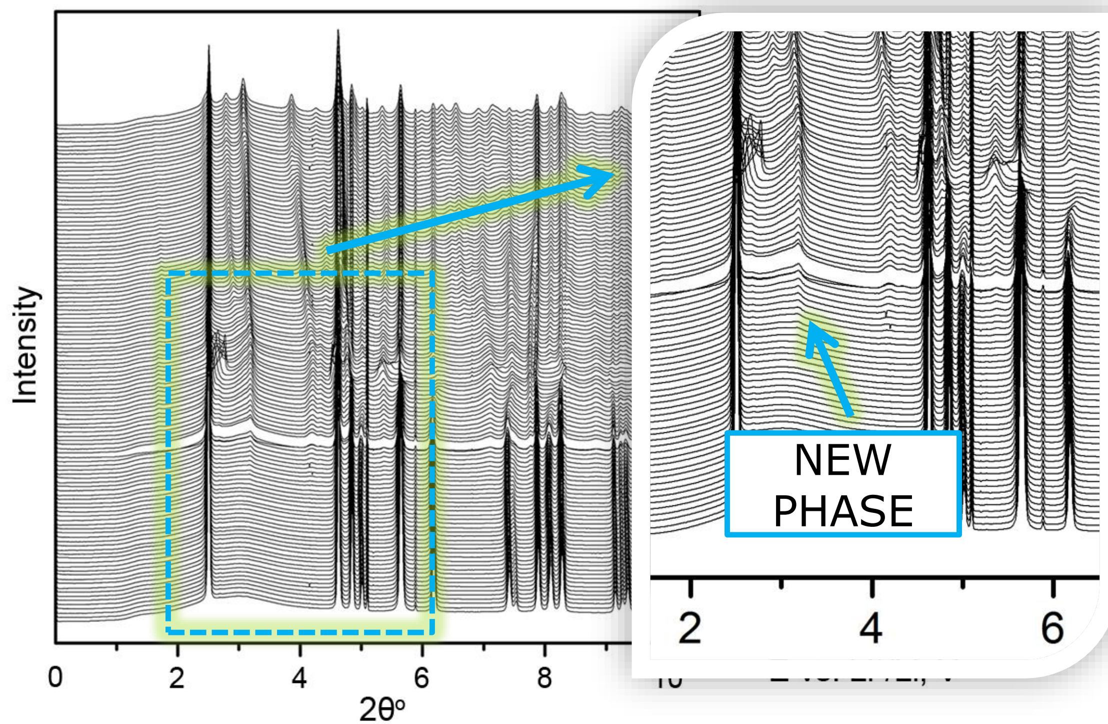

Mikhailova D. *et al*, *Inorg. Chem.* **2016**, *55*, 7079–7089

Li_xRhO_2

Structure solution:

1. SAED -> symmetry
2. EDT -> Rh and O positions
3. Monte Carlo simulations to optimize Li

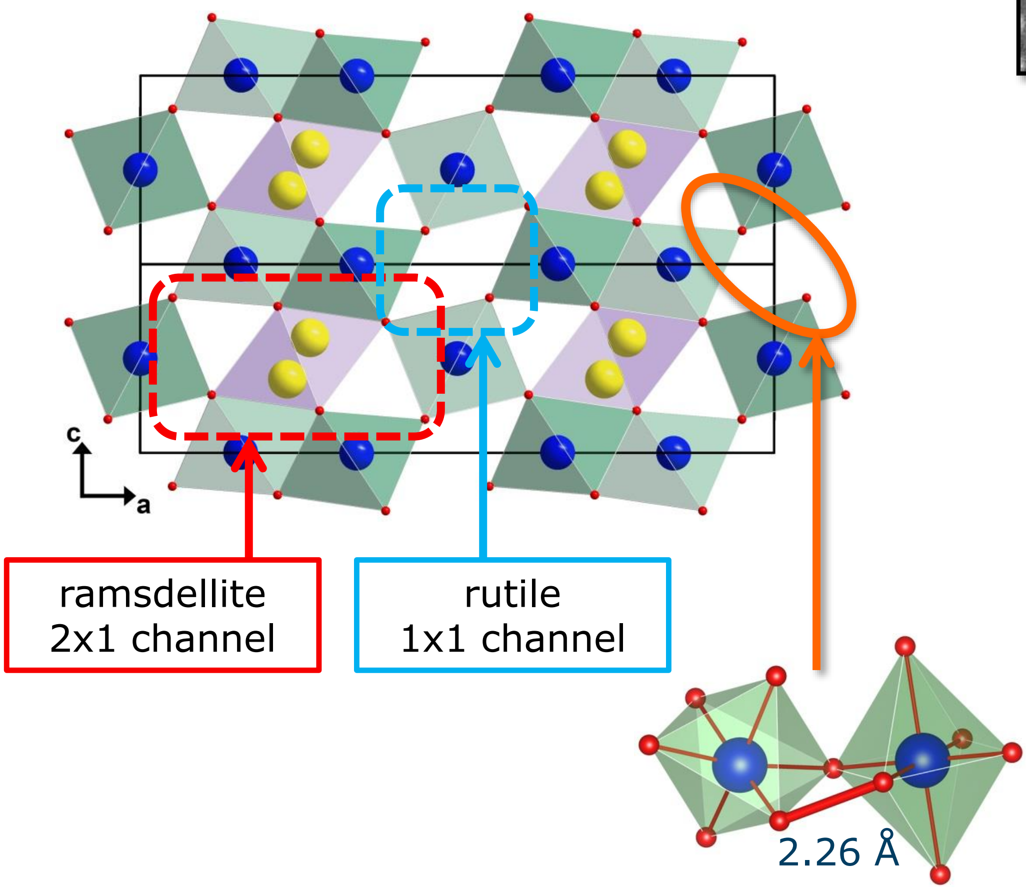

Structure confirmation: HAADF-STEM

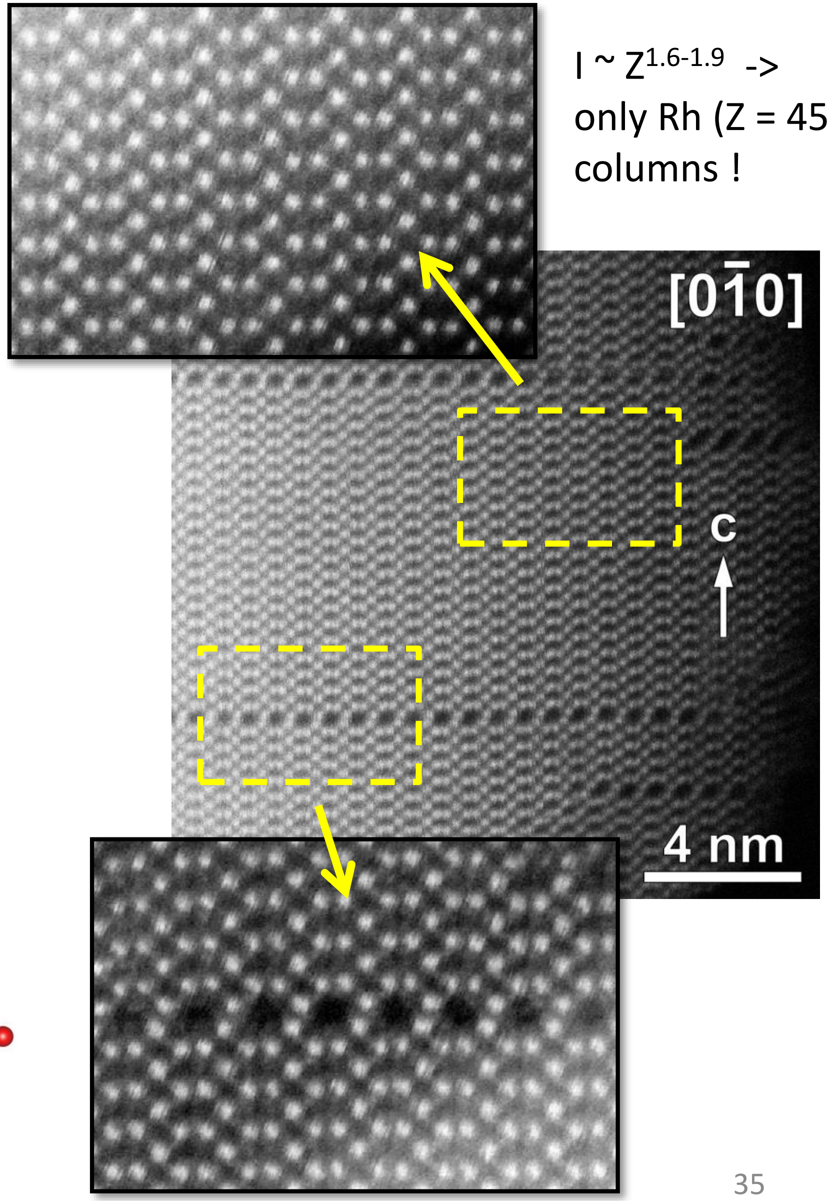

I ~ $Z^{1.6\text{-}1.9}$ -> only Rh (Z = 45) columns !

Mikhailova D. *et al*, *Inorg. Chem.* **2016**, *55*, 7079–7089

Li_xRhO_2 transformation mechanism

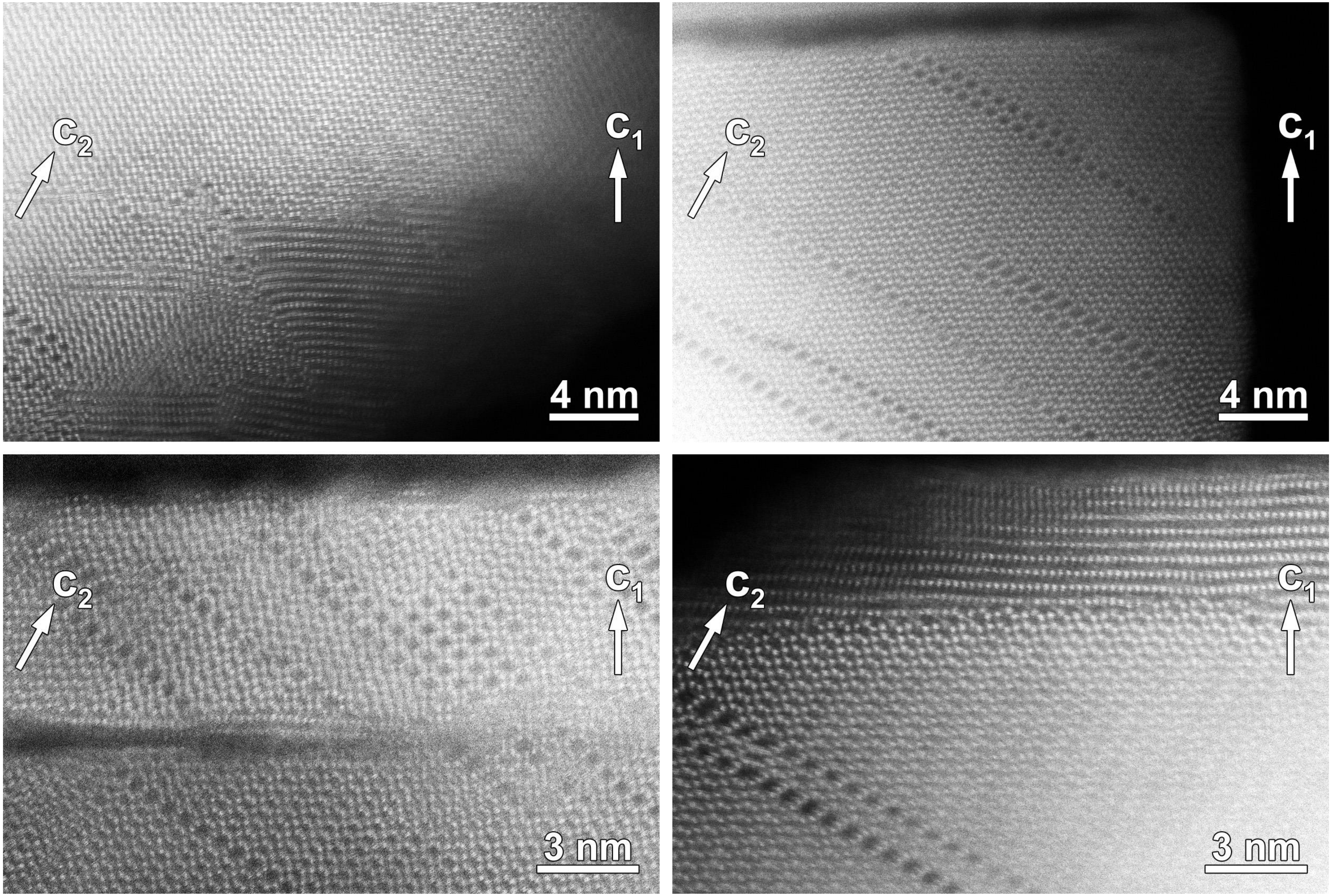

Mikhailova D. *et al*, *Inorg. Chem.* **2016**, *55*, 7079–7089

Li_xRhO_2 transformation mechanism

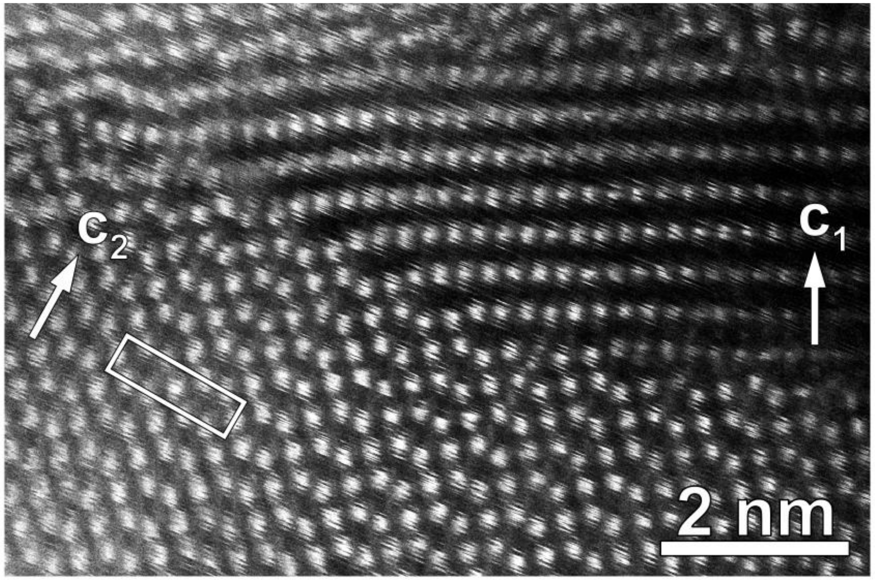

Partial O oxidation triggers corrugation of the RuO_2 layers

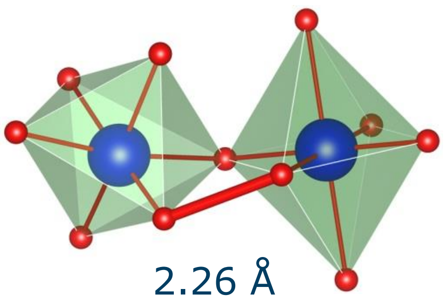

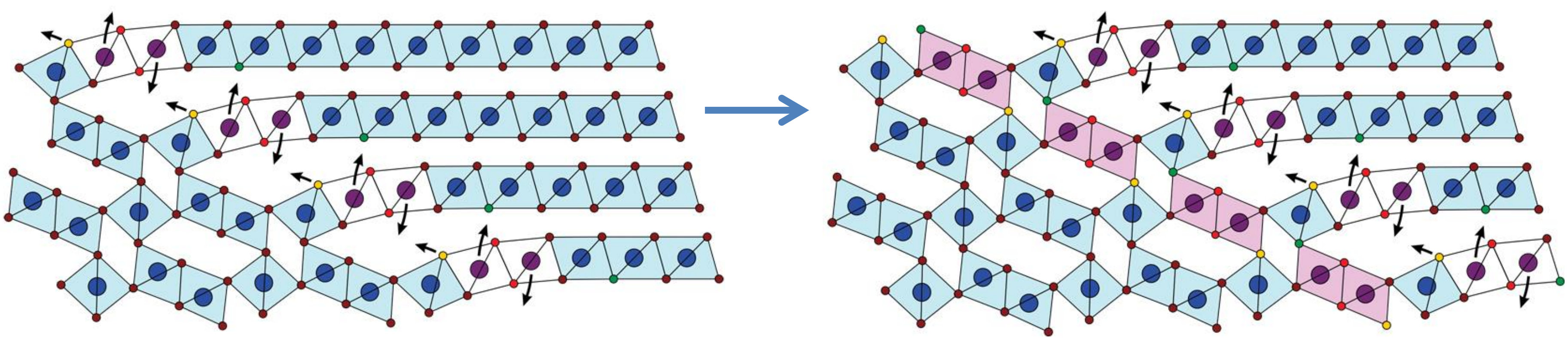

Mikhailova D. *et al*, *Inorg. Chem.* **2016**, *55*, 7079–7089

Li_xRhO_2 transformation mechanism

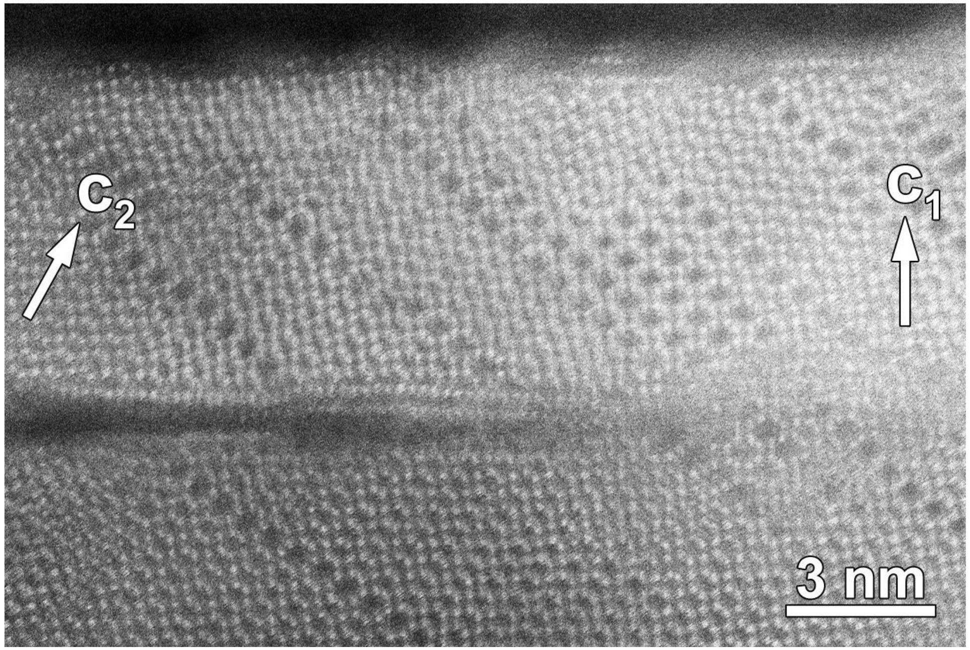

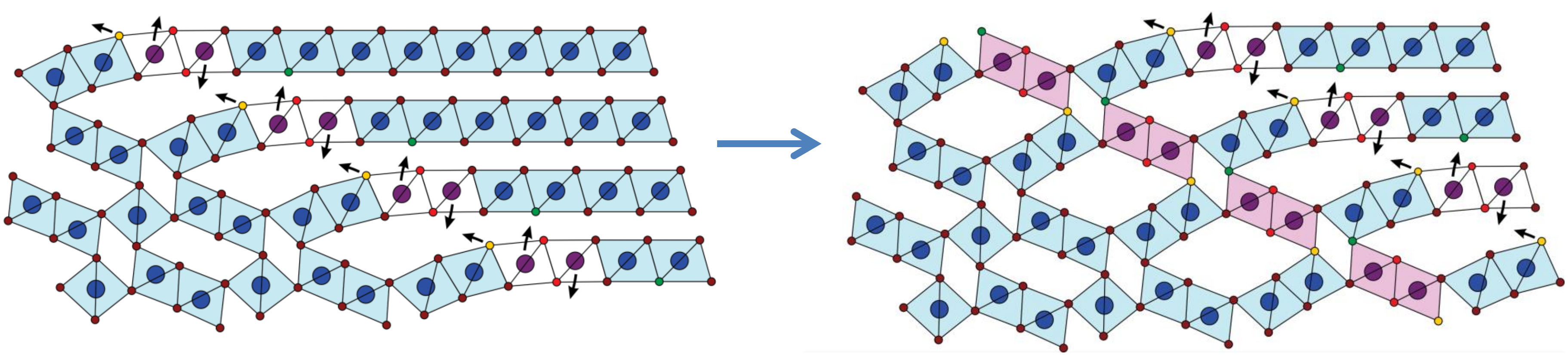

Mikhailova D. *et al*, *Inorg. Chem.* **2016**, *55*, 7079–7089

Li_xRhO_2 lithiation of the 3D structure

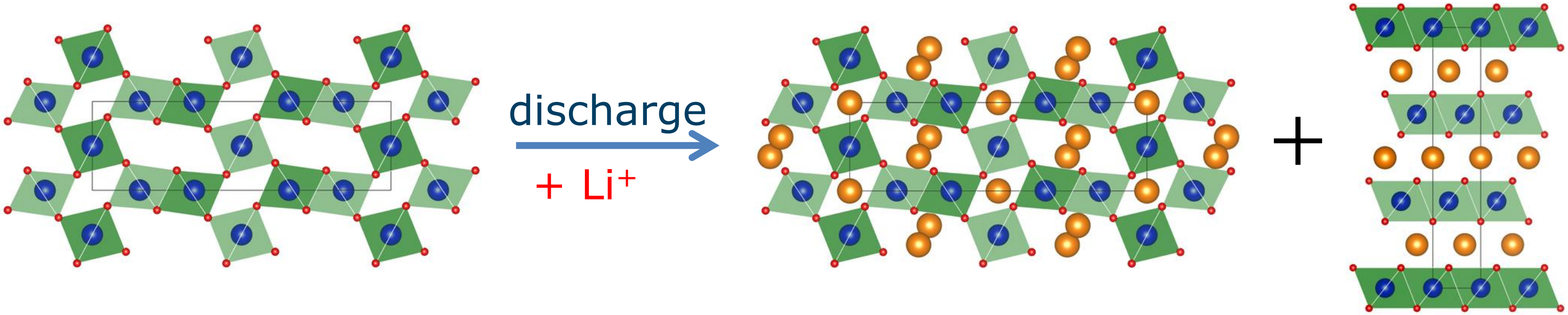

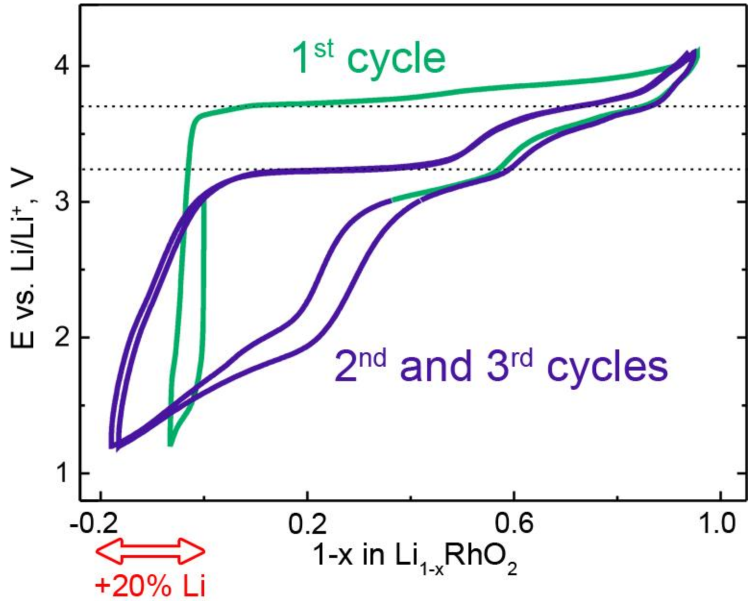

1. Partially reversible transformation 3D→ 2D

2. 3D structure hosts extra 20% Li in rutile channels

Mikhailova D. *et al*, *Inorg. Chem.* **2016**, *55*, 7079–7089

$Li_3Ru_{1-y}Nb_yO_4$: Li-rich structures

Rock-salt structures, but the topology of (Ru,Nb) distribution is different

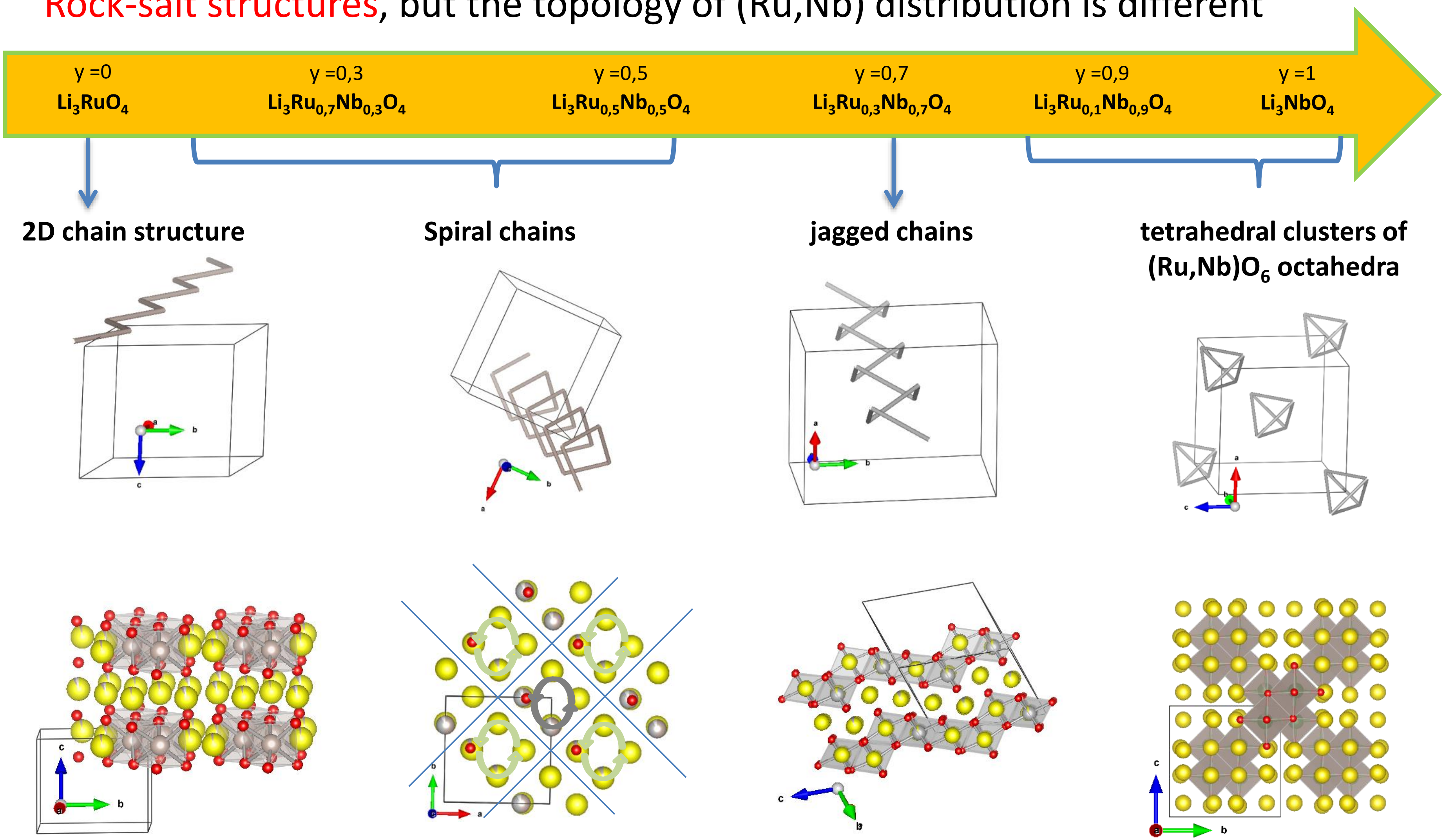

Isostructural with Ag_3RuO_4

Isostructural with Li_3TaO_4

Jacquet Q. *et al*, *Chem. Mater.* **2017**, *29*, 5331–5343

Li_3RuO_4

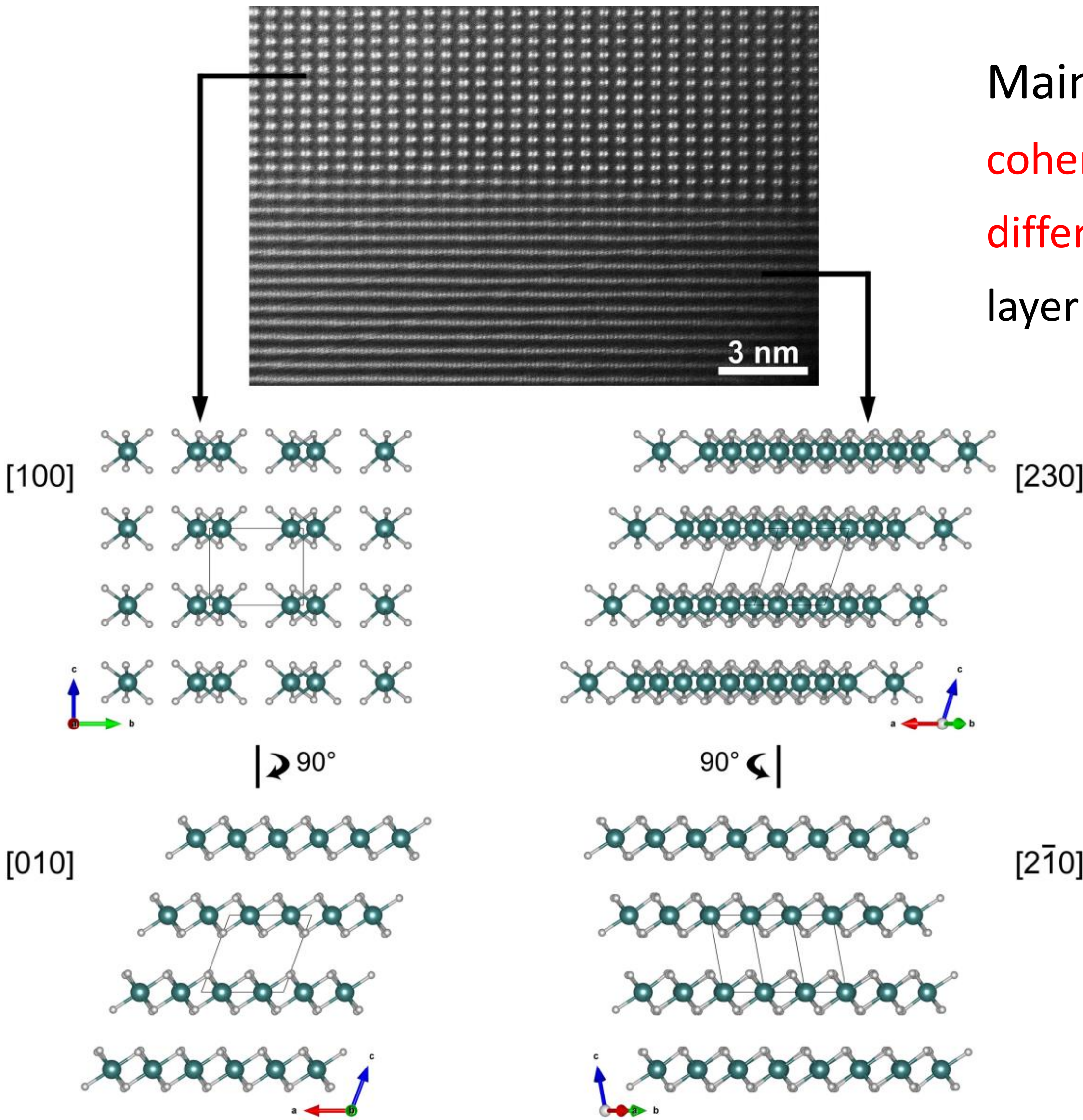

Main type of defects:

coherent intergrowths of domains with different orientation of the Li and (LiRu) layer stacking

O sublattice uninterrupted

No local antisite disorder !

Fairly large coherent domains

smooth structure refinement with XRD + NPD

Jacquet Q. *et al*, *Chem. Mater.* **2017**, *29*, 5331–5343

$Li_3Ru_{0.5}Nb_{0.5}O_4$

Spiral $(Ru,Nb)O_6$ chains
each segment 2 octahedra

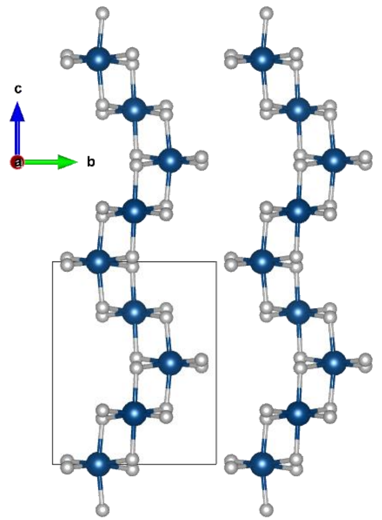

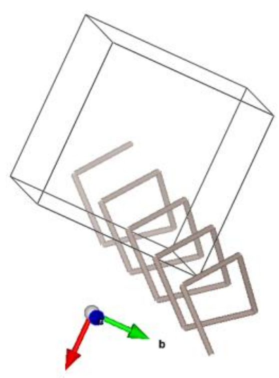

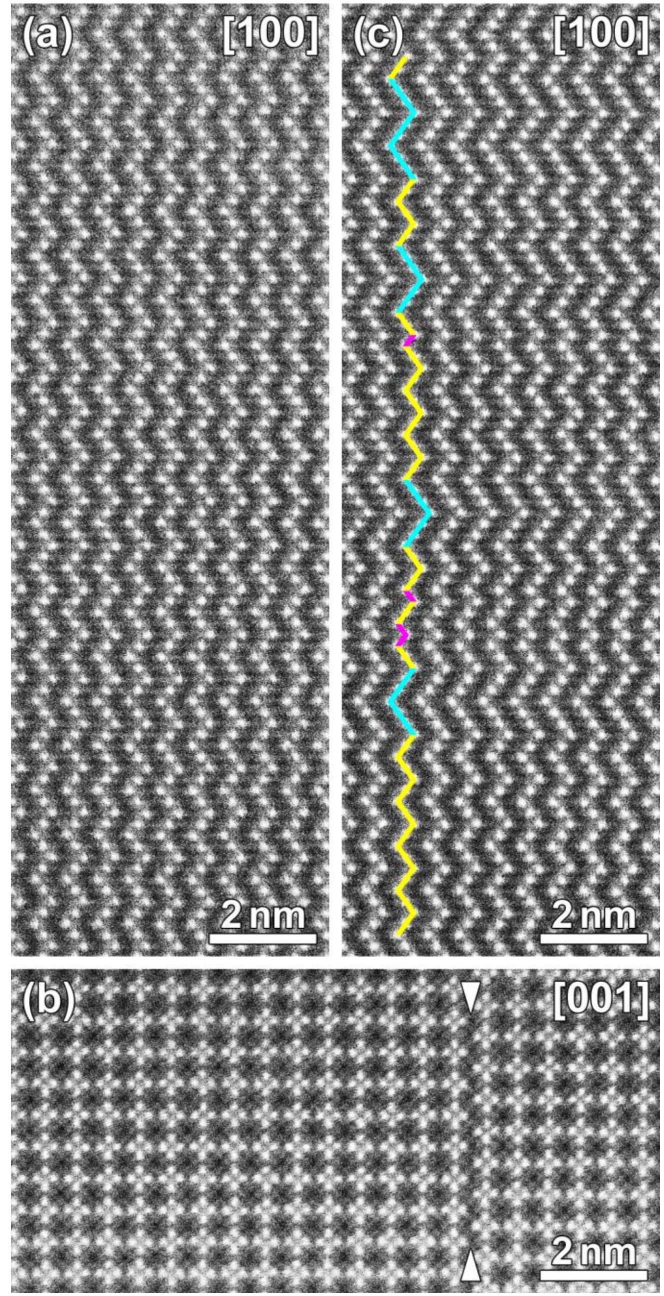

Defects:

1. (100) APBs that shift the spirals over *a*/2
2. cooperative variations in the Li/(Ru,Nb) ordering pattern

↓

XRD + NPD refinement: partial Li/(Ru,Nb) mixing

Jacquet Q. *et al*, *Chem. Mater.* **2017**, *29*, 5331–5343

$Li_3Ru_{0.3}Nb_{0.7}O_4$

Jagged $(Ru,Nb)O_6$ chains each segment 2 octahedra

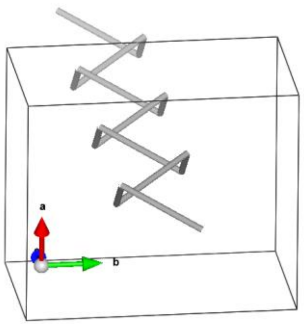

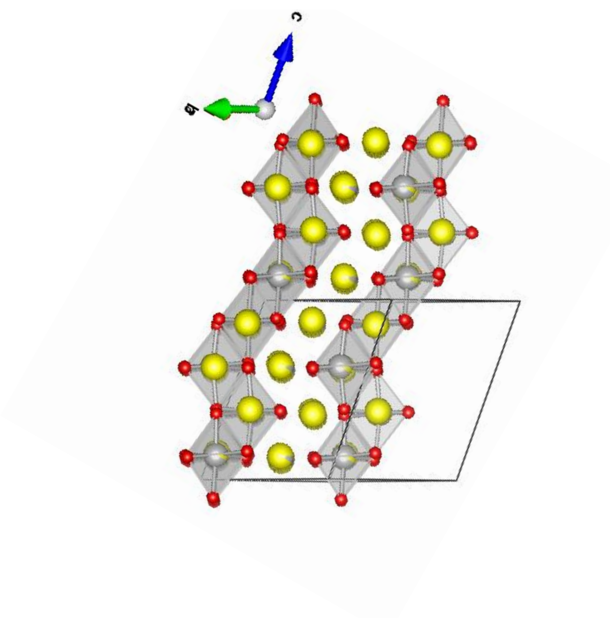

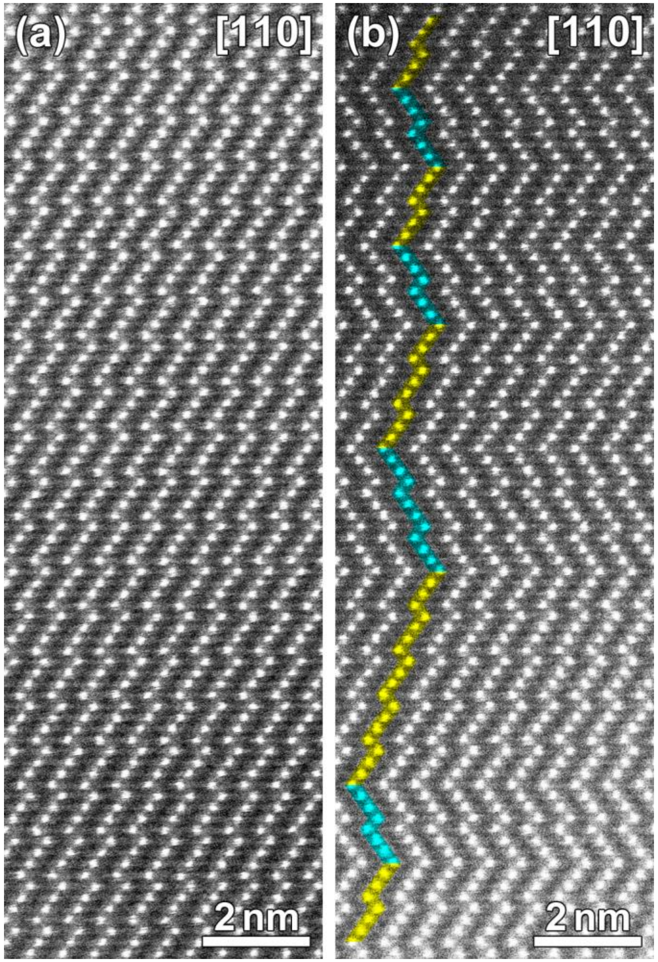

Defects:

cooperative variations in the Li/(Ru,Nb) ordering pattern

↓

XRD + NPD refinement: partial Li/(Ru,Nb) mixing

Jacquet Q. *et al*, *Chem. Mater.* **2017**, *29*, 5331–5343

$Li_3Ru_{0.1}Nb_{0.9}O_4$

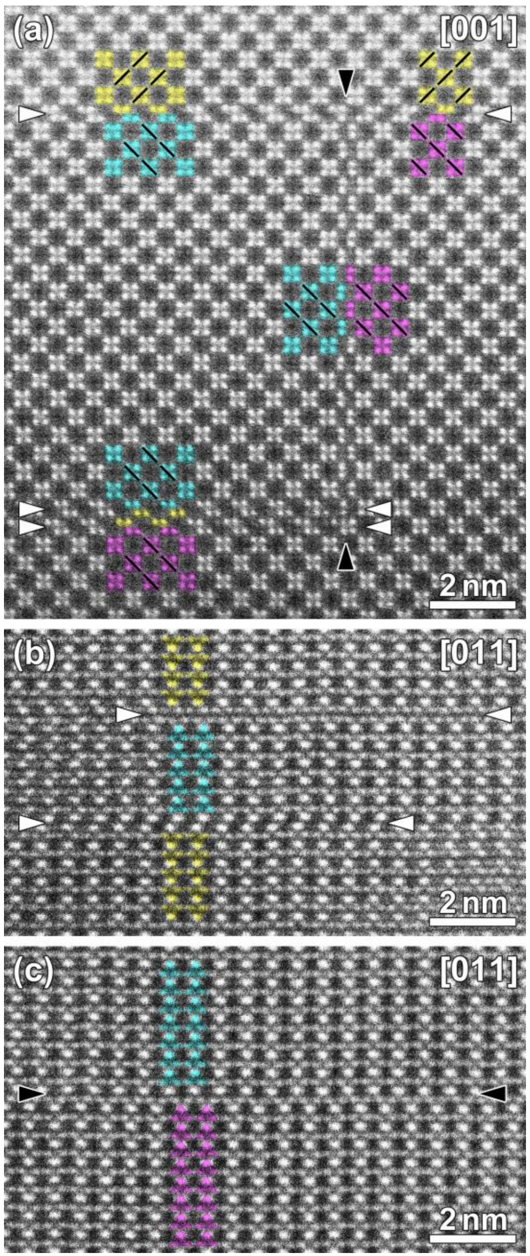

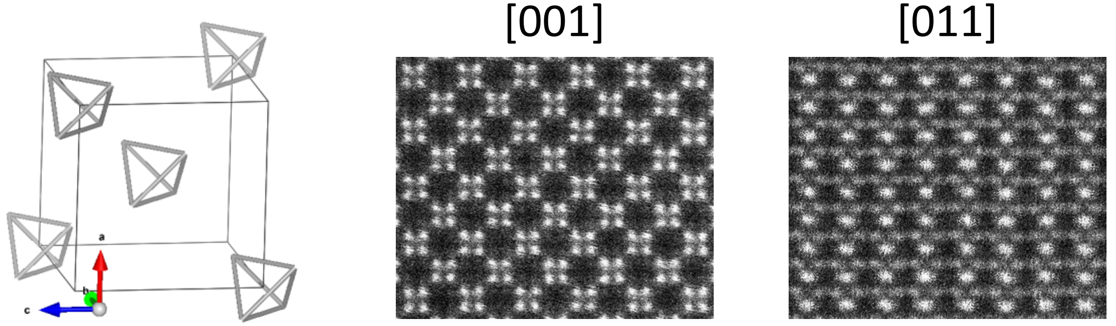

APB type 1 (▹ ◃): shift over *a*/4 + 90° rotation

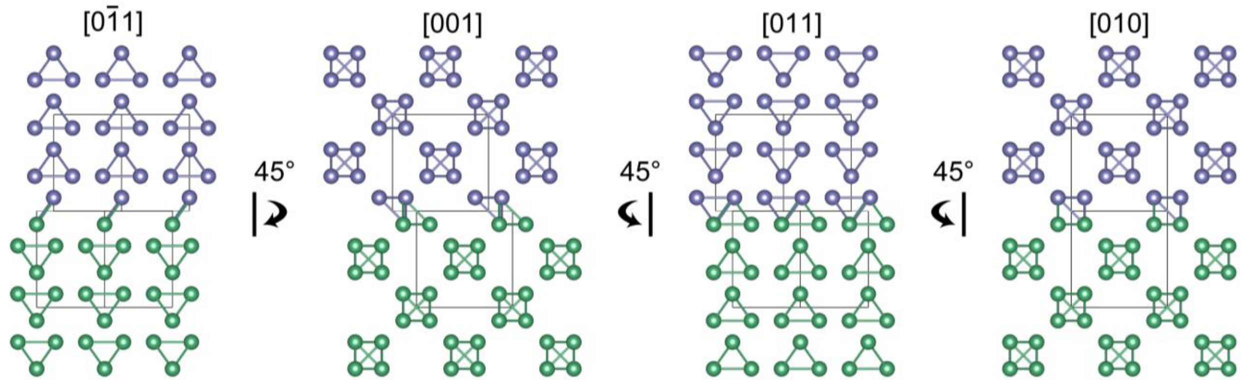

APB type 2 (▸ ◂): shift over *a*/2

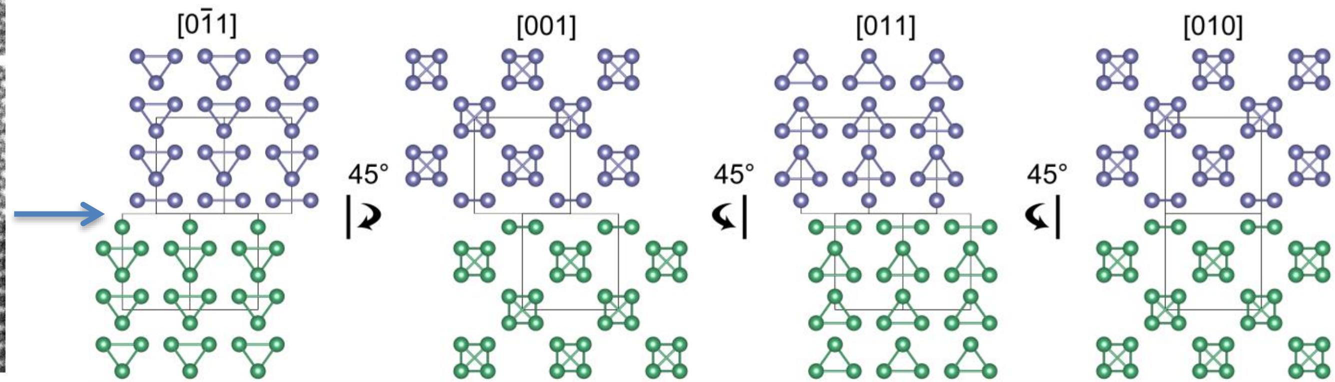

Jacquet Q. *et al*, *Chem. Mater.* **2017**, *29*, 5331–5343

$Li_3Ru_{0.1}Nb_{0.9}O_4$

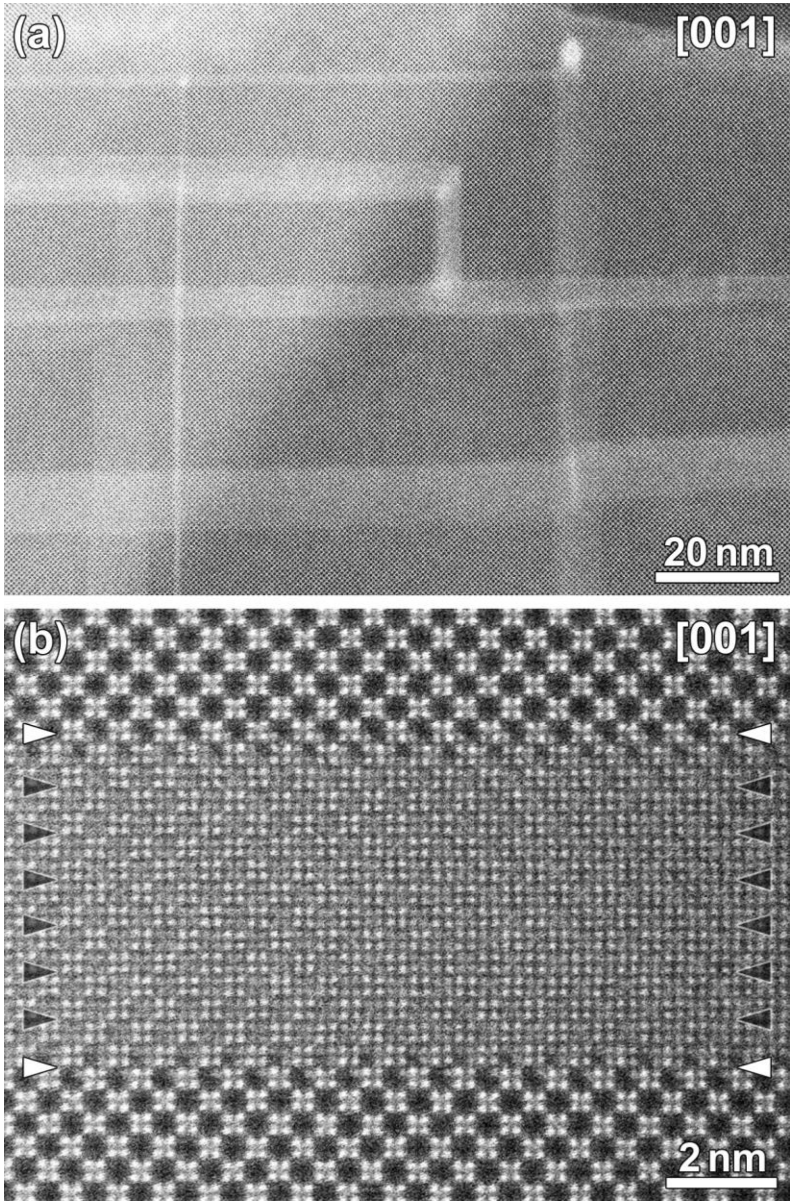

O sublattice uninterrupted

Small size of the coherent domains

anisotropic reflection broadening in the XRD + NPD refinement

Jacquet Q. *et al*, *Chem. Mater.* **2017**, *29*, 5331–5343

ABF-STEM vs. HAADF-STEM

signal is incoherent, dominated by Rutherford and thermal diffuse scattering

$I \sim Z^{1.6\text{-}1.9}$

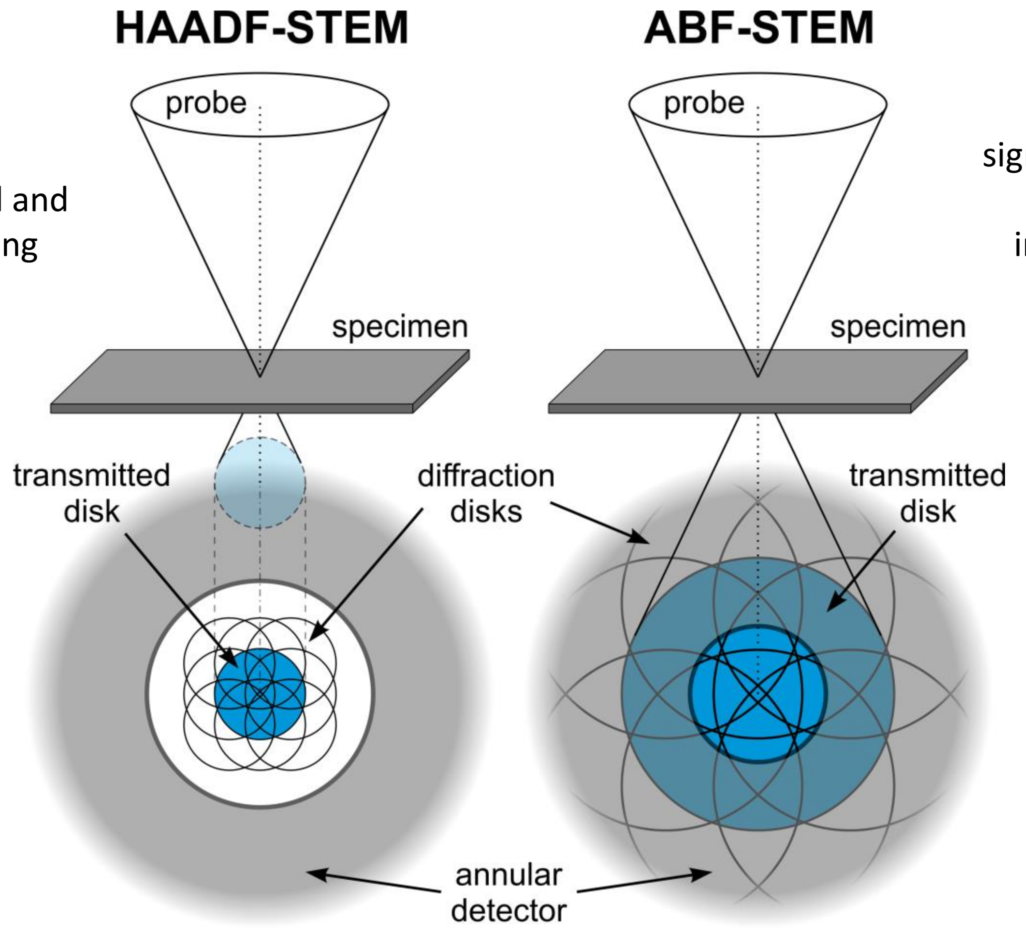

signal has contribution of both coherent and incoherent scattering

$I \sim Z^{1/3}$

✓ straightforward interpretation of STEM images
✓ contrast robust to thickness variations

✘ sensitive to the design of the microscope (i.e. type of gun, probe-corrector)

$Na_x(Ni_{0.2}Mn_{0.6}Co_{0.2})O_2$

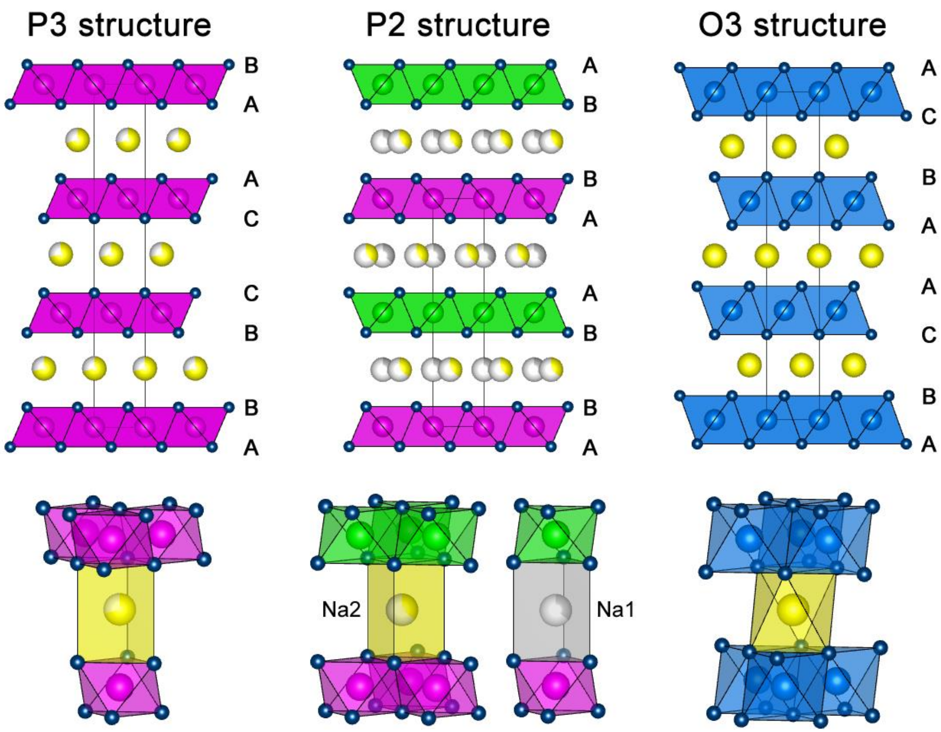

$x < 0.7$ $x \approx 0.7-1$ $x \approx 1$

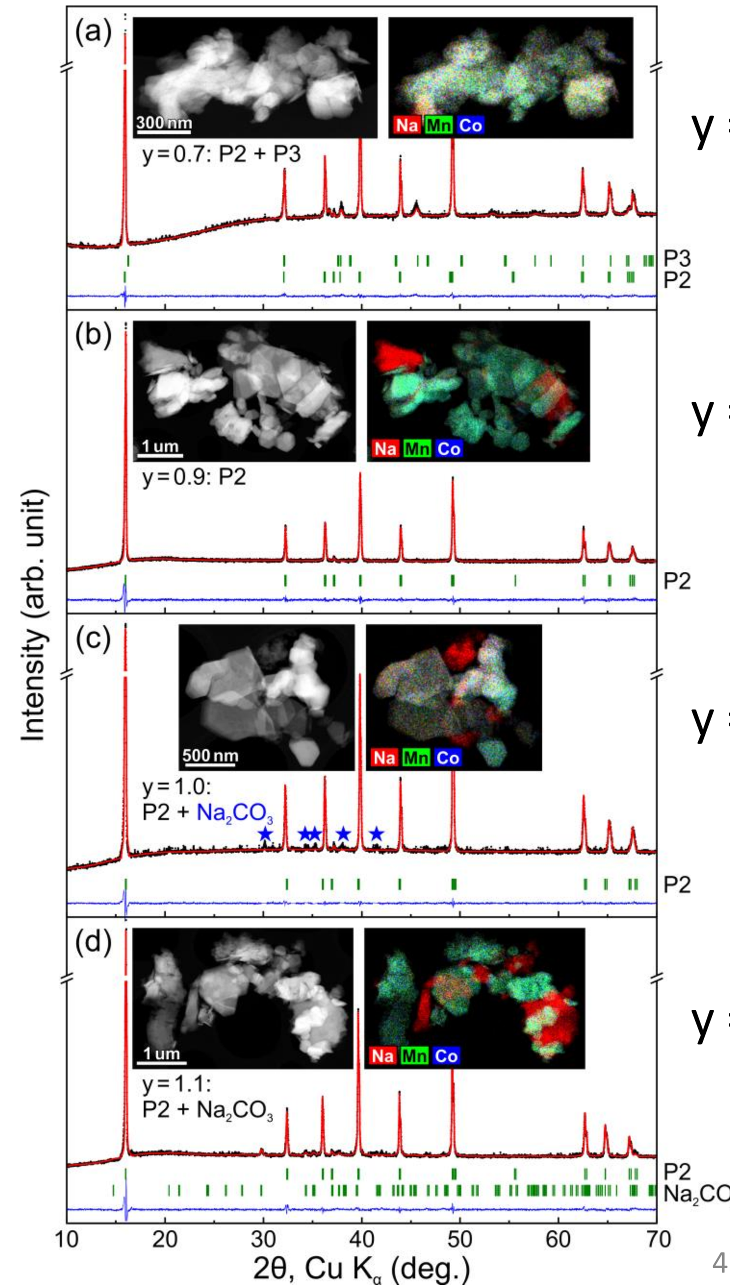

y = 0.7

y = 0.9

y = 1.0

y = 1.1

Stabilization of the P2 phase using Na_2CO_3 excess

y – total Na/M ratio

Sathiya M. *et al*, *Chem. Mater.* **2017**, *29*, 5948–5956

$Na_x(Ni_{0.2}Mn_{0.6}Co_{0.2})O_2$ stacking of metal layers

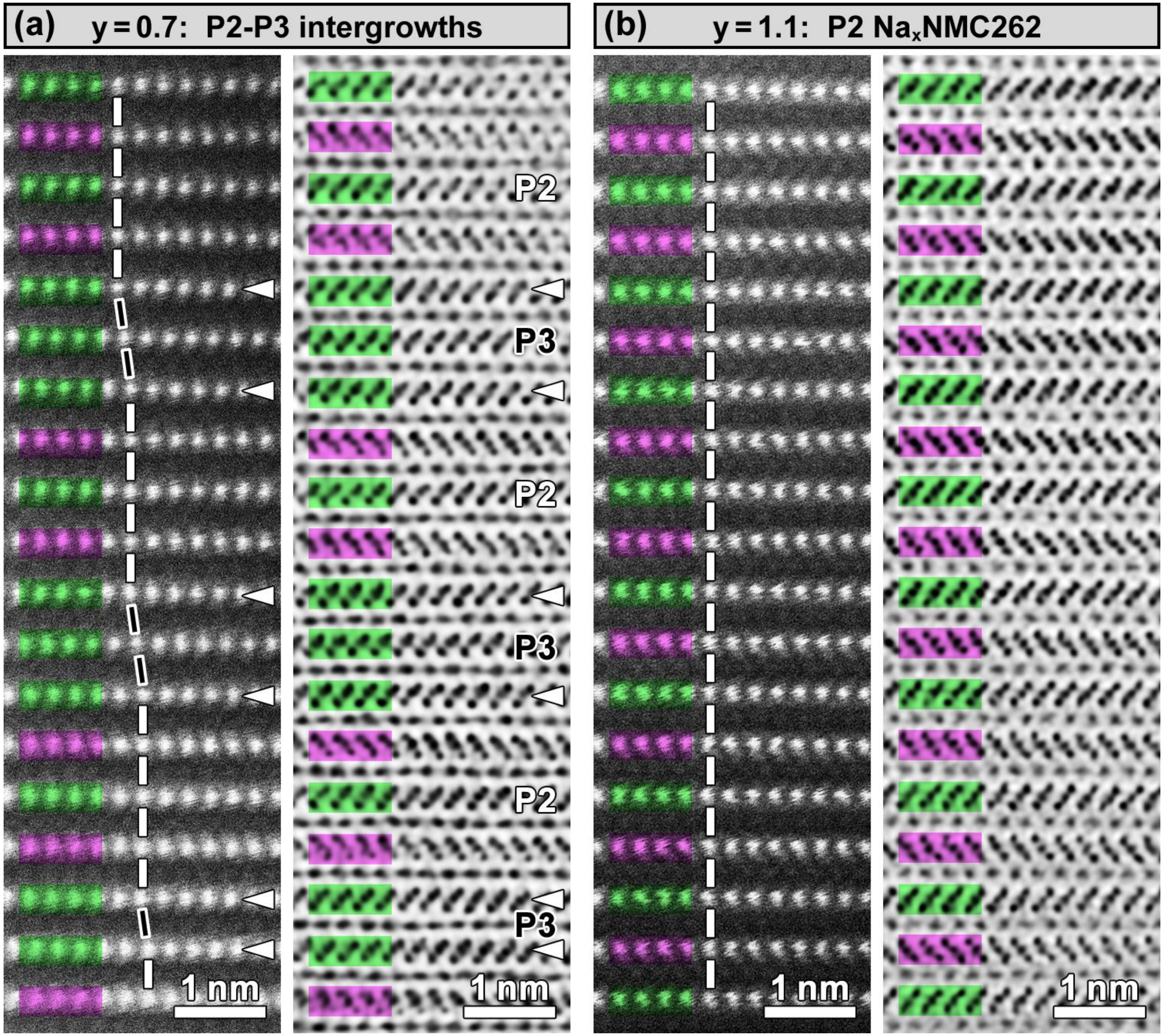

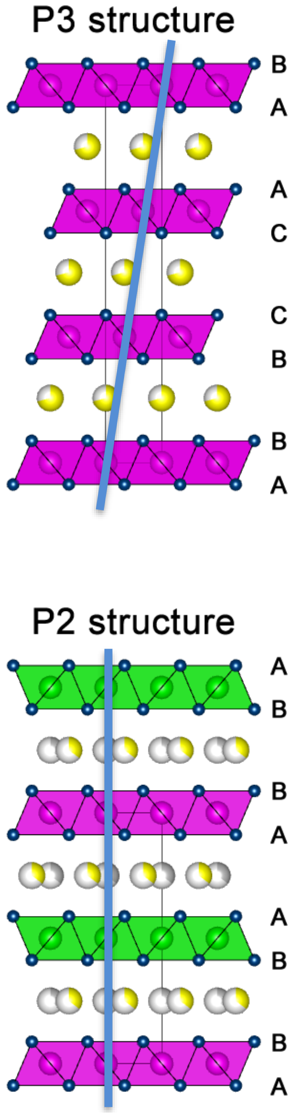

Sathiya M. *et al*, *Chem. Mater.* **2017**, *29*, 5948–5956

Na positions in P2 structure

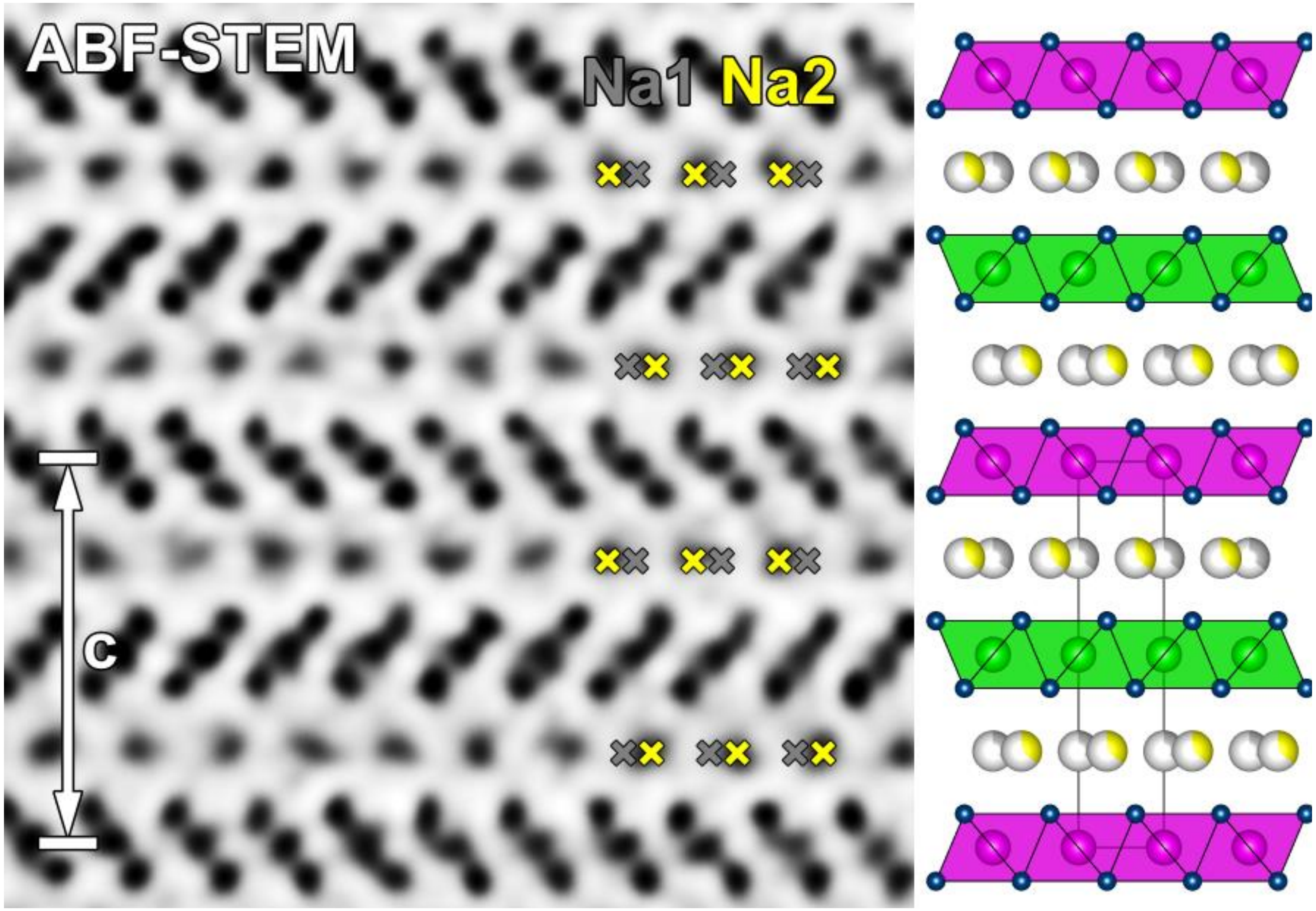

Na2 positions are preferentially occupied in the structure

Sathiya M. *et al*, *Chem. Mater.* **2017**, *29*, 5948–5956

Turbostratic defects in P2 structure, y = 0.7

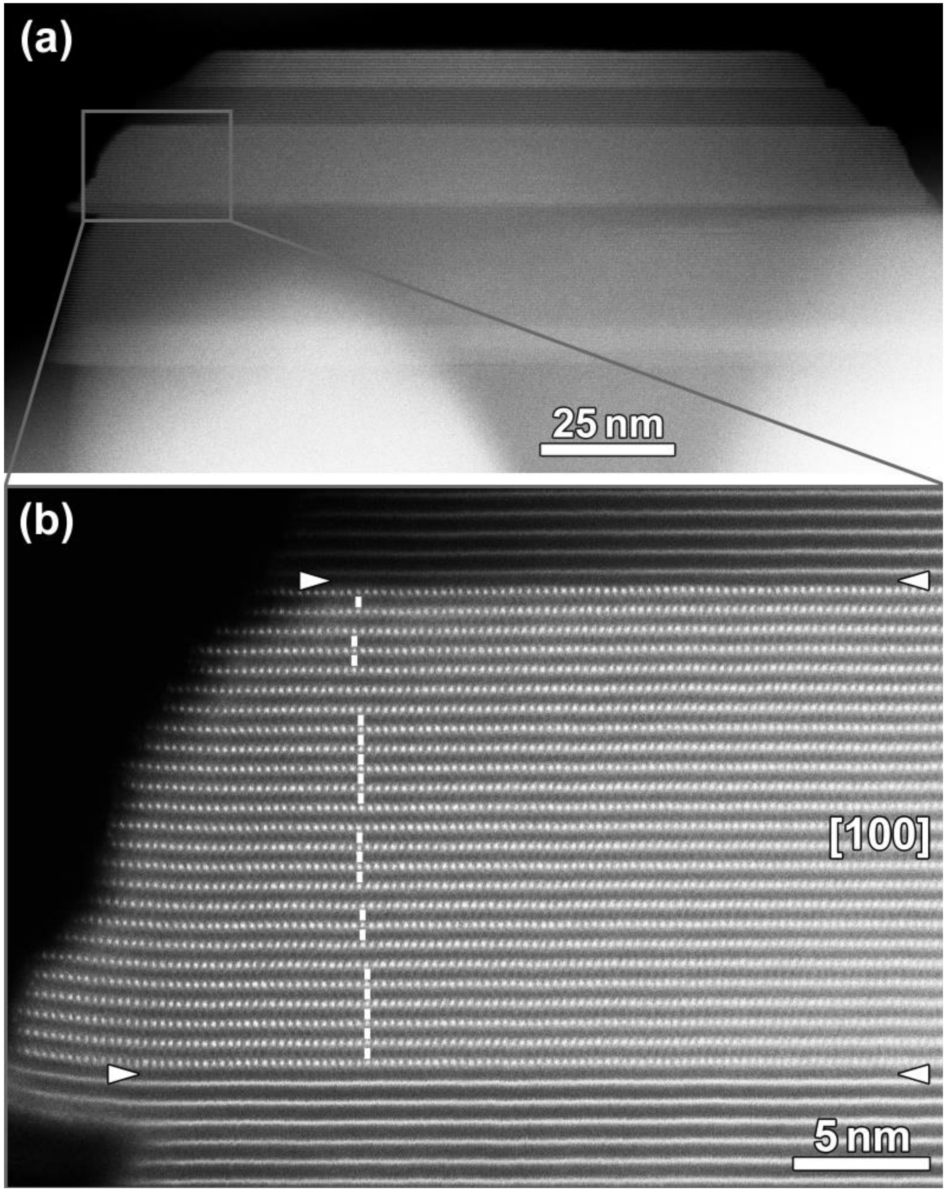

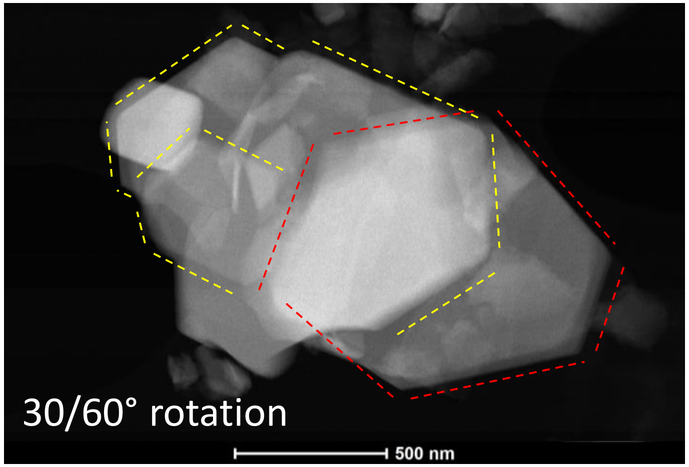

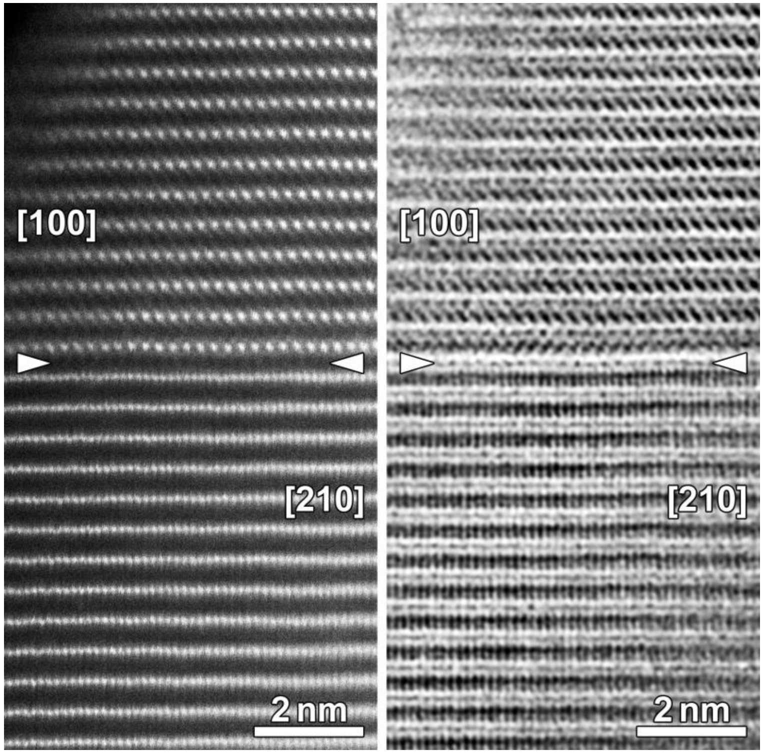

Sathiya M. *et al*, *Chem. Mater.* **2017**, *29*, 5948–5956

Na_2IrO_3 structure of the pristine material

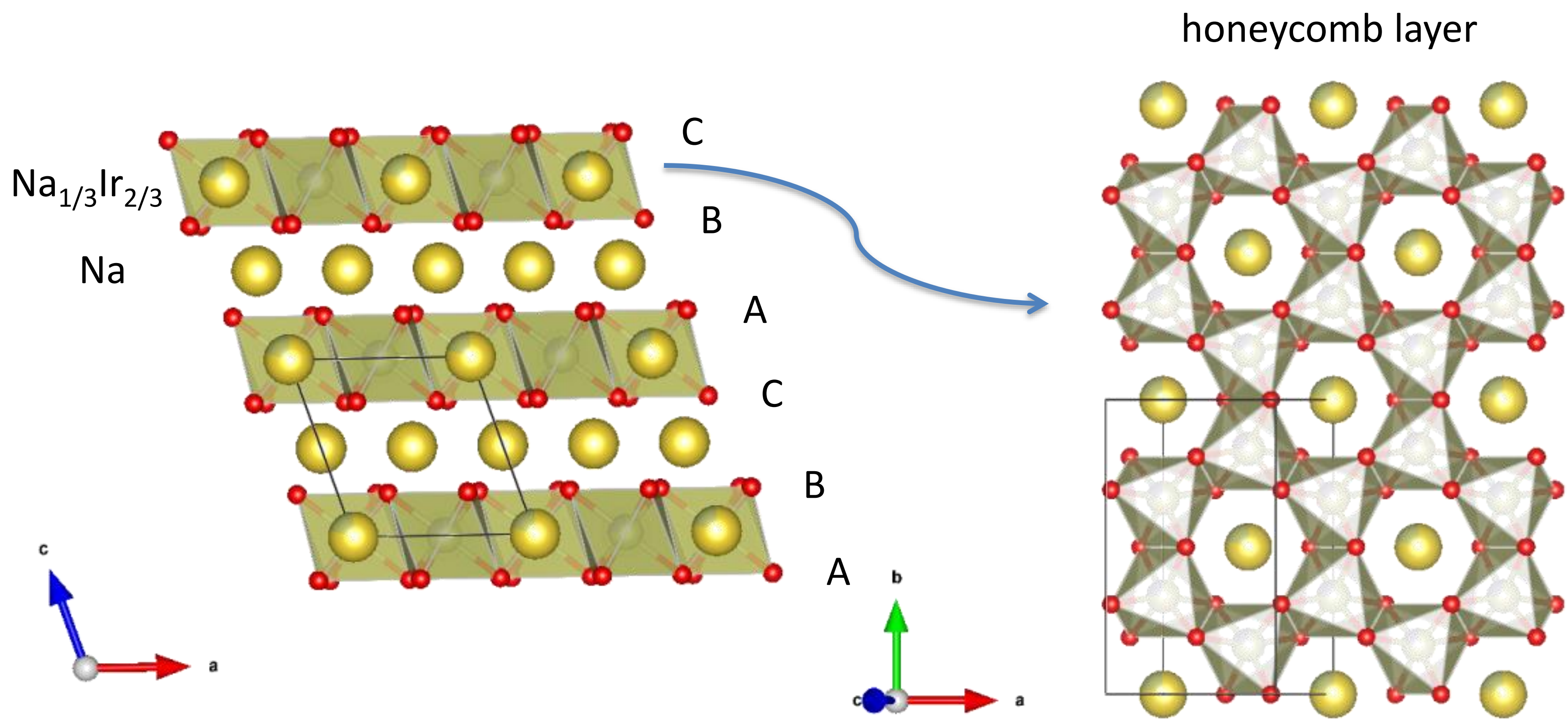

1. cubic close packing of O atoms
2. Every second octahedral layer is occupied by Ir, which alternate with Na layers
3. 1/3 of the Ir atoms is replaces with Na forming a honeycomb arrangement of Ir atoms

Perez A. J. *et al*, J.-M. M. *Chem. Mater.* **2016**, *28*, 8278–8288

$Na_{2-x}IrO_3$ pristine

Measured Na:Ir = 1.61(17) → normalised to Na:Ir = 2

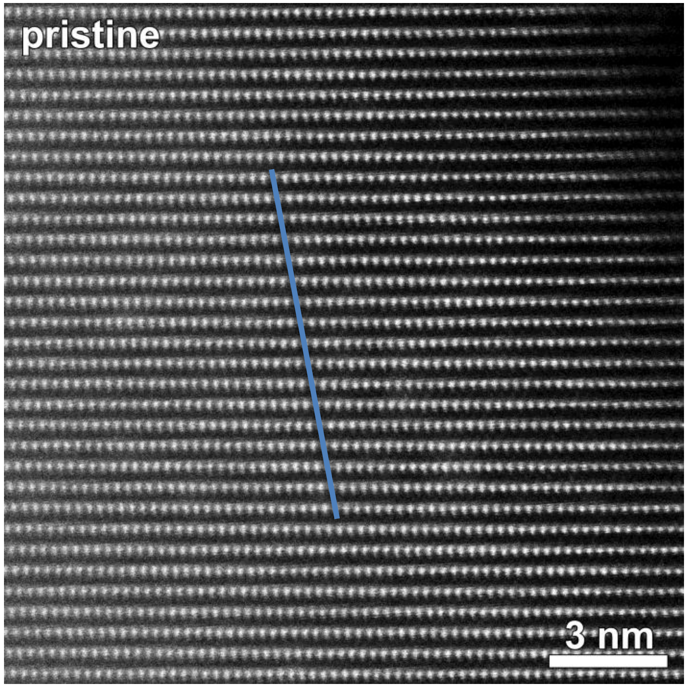

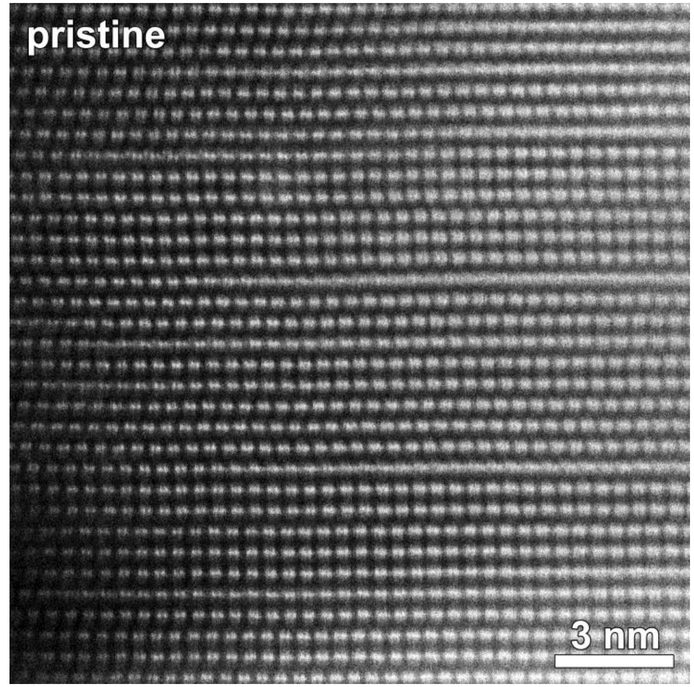

O3 structure:

1) *ccp* O packing

2) systematic shifts of the honeycomb layers

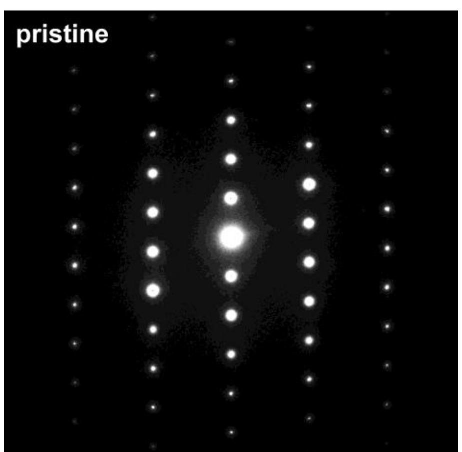

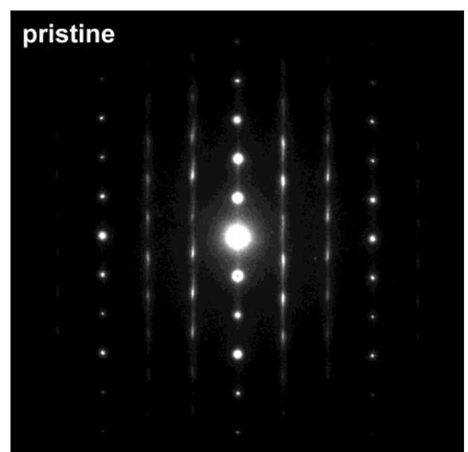

Perez A. J. *et al*, J.-M. M. *Chem. Mater.* **2016**, *28*, 8278–8288

Electrochemical oxidation

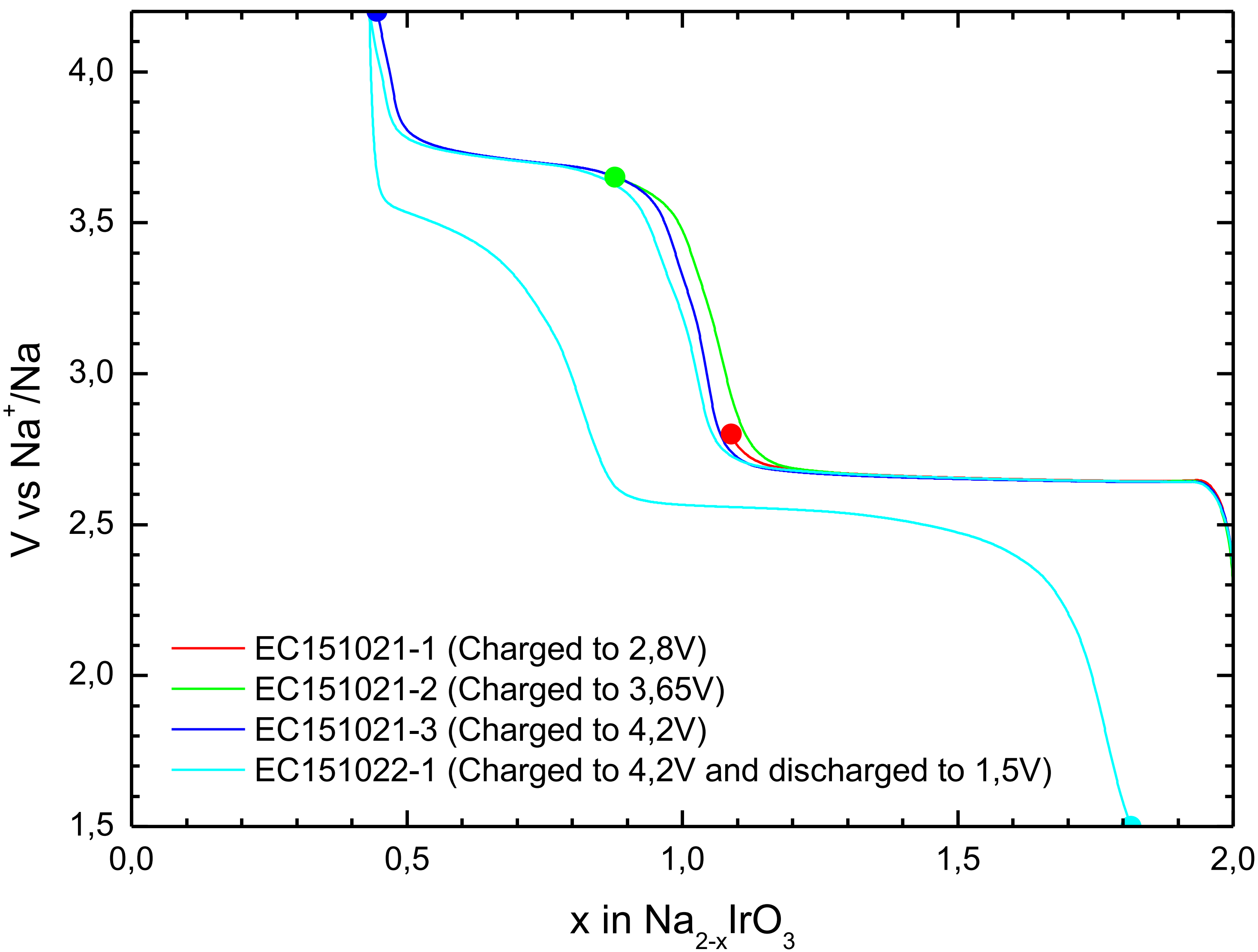

Perez A. J. *et al*, J.-M. M. *Chem. Mater.* **2016**, *28*, 8278–8288

$Na_{2-x}IrO_3$ charged to 3.65 V

Measured Na:Ir = 0.62(6) → normalised to Na:Ir = 0.77(11)

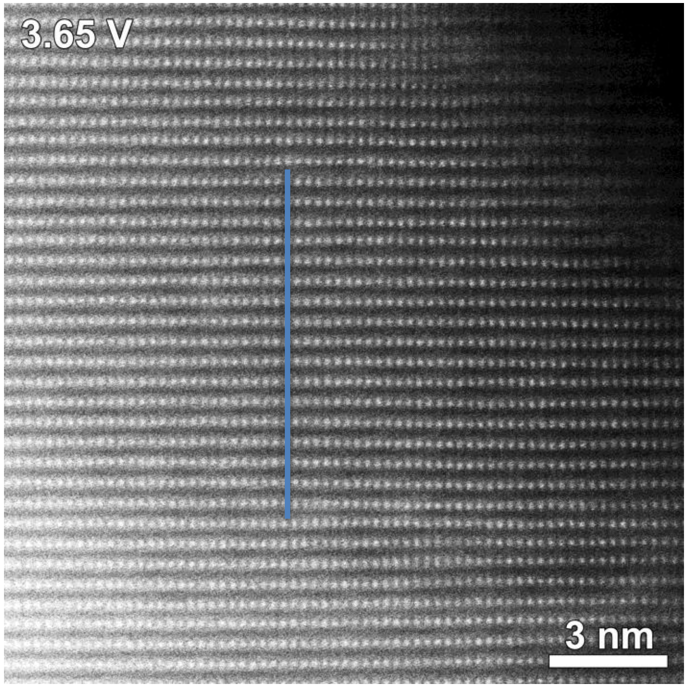

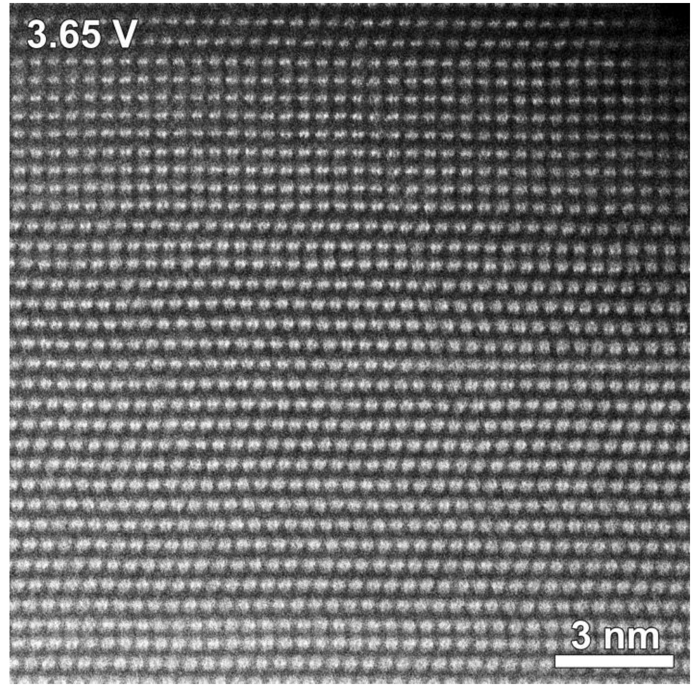

1) *hcp* O packing
2) systematic shifts of the honeycomb layers

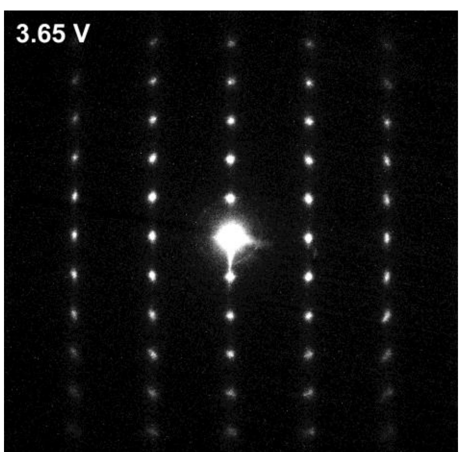

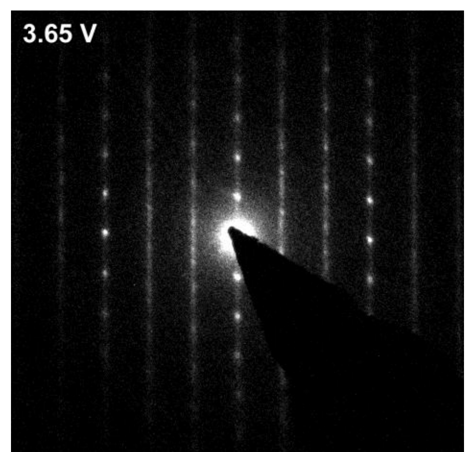

Perez A. J. *et al*, J.-M. M. *Chem. Mater.* **2016**, *28*, 8278–8288

$Na_{2-x}IrO_3$ charged to 4.2 V

Measured Na:Ir = 0.62(6) → normalised to Na:Ir = 0.77(11)

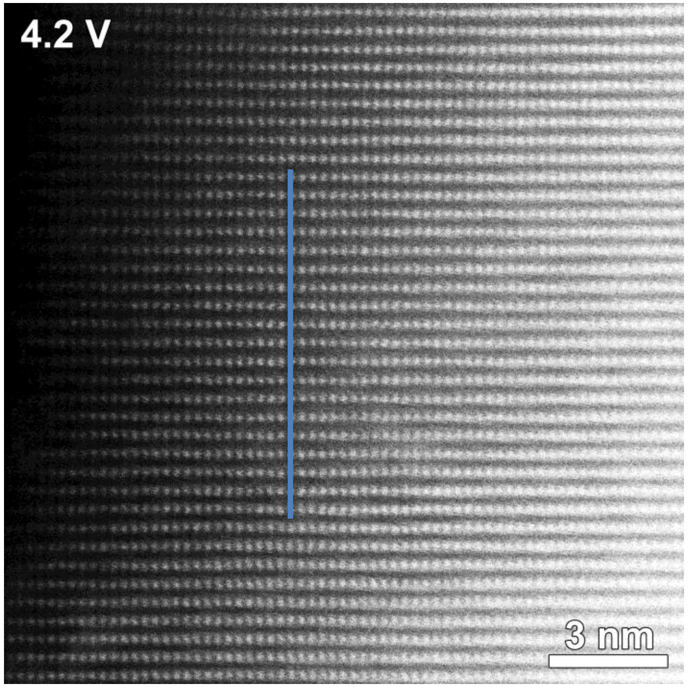

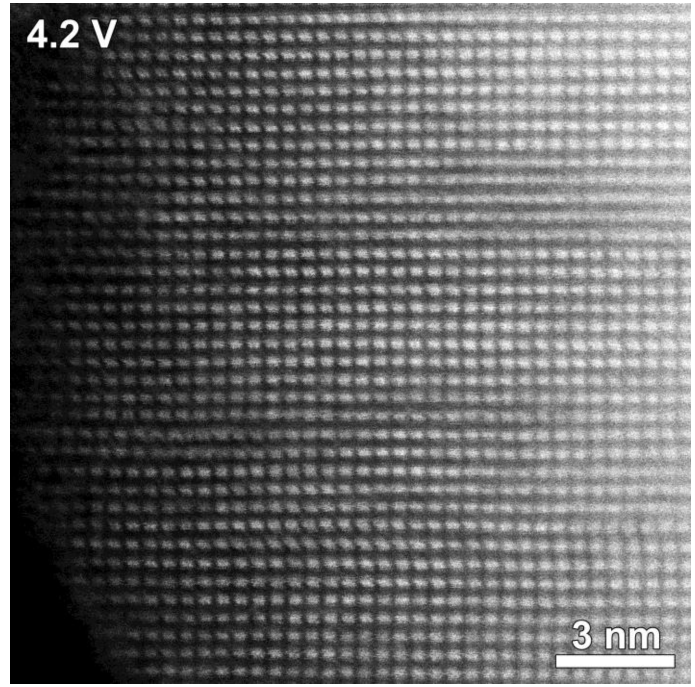

O1 structure:

1) *hcp* O packing

2) honeycomb layers on top of each other

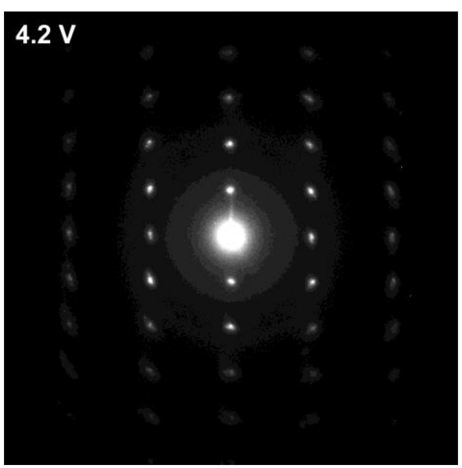

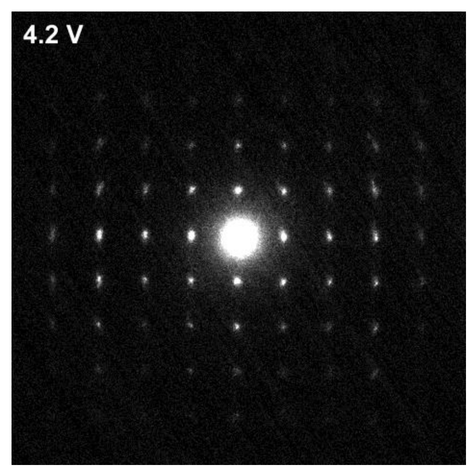

Perez A. J. *et al*, J.-M. M. *Chem. Mater.* **2016**, *28*, 8278–8288

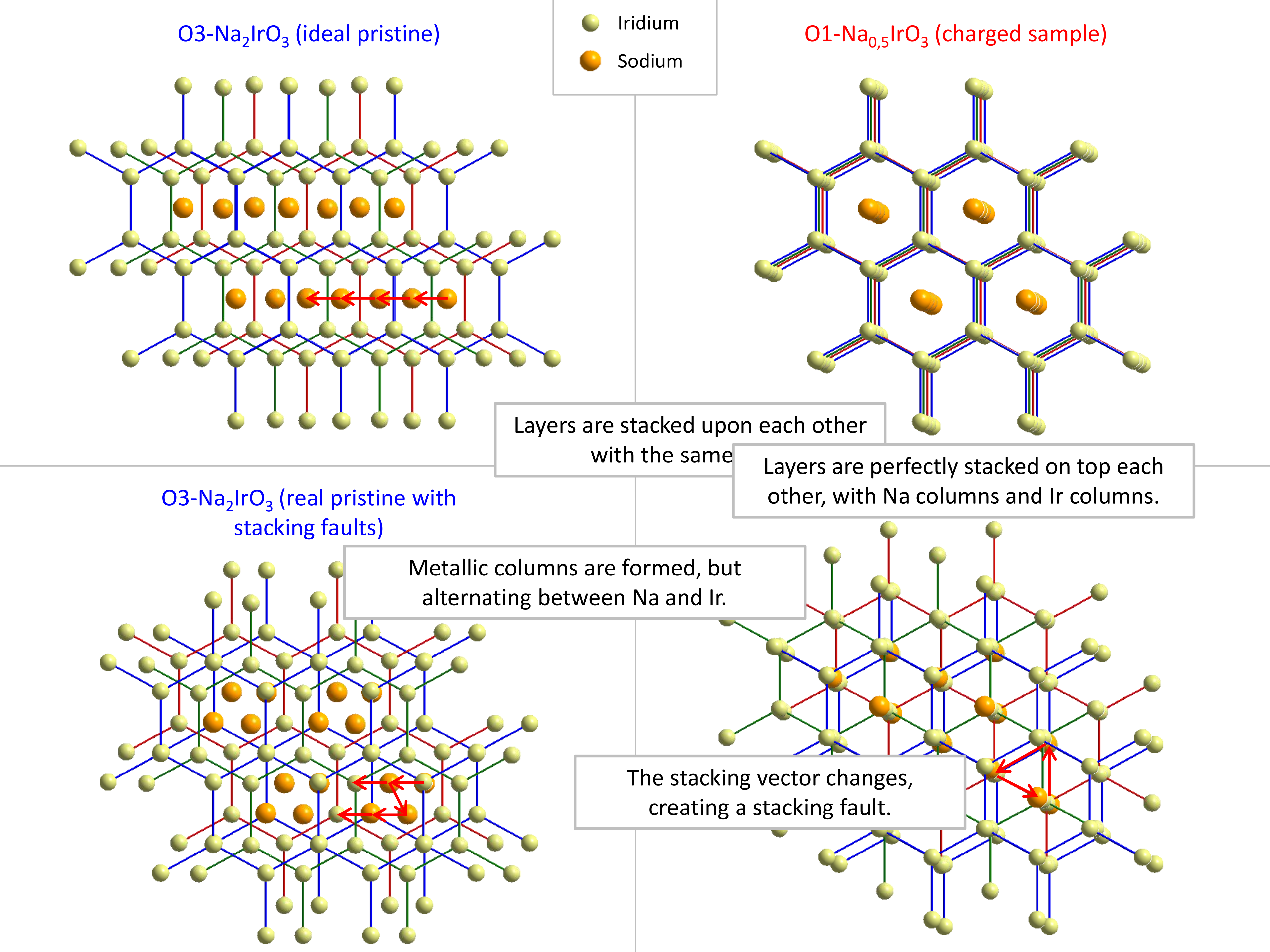

O3-Na_2IrO_3 (ideal pristine)
Iridium
Sodium
O1-$Na_{0,5}IrO_3$ (charged sample)
Layers are stacked upon each other
with the same
Layers are perfectly stacked on top each other, with Na columns and Ir columns.
O3-Na_2IrO_3 (real pristine with stacking faults)
Metallic columns are formed, but alternating between Na and Ir.
The stacking vector changes, creating a stacking fault.

Na_xIrO_3: anion redox

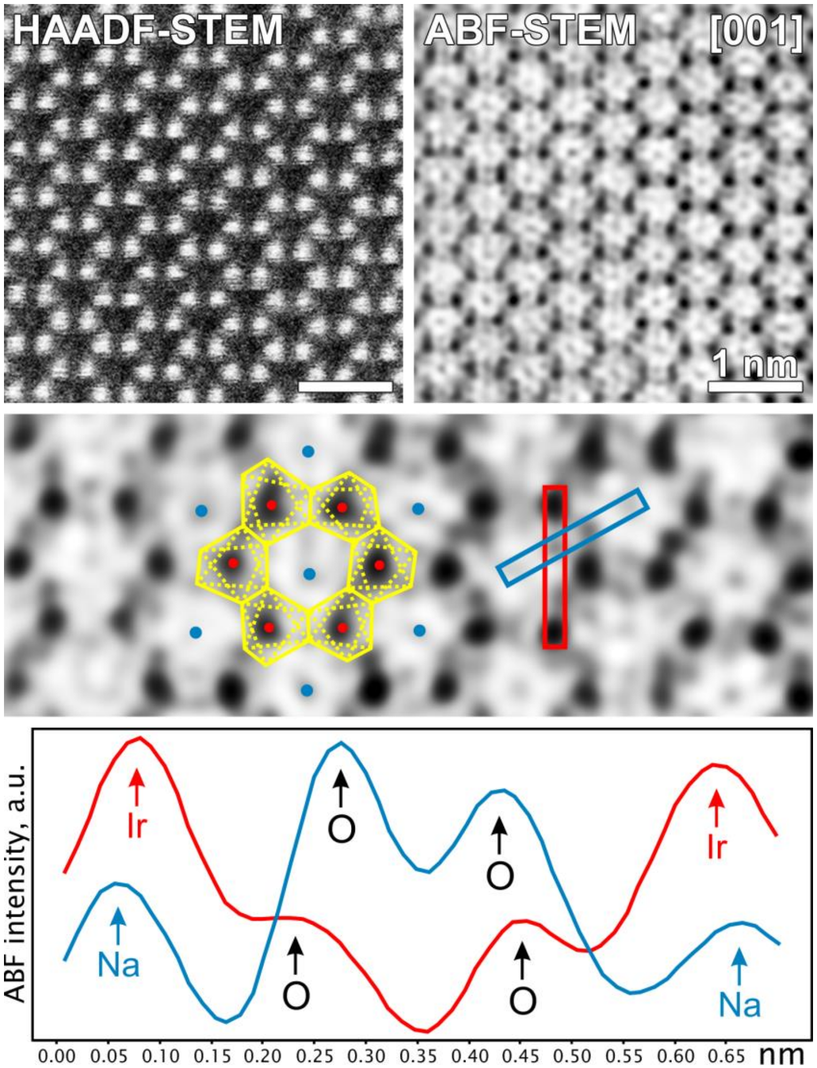

Fully charged Na_xIrO_3 (4.3 V)

shortening of 3 out of 6
O-O (projected) distances:
formation peroxo-like dimers

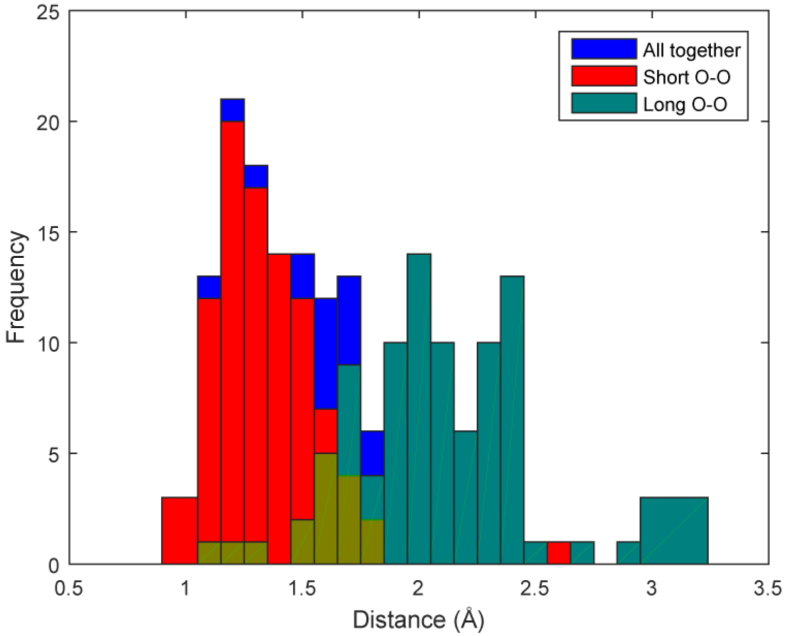

Data consistent with the NPD refinement!

Perez A. J. *et al*, J.-M. M. *Chem. Mater.* **2016**, *28*, 8278–8288

Li_2IrO_3 polymorphs

α-Li_2IrO_3

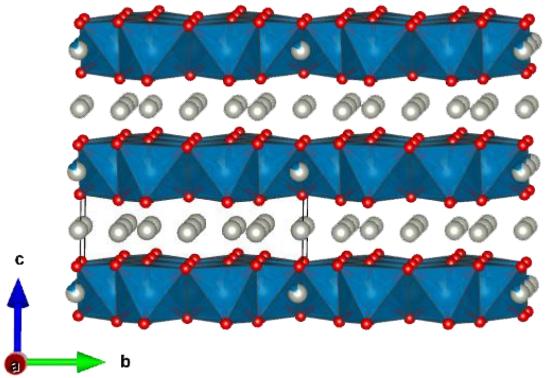

$[111]_{NaCl}$

β-Li_2IrO_3

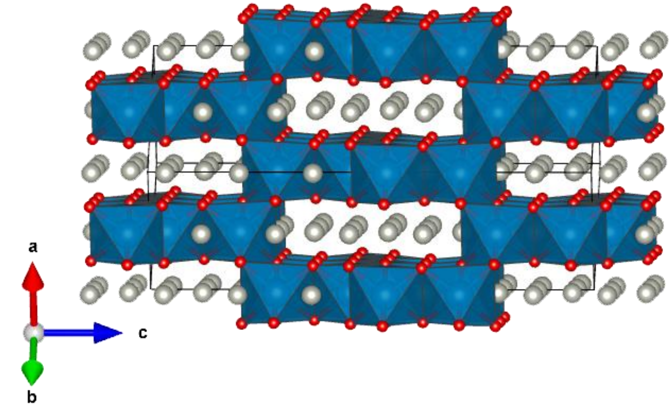

1. Both are based on the cubic close packing of the O atoms
2. In the pristine state Ir and Li occupy octahedral sites

"honeycomb" arrangement of Ir atoms

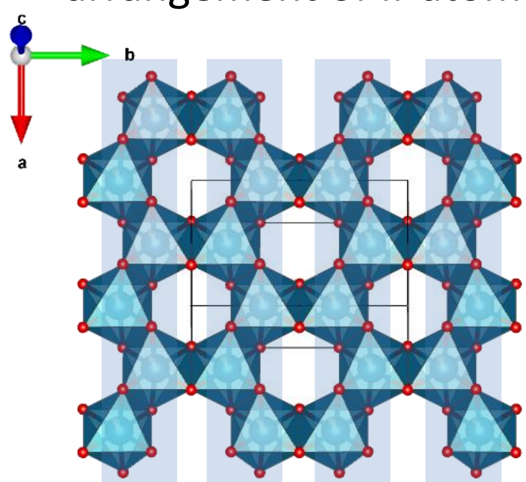

$[111]_{NaCl}$

interpenetrating zig-zag chains of IrO_6 octahedra

[110]

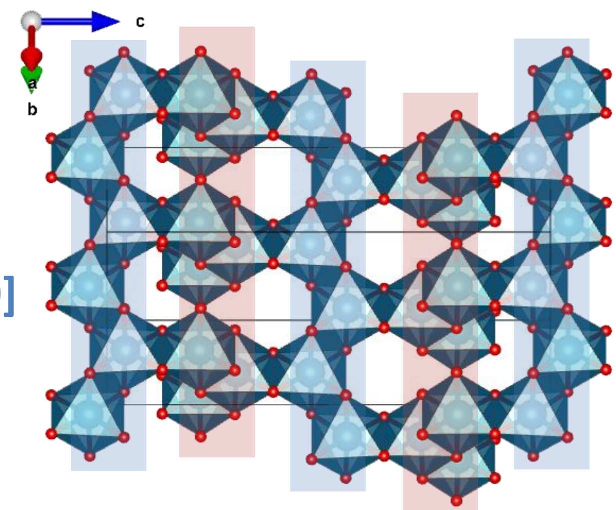

$[1\bar{1}0]$

Pearce P. E. *et al*, *Nat. Mater.* **2017**, 1–8

β-Li_2IrO_3

Electron diffraction

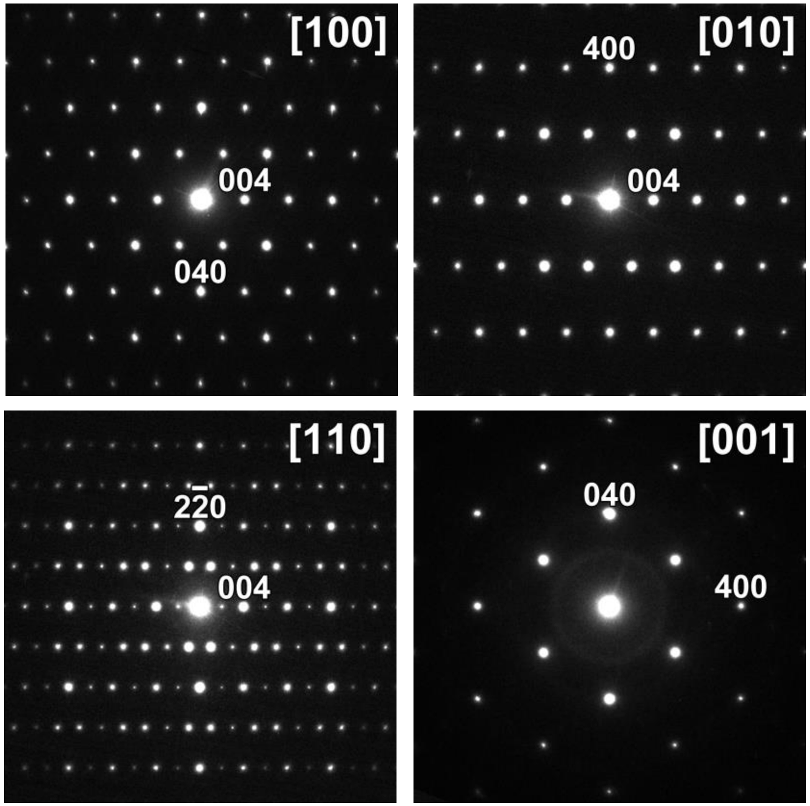

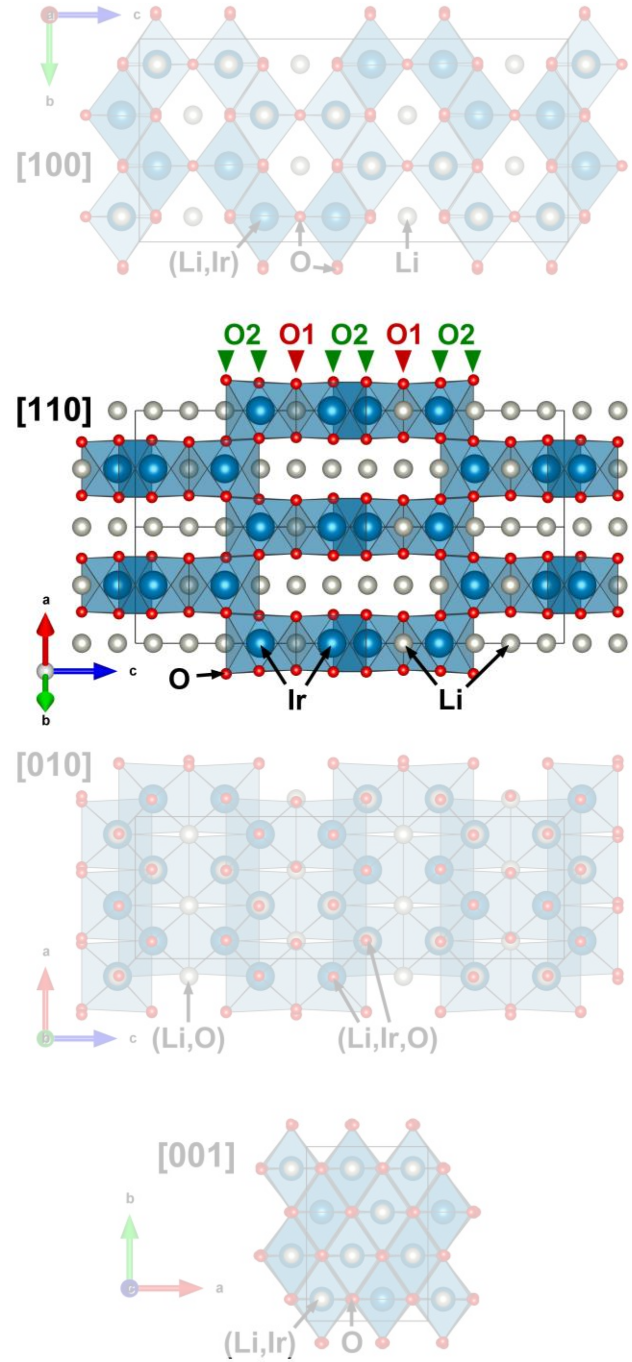

S.G. *Fddd*

$a \approx 5.9$ Å

$b \approx 8.4$ Å

c ≈ 17.8 Å

Pearce P. E. *et al*, *Nat. Mater.* **2017**, 1–8

Structure evolution of β-Li_xIrO_3 upon the electrochemical oxidation

Ir arrangement does not change!

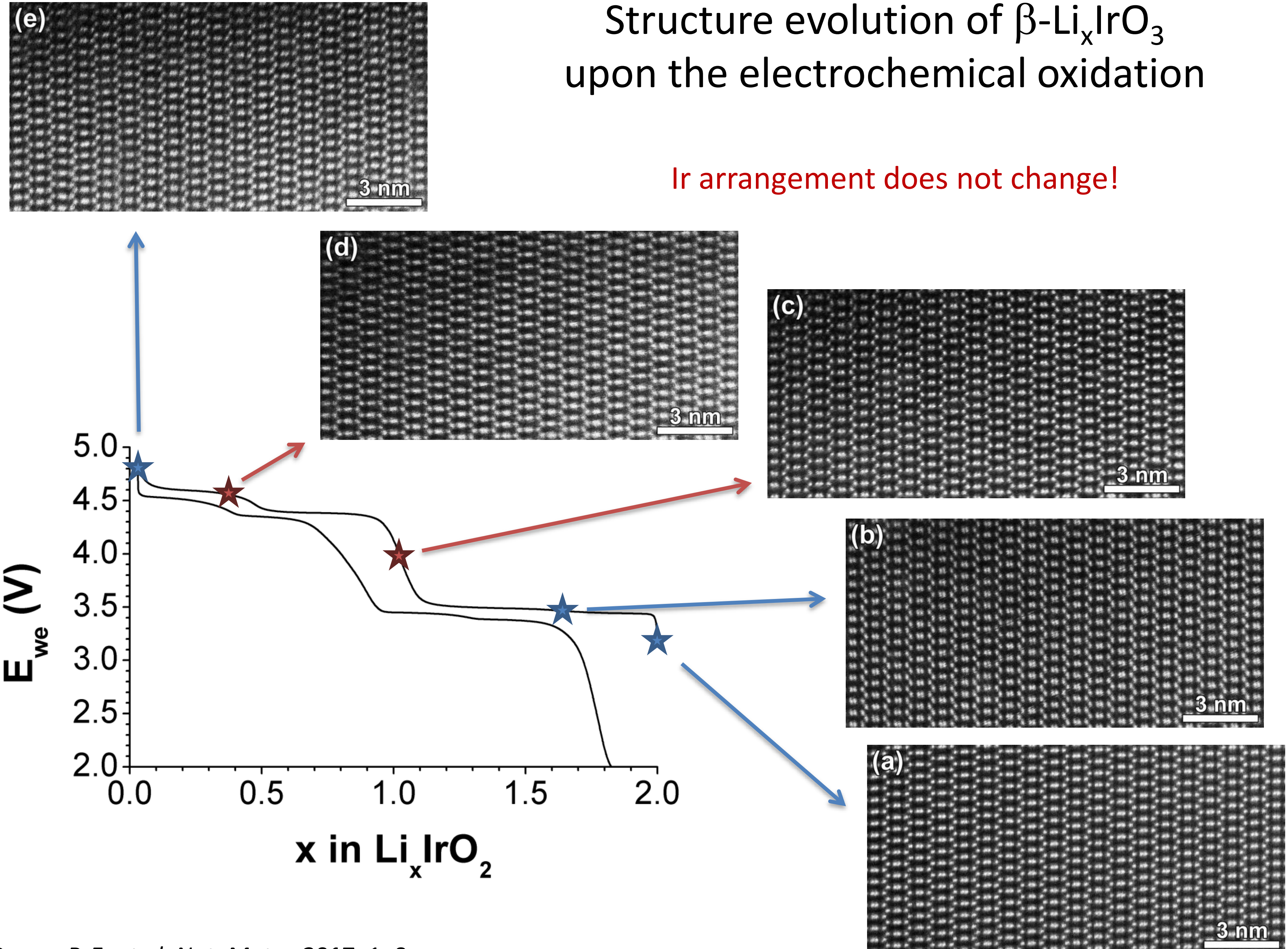

Pearce P. E. *et al*, *Nat. Mater.* **2017**, 1–8

β-Li_2IrO_3: anion redox

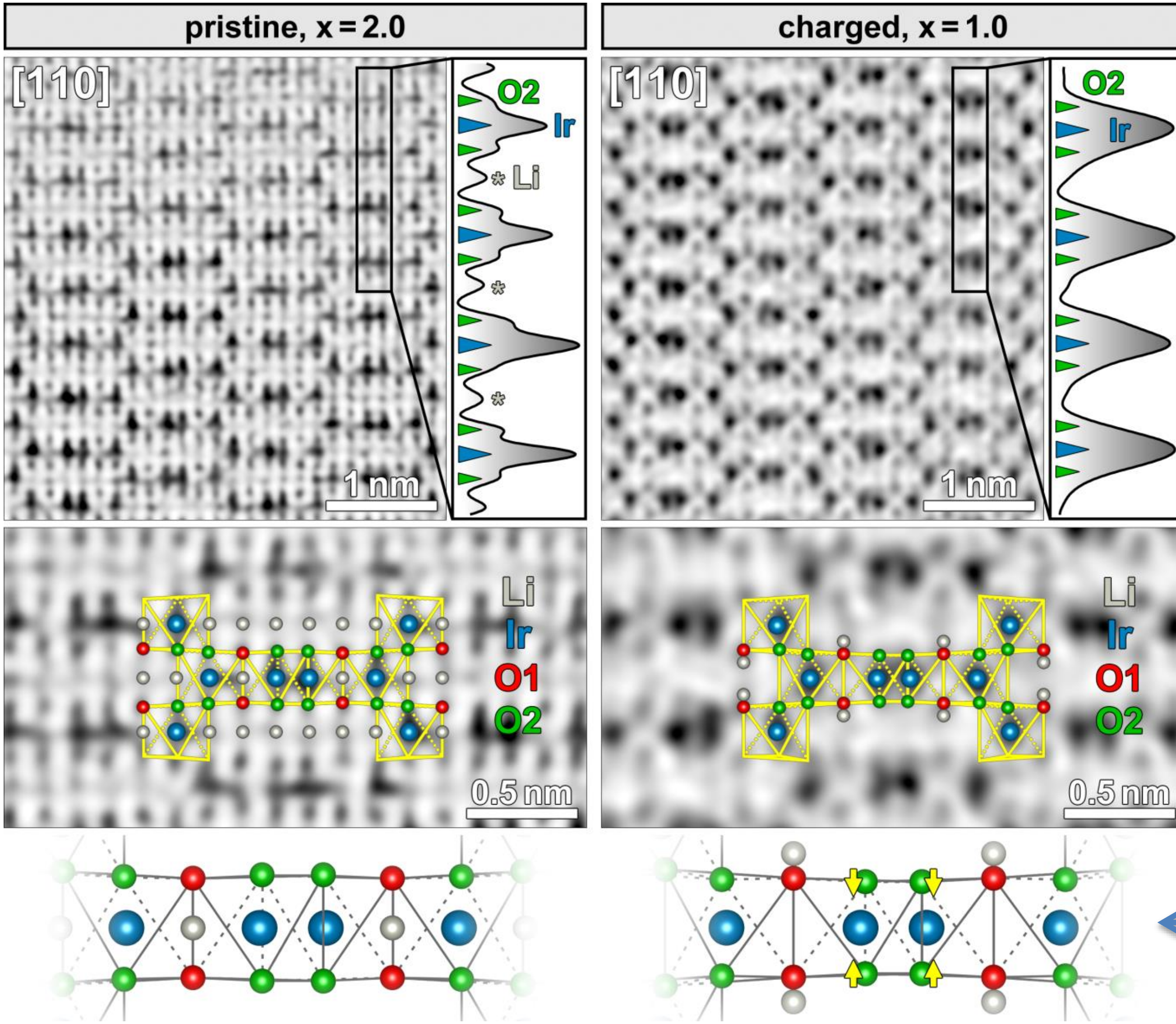

refined structures from NPD

Pearce P. E. *et al*, *Nat. Mater.* **2017**, 1–8

Electron Energy Loss Spectroscopy (EELS)

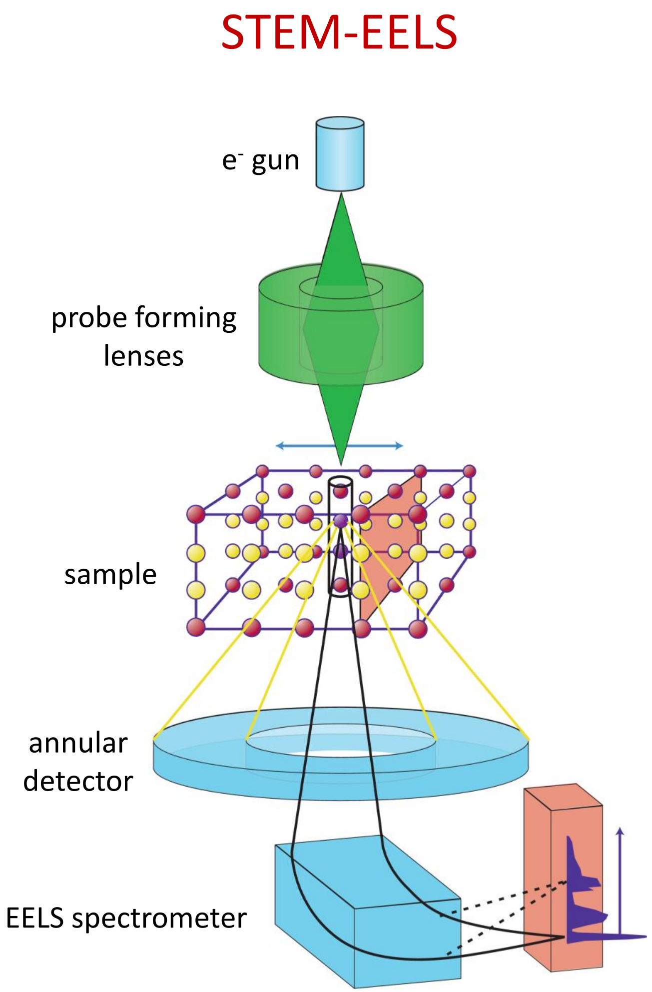

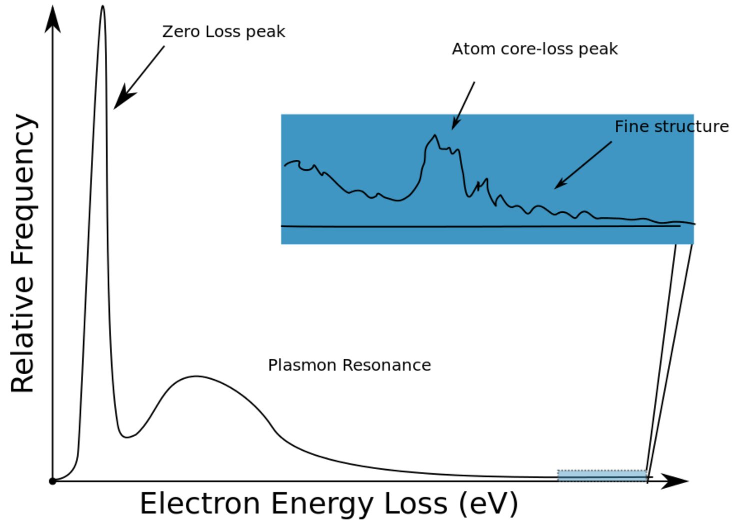

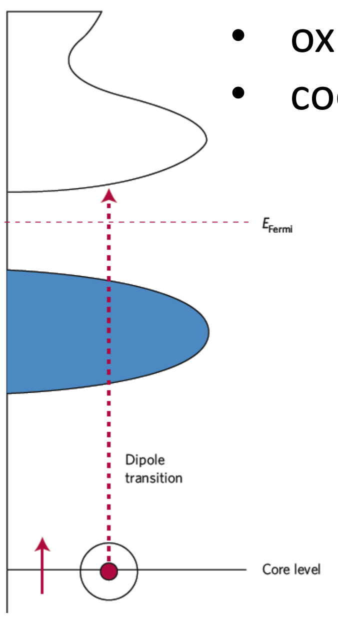

Fine structure of the absorption edge:

- oxidation state
- coordination environment

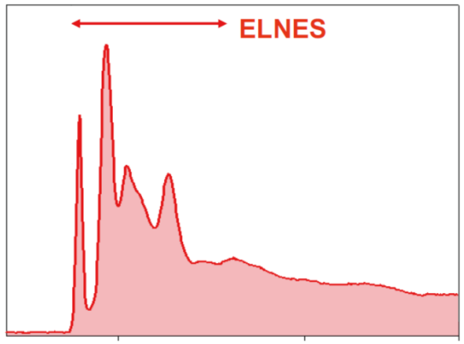

Electron Energy Loss Near Edge Structure

EELS for determining oxidation state

isostructural

$RuVPO_4F$ (V^{3+}) | $KV(PO_4)O$ (V^{4+}) | $Na_3V_2(PO_4)_3$ (V^{3+})

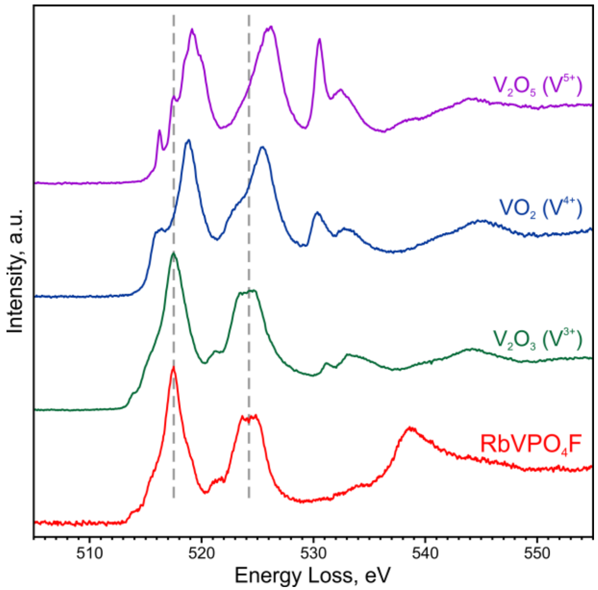

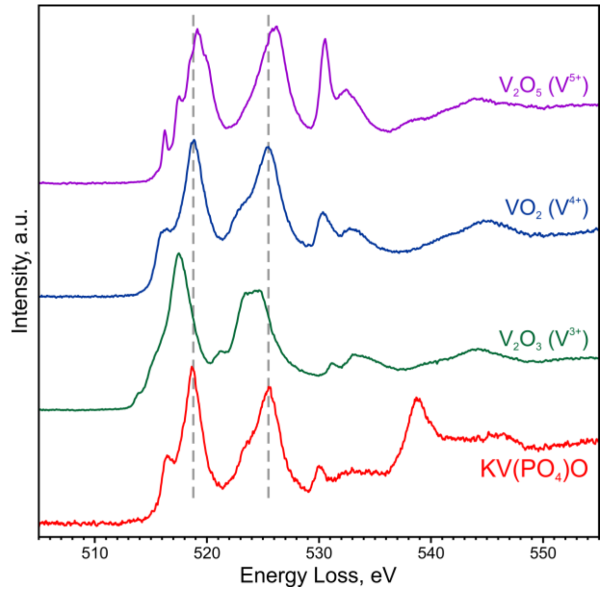

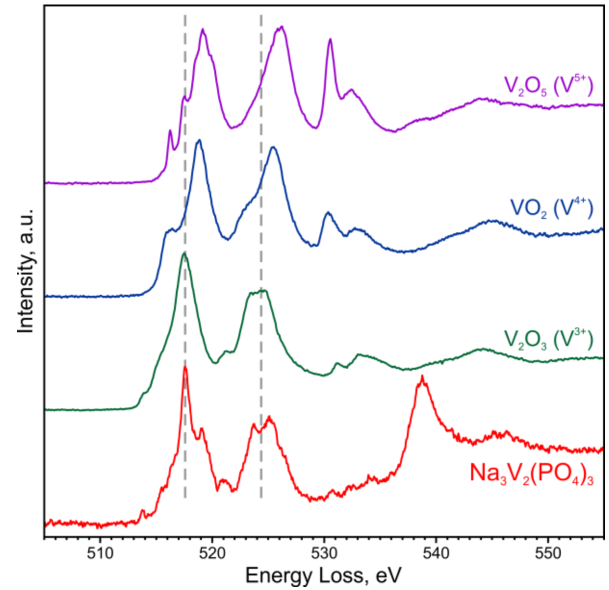

different local coordination

MnO + LiF composites

$$xLiF + MnO \xrightarrow{charge} MnOF_x + xLi^+ + xe^-$$

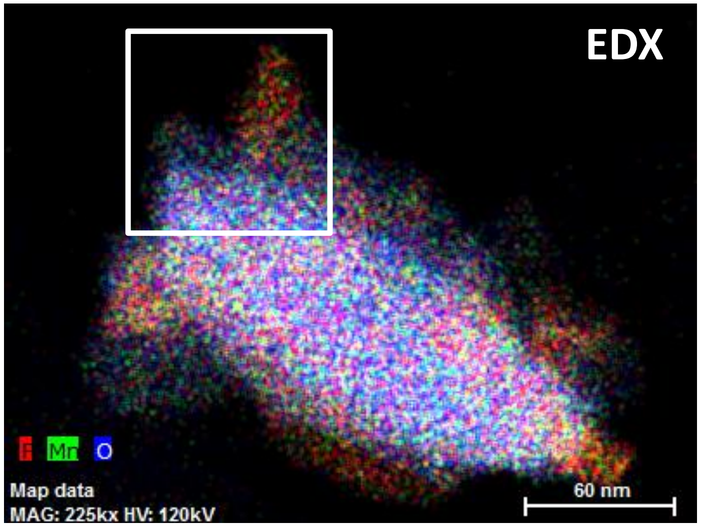

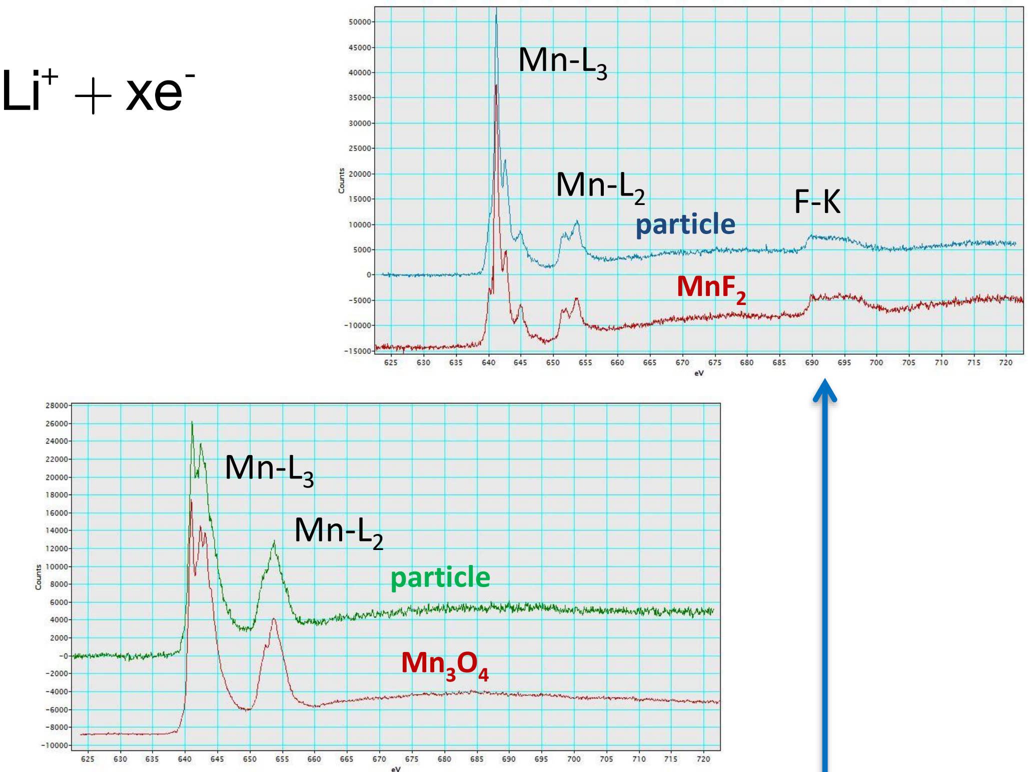

F-rich – MnF_2 // O-rich – Mn_3O_4

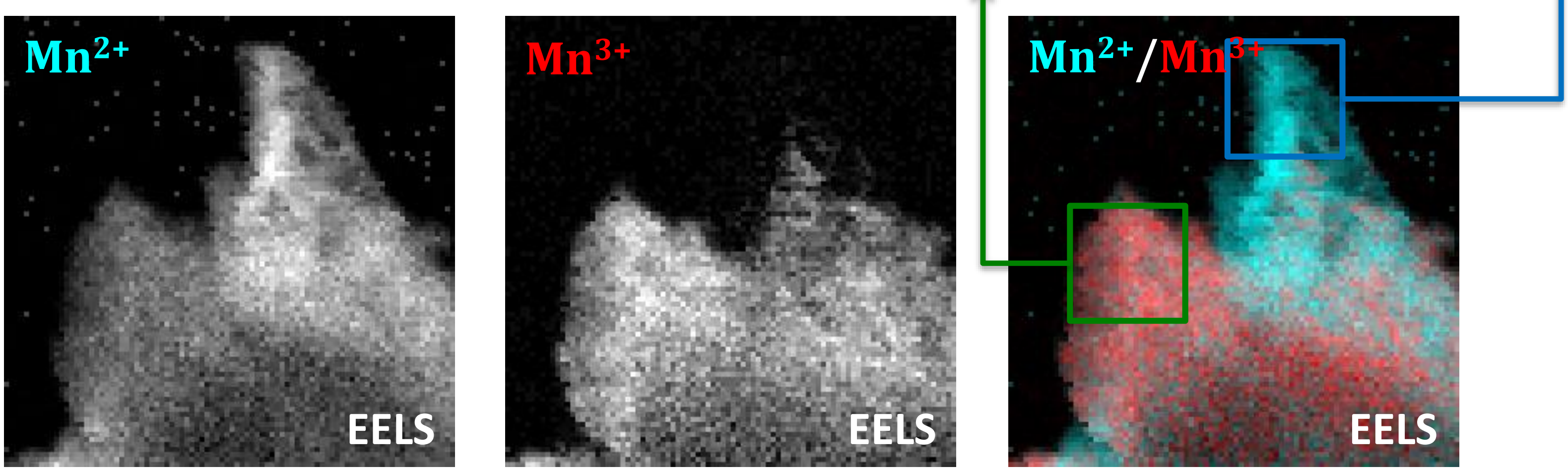

Energy Dispersive X-ray analysis

electron transitions in the atoms

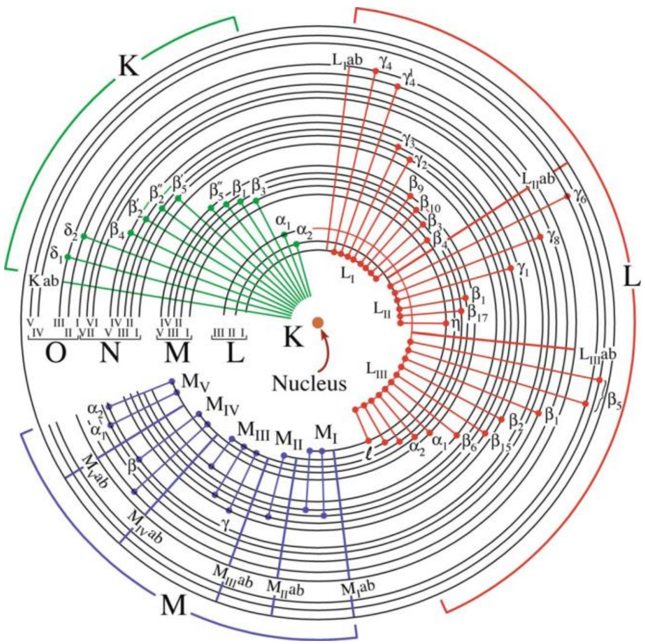

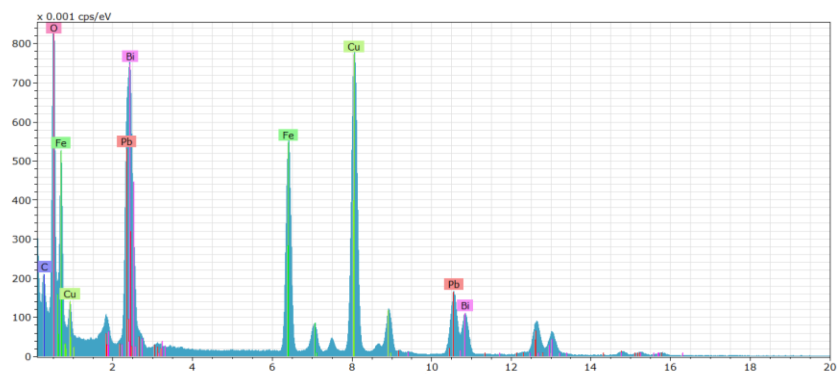

EDX spectrum – set of emission lines

STEM-EDX

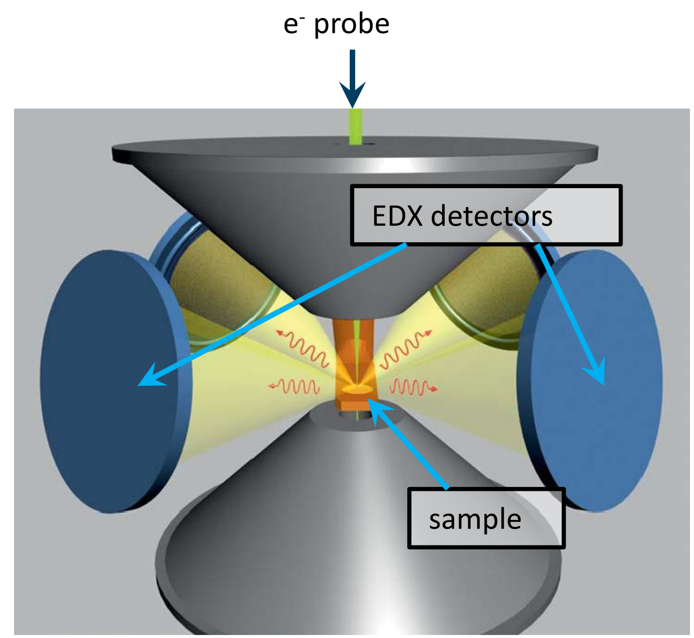

4 detector configuration:

- high count rate
- higher reliability

Quantitative EDX

$K_2Cu_2(SO_4)_3$

K : Cu : S = 1.97(7) : 1.95(14) : 3.07(14)

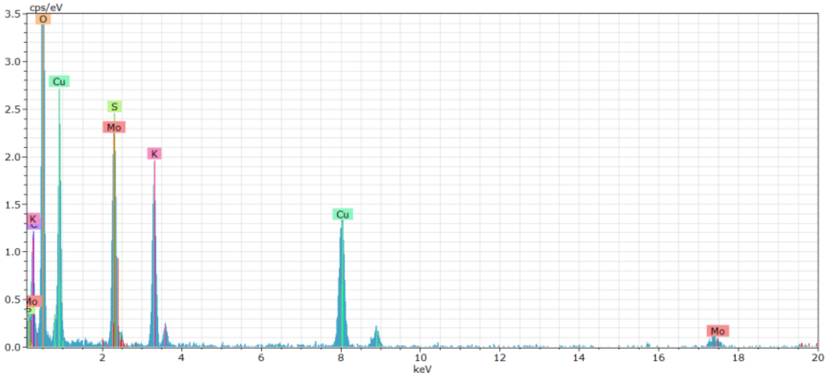

NaO_2

Na : O = 0.33(3) : 0.66(3)

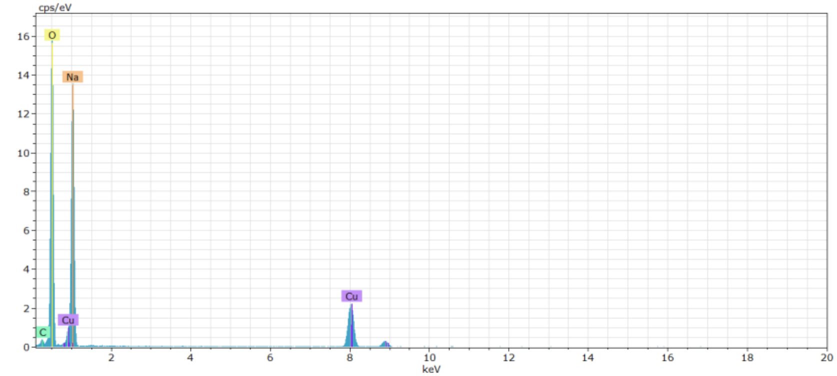

One should be careful !

$Na_{2-x}IrO_3$ systematic discrepancy

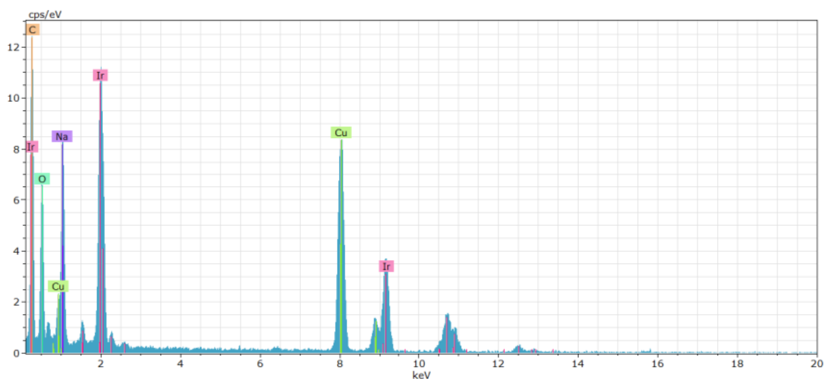

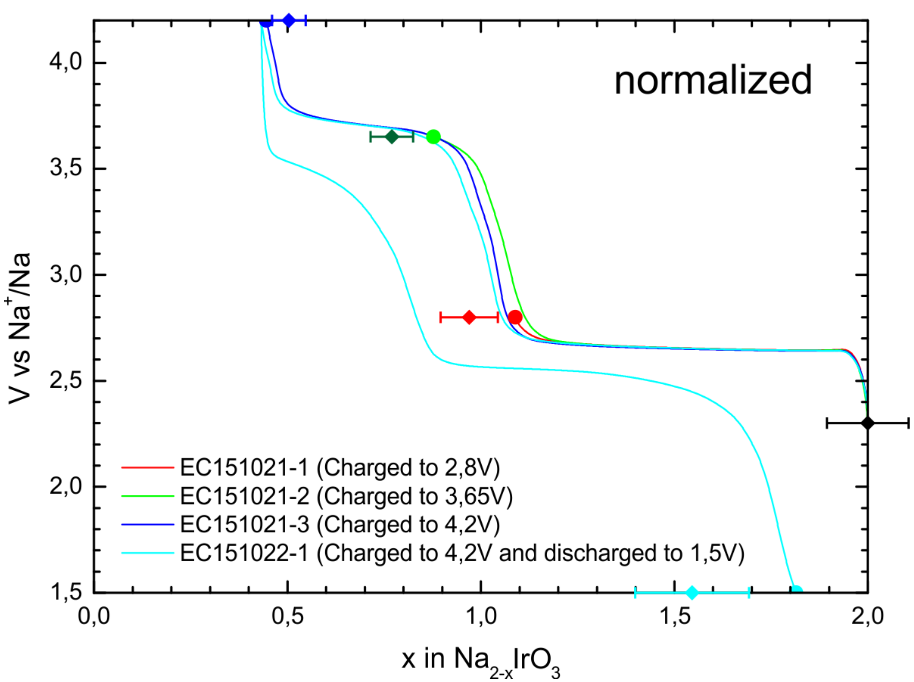

EDX elemental mapping

$Na_x(Ni_{0.2}Mn_{0.6}Co_{0.2})O_2$

+

Na_2CO_3

$y = Na^{tot}/M$

y = 0.7

y = 0.9

y = 1.0

y = 1.1

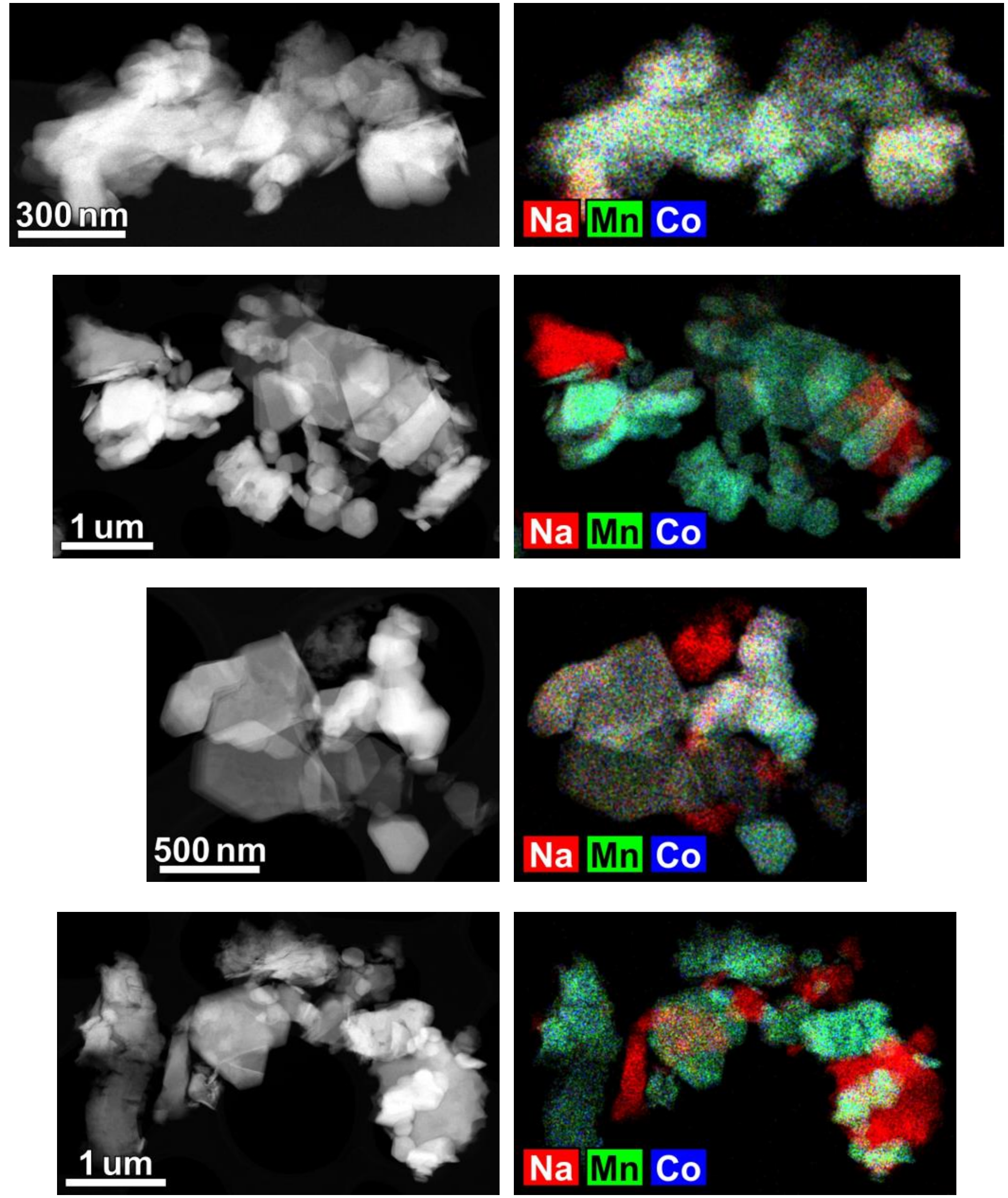

Sathiya M. *et al*, *Chem. Mater.* **2017**, *29*, 5948–5956

EDX elemental mapping

$$xLiF + MnO \xrightarrow{\text{charge}} MnOF_x + xLi^+ + xe^-$$

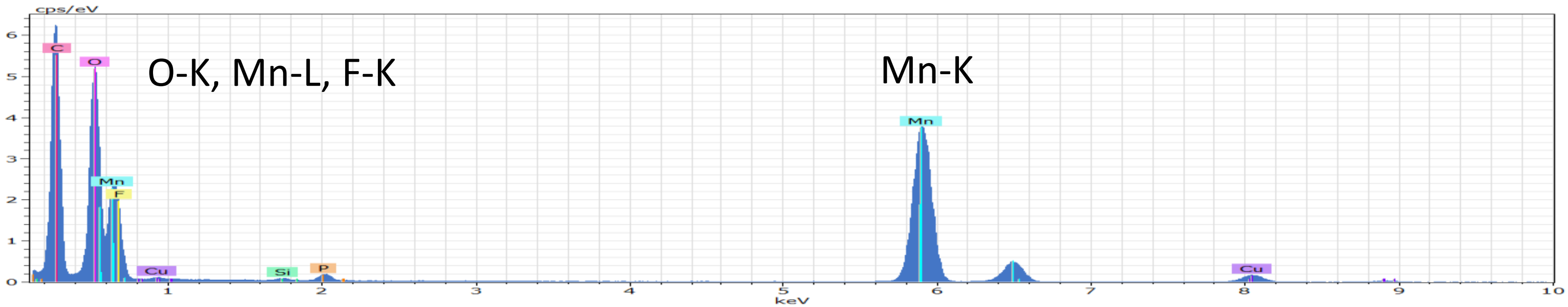

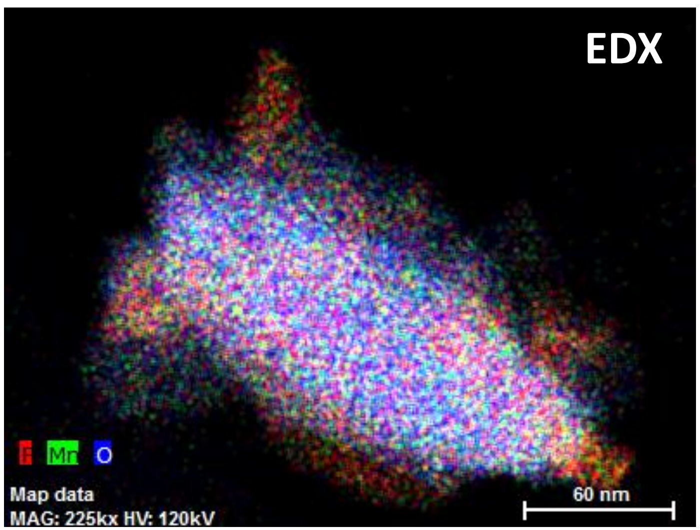

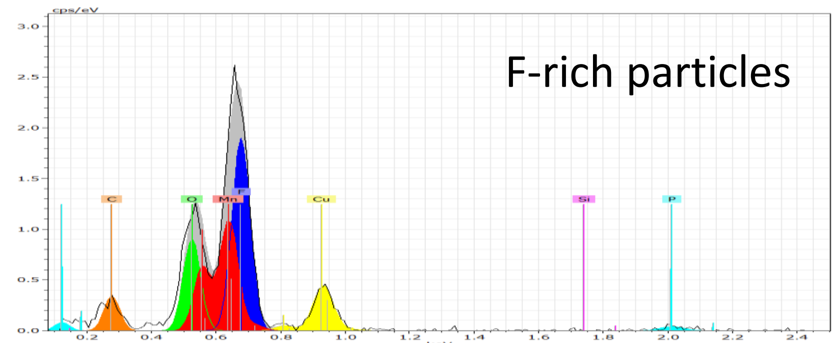

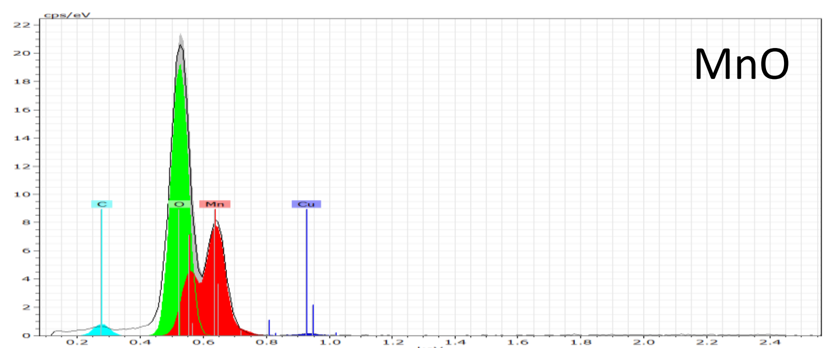

Mn-O-F: quantification unreliable

MnO, O:Mn = 1.05(6); Mn_2O_3, O:Mn = 1.53(14);
MnO_2, O:Mn = 2.09(15); MnF_2, F:Mn = 1.76(33)

Concluding remarks

- TEM is a versatile tool providing structural and chemical information on a very local scale
- Different TEM techniques provide complementary information, which can also be combined with other experimental method (i.e. XRD/NPD, XPS, bulk chemical analysis…)
- Often application of advanced TEM is challenged the material, i.e. poor crystallinity, beam sensitivity, contamination issues, etc.

Thank you for your attention!

Acknowledgement

Promoters: Prof. Joke Hadermann
Dr. Artem Abakumov

HAADF-STEM imaging: Dr. Dmitry Batuk

Collaborators: V. Sumanov
Dr. O. Drozhzhin
Dr. N. Khasanova
Dr. E. Antipov

Moscow State University, Moscow, Russia

Dr. D. Mikhailova

Max Planck Institute for Chemical Physics of Solids, Dresden, Germany

Bulk EDX data

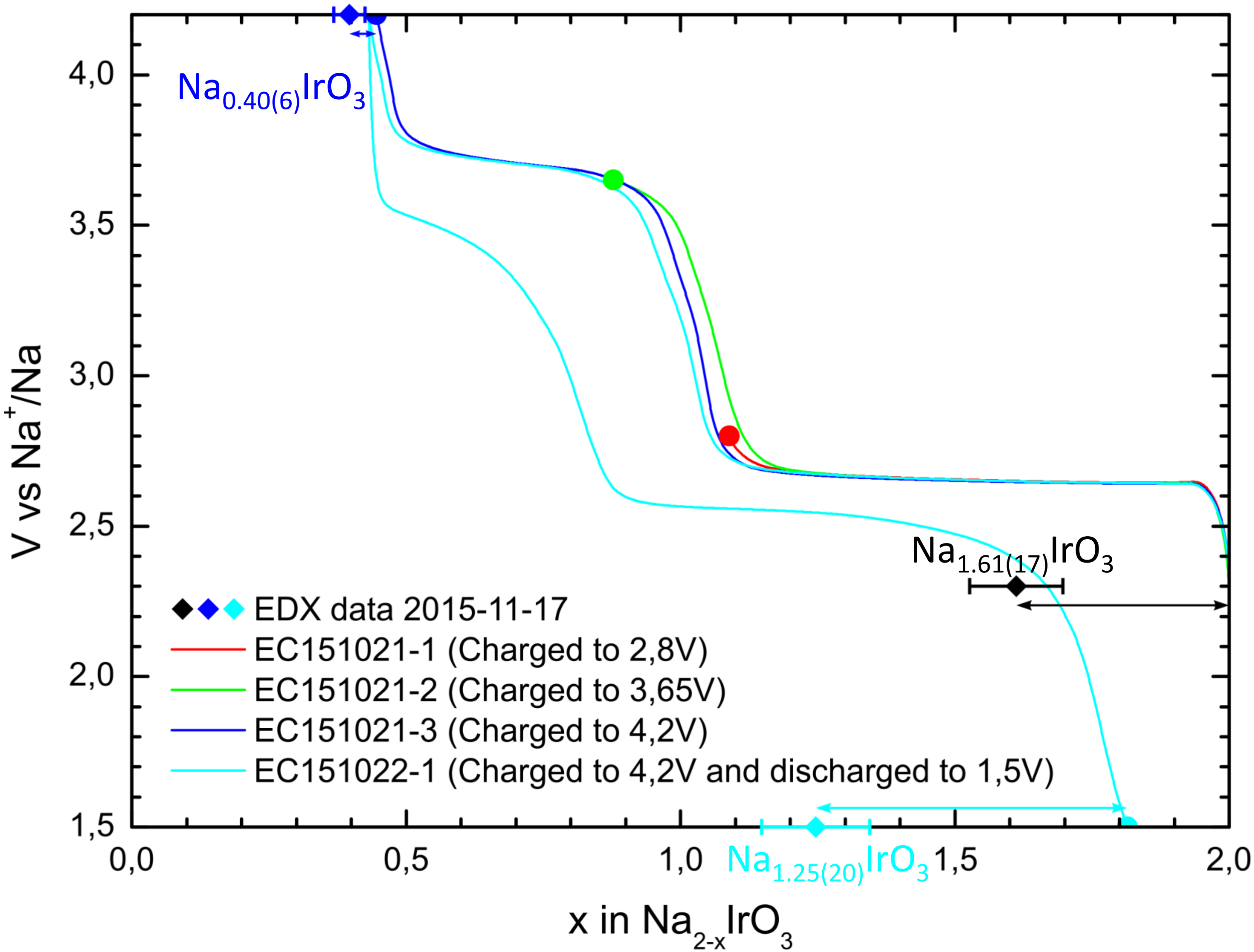

The composition is calculated for 30-60 crystals using the Na-K and Ir-L lines

Reciprocal lattice

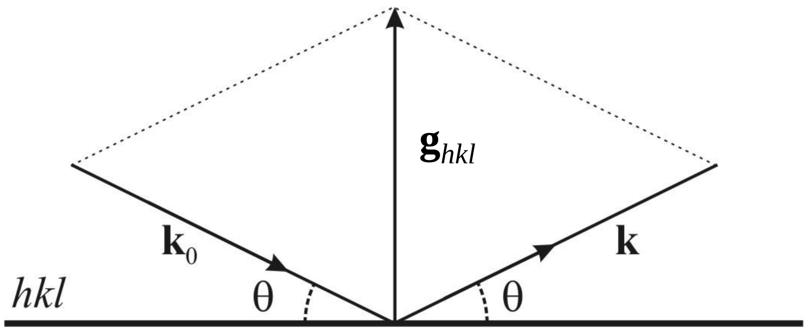

$\mathbf{k}_0$ – wave vector of the incident beam, $|\mathbf{k}_0| = 1/\lambda$

$\mathbf{k}$ – wave vector of the diffracted beam, $|\mathbf{k}| = 1/\lambda$

$\mathbf{g}_{hkl} \perp hkl$ plane, $\mathbf{g} = \mathbf{k} - \mathbf{k}_0$

Bragg's condition is satisfied if $|\mathbf{g}| = 2\sin\theta/\lambda = 1/d_{hkl}$

Set of the $\mathbf{g}_{hkl}$ vectors form a reciprocal lattice of crystal

$\mathbf{a^*} \perp \mathbf{bc}$ plane $\mathbf{b^*} \perp \mathbf{ac}$ plane $\mathbf{c^*} \perp \mathbf{ab}$ plane

$\mathbf{aa}^* = \mathbf{bb}^* = \mathbf{cc}^* = 1$

$\mathbf{ab}^* = \mathbf{ba}^* = \ldots = \mathbf{ac}^* = 0$

$\mathbf{a}^* = p\,(\mathbf{b}\times\mathbf{c})$ $\mathbf{b}^* = p\,(\mathbf{a}\times\mathbf{c})$ $\mathbf{c}^* = p\,(\mathbf{a}\times\mathbf{b})$

$\mathbf{aa}^* = p\,[(\mathbf{b}\times\mathbf{c})\,\mathbf{a}] = pV = 1$

$p = 1/V$, V – unit cell volume

$\mathbf{a}^* = (\mathbf{b}\times\mathbf{c})/V$ $\mathbf{b}^* = (\mathbf{a}\times\mathbf{c})/V$ $\mathbf{c}^* = (\mathbf{a}\times\mathbf{b})/V$

$\mathbf{g}_{hkl} = h\mathbf{a}^* + k\mathbf{b}^* + l\mathbf{c}^*$

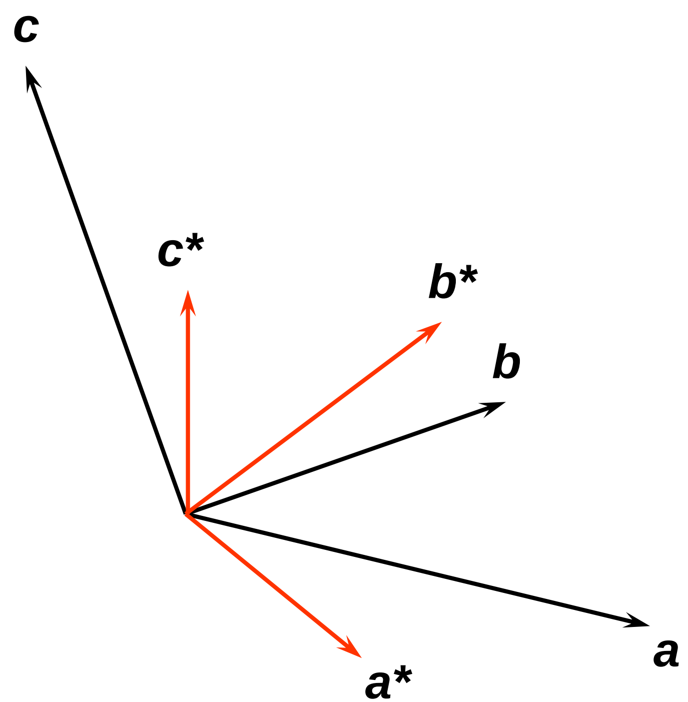

EELS – electron energy loss spectroscopy

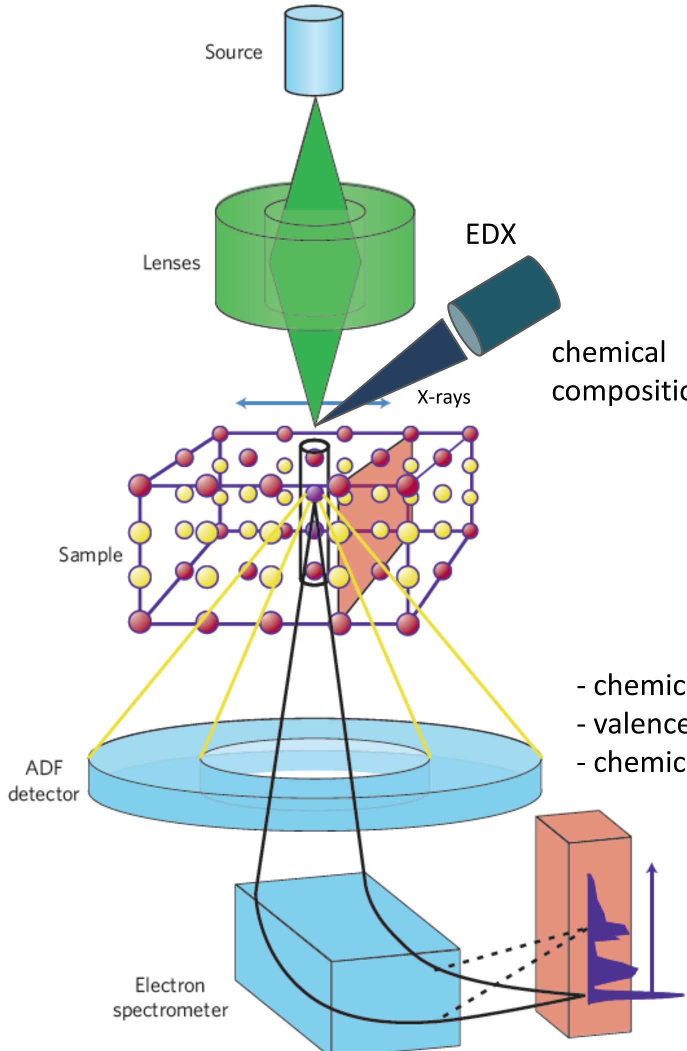

- chemical composition
- valence
- chemical bonding

Mapping of
- oxidation state
- coordination number

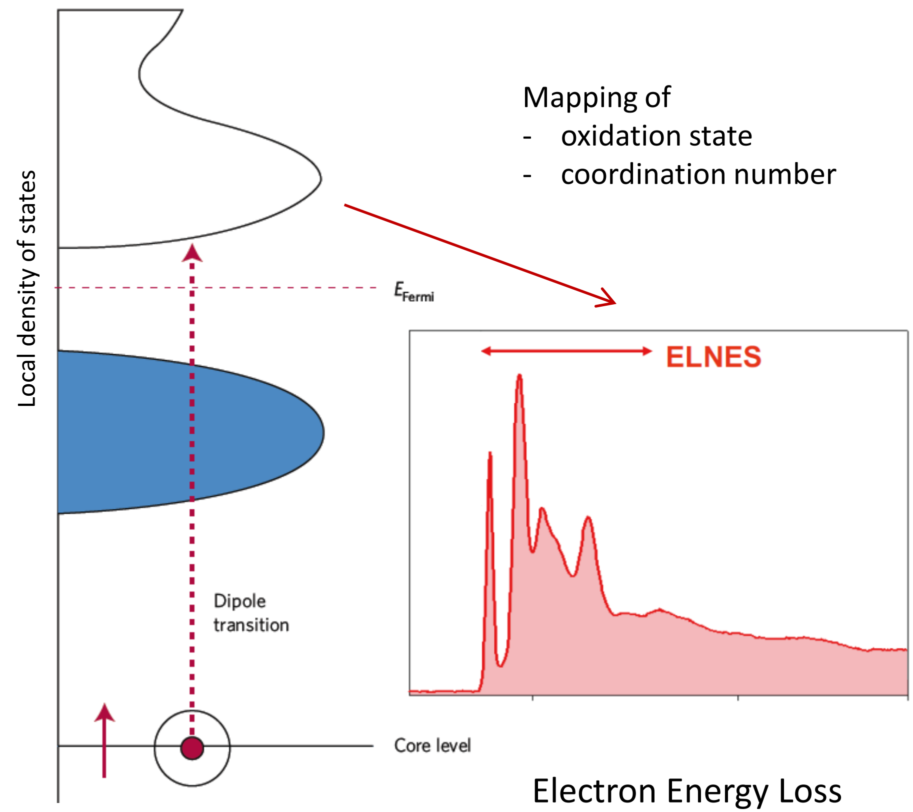

Electron Energy Loss Near Edge Structure